AD_____

Award Number:
W81XWH-09-1-0316

TITLE: Nanoscale Proteomic Analysis of Oncoproteins in Hematopoietic Cancers

PRINCIPAL INVESTIGATOR: Dean W. Felsher, M.D., Ph.D.

CONTRACTING ORGANIZATION: Stanford University
Menlo Park, CA 94025

REPORT DATE: May 2012

TYPE OF REPORT: Final

PREPARED FOR: U.S. Army Medical Research and Materiel Command
Fort Detrick, Maryland 21702-5012

REPORT DOCUMENTATION PAGE

Form Approved
OMB No. 0704-0188

1. REPORT DATE	2. REPORT TYPE	3. DATES COVERED
May 2012	Final	15 April 2009 – 14 April 2012

4. TITLE AND SUBTITLE
Nanoscale Proteomic Analysis of Oncoproteins in Hematopoietic Cancers

5a. CONTRACT NUMBER

5b. GRANT NUMBER
W81XWH-09-1-0316

5c. PROGRAM ELEMENT NUMBER

6. AUTHOR(S)

Dean Felsher

E-Mail: dfelsher@stanford.edu

5d. PROJECT NUMBER

5e. TASK NUMBER

5f. WORK UNIT NUMBER

7. PERFORMING ORGANIZATION NAME(S) AND ADDRESS(ES)

Stanford University
Menlo Park, CA 94205

8. PERFORMING ORGANIZATION REPORT NUMBER

9. SPONSORING / MONITORING AGENCY NAME(S) AND ADDRESS(ES)
U.S. Army Medical Research and Materiel Command
Fort Detrick, Maryland 21702-5012

10. SPONSOR/MONITOR'S ACRONYM(S)

11. SPONSOR/MONITOR'S REPORT NUMBER(S)

12. DISTRIBUTION / AVAILABILITY STATEMENT
Approved for Public Release; Distribution Unlimited

13. SUPPLEMENTARY NOTES

14. ABSTRACT
The goal of our grant was to develop two novel nanoscale proteomic technologies, NIA and AutoChIP, for the analysis of clinical specimens in response to targeted therapeutics. Over the three-year funding period, we have made excellent progress achieving these goals. Indeed, we have exceeded our objectives as follows: 1). We have identified the molecular mechanism of a novel PLK1 inhibitor, ON01910.Na, for the treatment of MDS. 2). We have identified biomarkers that appear to predict the clinical activity of this drug for MDS. 3). We have built an independent AutoChIP instrument in the Felsher laboratory, which enables us to unlimited access to this technology. 4). We have optimized conditions for AutoChIP-seq that will enable us to understand the molecular mechanism of targeted therapeutics by profiling global changes of gene activation and inactivation. Finally, during the three years of funding period, we have generated five published papers, two manuscripts in preparation, and we have also presented the DoD supported work in over 50 oral and poster presentations.

15. SUBJECT TERMS
NIA (nanoscale immunoassay), AutoChIP, ChIP-seq, c-MYC, signaling proteins, BCR-ABL, lymphoma, leukemia, MDS, atorvastatin, imatinib, apoptosis, cell proliferation, cellular senescence, tumor regression.

16. SECURITY CLASSIFICATION OF:			17. LIMITATION OF ABSTRACT	18. NUMBER OF PAGES	19a. NAME OF RESPONSIBLE PERSON
					USAMRMC
a. REPORT	b. ABSTRACT	c. THIS PAGE			19b. TELEPHONE NUMBER *(include area code)*
U	U	U	UU	77	

Table of Contents

Page

INTRODUCTION:
A major challenge in the development of better therapeutics for cancers is the ability to evaluate whether a targeted therapy is successfully inactivating the expected pathway. Current approaches for detecting potential efficacy of a therapy *in vivo* are usually static measurements, often insensitive and require large amounts of clinical material precluding serial analysis of therapeutic activity. To overcome this barrier, we have proposed in our grant to develop and utilize NIA and AutoChIP (in the original proposal, we called this micro-chip-ChIP) as tools to interrogate the mechanism of clinical response of patients with lymphoma to atorvastatin and the clinical response of leukemia to imatinib *in vitro* and *in vivo*. For the entire period of funding, we have fulfilled our proposed aims and moreover, we have surpassed our objectives and obtained exciting results. In summary, we have generated five published papers, two manuscripts in preparation, and we have also presented the DoD supported work in over 50 invited oral and poster presentations (list below).

BODY:
Specific Aim 1: To develop NIA and AutoChIP as tools for analyzing oncoprotein and signaling protein expression, phosphorylation and DNA binding in response to atorvastatin and imatinib *in vitro* in mouse and human cell lines.
To address the deficiency of existing methods to measure oncoprotein and signaling protein expression or phosphorylation in limited clinical specimens, we proposed to develop NIA, a highly sensitive, quantitative and automated technique as a tool to detect expression and phosphorylation changes of oncoproteins and signaling proteins in response to atorvastatin and imatinib. In addition, we proposed to develop AutoChIP, another highly sensitive and automated technique as a tool to measure DNA binding changes in response to atorvastatin and imatinib as our Specific Aim 1.

Over the past three years, we have developed NIA protocols and optimized NIA conditions for several proteins including oncoproteins such as c-MYC and BCL2, signaling proteins including AKT2, AKT1/2/3, Erk1/2, MEK1, MEK2, pStat5, pStat3, apoptotic proteins such as cleaved caspase 3 and pJNK, and cell cycling proteins including CDC2 and p15 in *in vitro* cell lysates and *in vivo* mouse and human specimens [**2010 Progress Report**, **2011 Progress Report**, **appended paper 1, Figure 1**, **and Figure 2**]. The development of these NIA assays enables us to have direct readouts for monitoring the molecular mechanism of response to targeted therapeutics in cells.

Through the use of *in vitro* cell lines, we investigated the mechanism of atorvastatin's and imatinib's anti-cancer effects. We found that atorvastatin treatment significantly decreases phosphorylation of c-MYC. Moreover, we found that lymphoma cells overexpressing phospho-MYC mutants are more resistant to atorvastatin treatment. Our findings support our central hypothesis proposed in our grant: Statin treatment mediates its anti-cancer effects by blocking c-MYC phosphorylation, resulting in either its degradation or its disassociation from E- box promoter region of target genes [**2010 Progress Report**]. A manuscript concerning this work is in preparation.

Also, we found that in BCR-ABL-induced human leukemia cells, K562 cells, imatinib may suppress activation of several signaling pathways including MAPK/Erk and Stat3/5 pathways, inhibiting c-MYC expression and phosphorylation, thereby leading to cell cycle arrest, apoptosis, and senescence. These results provide evidence that MAPK/Erk signaling are essential for imatinib's clinical activity. Specifically, a change in Erk2 phosphorylation appears to be a biomarker for TKI clinical activity [**2010 and 2011 Progress Reports**].

Beyond the initial aims proposed in our grant, we further extended our study on targeted therapeutics by adding other agent (ON01910.Na, a PLK1 inhibitor for myelodysplastic syndrome, MDS) with collaboration of other professors at Stanford University. MDS is a hematological disorder characterized by different degrees of bone marrow failure and a propensity to evolve to acute myeloid leukemia (AML). PLK1 (polo-like kinase 1) is known to be essential for mitosis and maintenance of genomic stability. PLK1 is overexpressed in leukemia and PLK1 inhibitors have some activities in phase I studies of MDS patients [1-2]. The mechanism by which ON01910.Na affects pathogenesis and progression of MDS is unclear. Groopman's group reported that ON01910.Na, a styryl sulfonyl compound, is a PLK1 inhibitor. It has anti-tumor activity against MCL (mantle cell lymphoma) by inducing cell cycle arrest and apoptosis through the mechanism of down-regulating cyclin D1 and c-MYC [3]. Based on the above studies, one of our collaborators initiated an IRB approved clinical trial of ONA01910.Na treatment with MDS patients at Stanford Hospital in 2009. As a member of the research team, we have first investigated the mechanism of the anti-MDS property of ON01910.Na in TF1 cells, a human MDS cell line. We have found that ON01910.Na blocks MEK/Erk signaling in TF1 cells by suppressing expression and phosphorylation of Erk1/2, MEK1 and MEK2, leading to cell cycling arrest and apoptosis **[2010 Progress Report**, **Figure 3 and 4]**.

In the first year of funding period, we built an independent microfluidics system to perform AutoChIP in the Felsher laboratory. This is beyond the goals we proposed in the original grant. It took us a great effort and time to build the first AutoChIP system in our laboratory, but this in-house AutoChIP system enables us to unlimited access to this technology in the following two years of research in this grant. Moreover, we tested and compared AutoChIP to conventional "Benchtop-ChIP", optimized the AutoChIP protocol regarding sensitivity and specificity, evaluated antibodies against MYC, and applied the AutoChIP technology to mouse lymphoma cells to monitor c-MYC's interaction with its target gene promoters. Some of these results have recently been published **[2010 and 2011 Progress Reports, appended paper 2]**. Additional results are currently in preparation for publication.

Specific Aim 2: To use NIA and AutoChIP assays for interrogating the mechanism of clinical response to atorvastatin and imatinib *in vivo* in transgenic mouse models.

We evaluated hypothesis one: statins inhibit MYC phosphorylation by blocking the Rac pathway, that then leads to reduced protein stability and/or loss of MYC DNA binding capacity to its target genes; and hypothesis two: Imatinib reverses leukemogenesis by altering phosphorylation states of signaling proteins in BCR-ABL signaling pathways. To go beyond our *in vitro* findings, we interrogated the mechanism by which atorvastatin or imatinib treatment inhibit progression of MYC-induced lymphoma or BCR-ABL-induced leukemia *in vivo* in transgenic mouse models.

First, we have identified that the inhibition of MYC activation is a possible mechanism for statin's anti-cancer properties in our transgenic mouse models of MYC-induced lymphoma and MYC-induced hepatocellular carcinoma (in our original grant we proposed to look at lymphoma but we also have looked at hepatocellular carcinoma). We have published some of these results **[2011 Progress Report and appended paper 3]**.

Second, we have established an essential function for immune system in the mechanism of sustained tumor regression of MYC-induced lymphoma and BCR-ABL-induced B-cell acute lymphocytic leukemia (B-ALL) upon MYC or BCR-ABL inactivation, respectively *in*

vivo. Our results were published in a high profile paper **[2011 Progress Report and appended paper 4]**.

Third, we have elucidated that the p19Arf gene is pivotal for tumor progression upon MYC activation and sustained tumor regression upon MYC inactivation *in intro* in MYC-induced mouse lymphoma cells and *in vivo* in MYC-induced lymphoma mouse model **[2011 Progress Report and Yetil and Adam *et al*., manuscript in review]**.

In our grant, we proposed to use NIA assays for interrogating the mechanism of clinical response to imatinib *in vivo* in transgenic mouse models. We made a strategic decision that it was important to focus our NIA studies on a clinical trial of MDS with the therapeutic agent ON01910.Na, a PLK1 inhibitor. This was a unique opportunity that although not part of our original proposal, was highly consistent with the overall objectives of our grant to develop NIA for the interrogation of drug activity in human patients. In this manner, we were able to translate our results into humans well ahead of schedule of our grant. Therefore, we chose to focus on these studies rather than focus on the use of our mouse models. We believed this was the correct decision since we felt going into humans with our work was the highest priority.

In our grant, we proposed to use AutoChIP assays for interrogating the mechanism of clinical response to atorvastatin and imatinib *in vivo* in transgenic mouse models. After we built an independent microfluidics system in the Felsher laboratory, tested it, and after we compared AutoChIP to conventional "Benchtop-ChIP", optimized the AutoChIP protocol regarding sensitivity and specificity, we realized that to better understand the molecular mechanism of targeted therapeutics, we should run whole-genome mapping of protein-DNA interaction with ChIP-sequencing. However, current methods for whole-genome mapping of protein-DNA interactions, performed by combining chromatin immunoprecipitation with next-generation sequencing (ChIP-seq), require large amounts of starting materials, which prevent their application to rare cell types. Therefore, we initiated optimization to combine the highly sensitive AutoChIP assay with Illumina and Helicos, next-generation sequencing in order to perform genome-wide location analysis (AutoChIP-seq) for transcription factors such as MYC and/or epigenetic mapping of histone modifications in very small cell numbers (as low as 2,000 cells) **[2011 Progress Report]**.

We used antibodies against MYC and H3K4me3, a well-known histone modification to activate gene transcriptions, to immunoprecipitate chromatin-protein complex in the mouse lymphoma cells from Tet-regulated conditional mouse model of MYC-induced lymphoma. After AutoChIP and prior to sequencing library construction, we performed qPCR on the AutoChIP samples to check for enrichment at a MYC target gene, Odc1. As shown in **Figure 5**, both MYC and H3K4me3 AutoChIP samples show enrichment in the transcription factor-binding site, E-box region of Odc1 over an upstream control region. Enrichment is very high in H3K4me3, as expected from a well-characterized antibody. The absolute signal for Odc1 E-box in the MYC AutoChIP samples is relatively lower, but still enriched compared to both the genomic loci negative control Odc1 Upstream, and compared to the IP background control FLAG. The AutoChIP appears to be quite clean, as FLAG pull-down, representing noise, is undetectable by qPCR. After validating enrichment, we constructed the sequencing libraries on these samples and did ChIP-sequencing on an Illumina platform.

Table 1 summarizes the sequencing statistics of this experiment, which was sequenced on an Illumina HiSeq machine using version 3 chemistry, generating single-ended 50 bp reads. We found that 911 gene-associated peaks (i.e. those peaks within 1.5 kbp of the TSS of a gene) were called in the H3K4me3 dataset, using a FDR cut-off of 0.01. We then cross-referenced these genes to the MYC Target Gene Database [4] to find overlaps, and we identified 29 genes as MYC target genes that also associated with H3K4me3, a mark of open chromatin in areas of active gene transcription **[Table 1]**. The database of target genes is curated from literature, and organisms and cell types listed in the **Table 1** are based on the original experiment in which the MYC binding was identified. The cell line used for this AutoChIP-seq is a lymphoma cell line that models human Burkitt's lymphoma. Thus, it is not surprising that most of the genes identified were originally identified in Burkitt's lymphoma cells, indicating that a similar set of MYC target genes are being actively transcribed in the mouse lymphoma model and hence also bear H3K4me3 marks.

After we optimized AutoChIP-seq protocol for H3K4me3, we are currently optimizing conditions for MYC. In addition, we have generated chromatins from atorvastatin-treated and untreated human lymphoma cells. Once we finish optimization of MYC AutoChIP-seq, we will perform AutoChIP-seq with these chromatin samples to profile changes of MYC binding genes upon atorvastatin treatment.

We are currently expanding application of the AutoChIP instrument in our lab. We have optimized AutoChIP-seq, which exceeds the original goals of our grant. We are now examining the DNA binding activity by MYC *in vivo* upon atorvastatin and imatinib treatments in transgenic mouse models.

Specific Aim 3: To use NIA and AutoChIP assays for defining proteomic signatures of clinical response in human patients with lymphoma to atorvastatin and with chronic myelogenous leukemia to imatinib.
In our grant, we proposed to identify proteomic biomarkers of clinical response in human patients to targeted therapeutics.

Over the last three years, we have collected and banked 110 fine needle aspiration (FNA) samples from 24 lymphoma patients before statin treatment and at serial time-points after statin treatment. Up to date, we have analyzed 24 FNA specimens by flow cytometry, and we have run NIA assays for five different proteins in 30 FNA specimens. We are in the process of analyzing our data from these flow cytometry and NIA assays and correlating our data with patients' clinical outcomes, in order to define biomarkers of clinical response in patients with lymphoma to atorvastatin. We will perform flow cytometry and NIA assays with more FNA samples. Our findings are being prepared for a manuscript.

Since the first year of this grant funding, we have extended our NIA detection tool to study the possible mechanism of and to identify possible response biomarkers for other targeted therapeutics (ON01910.Na, a PLK1 inhibitor for MDS). Our work goes beyond the aims we proposed in our grant proposal and has led us to great findings. Along with our *in vitro* study of ON01910.Na **[2010 Progress Report, Figure 3 and Figure 4]**, in the year 2 funding period, we started to optimize NIA conditions for sorted CD34+ bone marrow (BM) cells from human patients and initiated to analyze the changes of phosphorylation of some signaling proteins upon ON01910.Na treatments in BM samples from MDS patients in Dr. Peter Greenberg's Phase II clinical trial at Stanford

Hospital **[2011 Progress Report]**. In the year 3 funding period, we profiled the phosphorylation changes with NIA for sorted CD34+ bone marrow cells from MDS patients pre- and post-treatment of ON01910.Na. PI3K/AKT and MAPK/Erk/MEK signaling pathways are important to both pathogenesis and progression of many types of cancers including MDS and AML [5-7]. In AKT family, AKT2 is critical for metabolic signaling, protection against tumor cell apoptosis, and cancer cell invasion [8]. First, we compared percentages of pAKT2, pAKT2-isoform 3, pMEK1, and pCDC2 in CD34+ BM cells between MDS patients and normal BM donors. As shown in **Figure 6** and **Table 2**, we could not find specific distribution patterns in basal levels of phosphorylation of these proteins among MDS patients and normal BM donors. However, NIA analysis revealed a correlation between phosphorylation changes of these proteins in CD34+ BM cells from MDS patients and their clinical responses upon ON01910.Na treatment **[Figure 7 and Table 3]**. These data suggest that ON01910.Na might inhibit MDS progression through inactivation of both PI3K and MAPK pathways *in vivo* in MDS patients. Moreover, our data also suggest that measurement of specific phosphor-isoforms and percentage changes of the signaling protein phosphorylation with NIA may be developed as biomarkers for clinical outcome. Our work has resulted in one published paper **[appended paper 5]** and one manuscript in preparation **[Xu *et al*.]**.

The CD34+ bone marrow cells we have analyzed with NIA are all collected and isolated on the same day at Stanford Hospital. In order to open the possibility of analyzing BM specimens collected from other clinical centers, we need to develop a suitable specimen processing protocol to enable shipment of BM specimens from other institutes to Stanford for NIA analysis.

We purified CD34+ cells from patient BM samples under various conditions **[Figure 8]**, did NIA analysis, and compared NIA results generated from different processing conditions. We found that bone marrow samples can be stored overnight at 4°C prior to CD34+ cell isolation for NIA analysis **[Figure 9]**. This enables other clinical centers ship BM samples with FedEx to us for further CD34+ cell isolation and NIA analysis. Because of the progresses we have made, Onconova Therapeutics, Inc. has started Phase III worldwide multi-center clinical trial for ON01910.Na on MDS patients.

To further define the molecular mechanism of ON01910.Na activity in MDS, we will measure changes in additional oncoproteins and cell cycling proteins in MDS patients from this clinical trial. We are in the process of optimizing NIA conditions for these additional proteins in patient samples. We will develop proteomic biomarkers to confirm the mechanism of biologic response and to predict clinical response of MDS to ON01910.Na in a larger cohort of patients.

Our work in MDS has been highly productive, yielded exciting biomarkers, helped identify novel therapy, validated a new approach for nanoscale proteomics and will result in multiple publications. We believe these studies have been highly interesting and useful. We believe these methods will also be useful for the examination of human patients with chronic myelogenous leukemia to imatinib, which we continue to pursue.

We have collected and banked all our human patient specimens pre- and post-treatment. We are planning to run AutoChIP-seq with these samples in the future in order to profile activation changes of gene expression upon targeted therapeutics.

KEY RESEARCH ACCOMPLISHMENTS:

- We have developed NIA assays and optimized NIA conditions for proteins including oncoproteins, signaling proteins, cell cycling, and cell senescence proteins so that we can have good readouts to directly evaluate the efficacy of a therapy and to interrogate the molecular mechanism of a therapy.
- We have built an AutoChIP system in the Felsher laboratory, which goes beyond the proposed goals. We also tested and optimized the AutoChIP protocol, and applied the AutoChIP technology to mouse lymphoma cells to monitor c-MYC's interaction with its target gene promoters. This work has been included in a paper that is in press (Wu *et al*., *Lab on a Chip*, 2012).
- We have also developed and optimized the protocol for AutoChIP-seq. We will be able to use AutoChIP-seq with the patient specimens we have collected and banked to understand the molecular mechanism of targeted therapeutics by profiling global changes of gene activation and inactivation upon the targeted therapeutics.
- We have found that the decreased expression and phosphorylation of proteins in MEK/Erk and Stat3/5 signaling pathways are the landmarks of efficacy of targeted therapies for hematopoietic cancers. Our findings have resulted in one publication (A. C. Fan *et al. Nature Medicine*, 2009).
- We have identified the inhibition of MYC activation as a possible mechanism for statin's anti-cancer properties in our transgenic mouse models of MYC-induced lymphoma and MYC-induced hepatocellular carcinoma (in our original grant we proposed to look at lymphoma but we have also looked at hepatocellular carcinoma). Our results have been published (Cao *et al*., *Cancer Research*, 2010).
- We have found that MYC protein levels are reduced in response to imatinib treatment of BCR-ABL-induced leukemia cells *in vitro*. Our results suggest an unanticipated mechanism of action for this therapeutic agent.
- We have established an essential function for immune system in the mechanism of sustained tumor regression of MYC-induced lymphoma and BCR-ABL-induced B-cell acute lymphocytic leukemia (B-ALL) upon MYC or BCR-ABL inactivation, respectively *in vivo*. Our results have been published in a high profile paper (Rakra *et al*., *Cancer Cell*, 2010).
- We have elucidated that p19Arf gene is pivotal for tumor progression upon MYC activation and sustained tumor regression upon MYC inactivation *in intro* in MYC-induced mouse lymphoma cells and *in vivo* in MYC-induced lymphoma mouse model. The results from this work have been included in a manuscript that has been reviewed and is now being revised for resubmission (Yetil and Adam *et al*., 2012).
- We have collected FNA specimens from the patients recruited in our statin clinical study before and after treatments. We have run the flow cytometry and NIA analyses on some of these FNA samples. After we run and finish the analyses with more FNA specimens, we will wrap up our findings as a paper.
- We have been provided with a unique ability to utilize NIA to identify the mechanism of action of a PLK1 inhibitor, ON01910.Na, in clinical specimens from patients with myelodysplastic syndrome (MDS). This exciting work goes beyond the aims we proposed in the grant and it has generated one published paper (Seetharam *et al*., *Leukemia Research*, 2012) and one manuscript in preparation (Xu et al., 2012).

- We have developed a feasible specimen processing protocol for NIA analysis, which has facilitated Onconova Therapeutics, Inc. to start the Phase III worldwide multi-central clinical trial of ON01910.Na on MDS patients.

REPORTABLE OUTCOMES:

1. Xu, L. *et al. In preparation* (2012). Nanoscale immunoassay reveals the biologic mechanism of clinical activity of rigosertib (ON001910.Na) on myelodysplastic syndrome and predicts its clinical outcomes.
2. Yetil and Adam *et al. In preparation* (2012). Loss of p19ARF tumor suppressor facilitates tumor recurrence upon MYC inactivation by abrogating cellular senescence.
3. Wu, A. *et al. Lab on a Chip*. In press (2012). High throughout automated chromatin immuoprecipitation as a platform for drug screening and antibody validation.
4. Seetharam, M. *et al. Leukemia Research*. 36(1) 98 (2012). Treatment of higher risk myelodysplastic syndrome patients unresponsive to hypomethylating agents with ON 01910.Na.
5. Z. Cao *et al*., *Cancer Res.* 71(6) 2286 (2011). MYC phosphorylation, activation, and tumorigenic potential in hepatocellular carcinoma are required by HMG-CoA reductase.
6. K. Rakhra *et al*., *Cancer Cell* 18 485 (2010). CD4+ T cells contribute to the remodeling of the microenvironment required for sustained tumor regression upon oncogene inactivation.
7. A. C. Fan *et al., Nature Medicine.* 15(5) 566 (2009). Nanofluidic proteomic assay for serial analysis of oncoprotein activation in clinical specimens.
8. A. C. Fan *et al., ASCO Annual Meeting* (2012). Use of nano-immuno assay to generate rapid, quantitative nanoscale proteomic profiling of the hypoxia pathway in renal cell carcinoma clinical specimens.
9. A. C. Fan *et al., ASCO Annual Meeting* (2012). Nano-immuno assay generates rapid, quantitative nano-scale proteomic profiling of the hypoxia pathway in renal cell carcinoma clinical specimens.
10. A. C. Fan *et al., AACR Annual Meeting* (2012). Nano-scale phospho-proteomic analysis to define diagnostic signatures and biomarkers of therapeutic activity in cancer.
11. D. W. Felsher, *Frontiers in Cancer Research and Therapy, Stockholm, Sweden* (2012). Modeling and predicting oncogene addiction.
12. D. W. Felsher, *Geron Corporation* (2012). Targeting MYC for the treatment of cancer.
13. D. W. Felsher, *St. Jude Children's Research Hospital, Memphis, TN* (2012). Modeling and predicting oncogene addiction.
14. A. C. Fan *et al., ASH Annual Meeting* (2011). A novel nano-immunoassay (NIA) reveals inhibition of PI3K and MAPK pathways in CD34+ bone marrow cells of patients with myelodysplastic syndrome (MDS) treated with the multi-kinase inhibitor: ON01910.Na (rigosertib).
15. A. C. Fan, *Nanoproteomics Meeting, NIH/NCI/Center for Cancer Research.* (2011). Developing novel biomarkers and therapeutics for cancer.
16. A. C. Fan, *Translational Medicine Program, Stanford University School of Medicine Research Seminar* (2011). Development of nano-immuno assay (NIA) to define diagnostic signatures and biomarkers of therapeutic activity in cancer.
17. A. C. Fan, *Mennonite Hospital. Grand Rounds* (2011). Developing novel diagnostics and therapeutics for lymphoma.

18. L. Xu *et al., ProteinSimple Annual User Meeting* (2011). A novel nano-immunoassay (NIA) reveals inhibition of PI3K and MAPK pathways in CD34+ bone marrow cells of patients with myelodysplastic syndrome (MDS) treated with the multi-kinase inhibitor ON01910.Na (rigosertib).
19. L. Xu *et al., Stanford Oncology and Hematology Research Retreat* (2011). A novel nano-immunoassay (NIA) reveals inhibition of PI3K and MAPK pathways in CD34+ bone marrow cells of patients with myelodysplastic syndrome (MDS) treated with the multi-kinase inhibitor ON01910.Na (rigosertib).
20. D. W. Felsher, *Systems Biology Conference, Stanford University* (2011). Modeling oncogene addiction.
21. D. W. Felsher, *Microbiology and Biochemistry Seminar Series, Southern Illinois University* (2011). Oncogene addiction inside and out.
22. D. W. Felsher, *CCRTP Conference, Stanford* (2011). Cancer therapy and biomarkers.
23. D. W. Felsher, *16th World Congress on Advances in Oncology* (2011). Reversing tumorigenesis through targeted oncogene inactivation.
24. D. W. Felsher, *MYC and the Pathway to Cancer. Cold Spring Harbor* (2011). MYC as a therapeutic target.
25. D. W. Felsher, *Cancer Conference* (2011). Modeling oncogene addiction.
26. D. W. Felsher, *Dormancy Workshop* (2011). Modeling Tumor Dormancy.
27. D. W. Felsher, *Molecular Biology, Microbiology and Biochemistry Seminar Series* (2011). Oncogene addiction inside and out.
28. D. W. Felsher, *Systems Biology Conference* (2011). Modeling oncogene addiction.
29. D. W. Felsher, *Amgen* (2011). Modeling oncogene addiction.
30. D. W. Felsher, *16th International AEK Cancer Congress* (2011). Modeling and predicting oncogene addiction.
31. D. W. Felsher, *Genentech* (2011). Nanoscale analysis of oncogene addiction.
32. D. W. Felsher*, Pulmonary Medicine and Biology Grand Rounds, Stanford University School of Medicine* (2011). Multi-scale modeling to predict therapeutic response in lung cancer.
33. D. W. Felsher*, SuperGen, Inc.* (2011). Targeting the MYC pathway to reverse cancer.
34. L. Xu *et al., Stanford Oncology and Hematology Research Retreat* (2010). Nanoscale proteomic analysis of protein phosphorylation changes in myelodysplastic syndrome (MDS) upon ON01910.Na treatment.
35. A. C. Fan *et al.*, *ASCO Annual Meeting.* (2010). ERK and MEK isoforms as novel biomarkers for solid tumors.
36. A. C. Fan *et al.*, *AACR Molecular Diagnostics Meeting* (2010). Nanoscale approaches to define biologic signatures and measure proteomic response to targeted therapies in hematologic and solid tumors.
37. A. C. Fan *et al.*, *AACR Annual Meeting* (2010). Nanoscale analysis of biologic response to targeted therapeutics.
38. M. Seetharam *et al*. *ASH Annual Meeting* (2010). Treatment of high risk meylodysplastic syndrome patients unresponsive to hypomethylating agents with ON01910.Na.
39. D. W. Felsher, *Agilent*. (2010). Modeling oncogene targeted therapeutics.
40. D. W. Felsher, *Cold Spring Harbor Laboratory Meeting, Mechanisms & Models of Cancer* (2010). Modeling of oncogene addiction in transgenic mouse models.
41. D. W. Felsher, *ADAPT Biomarker Meeting* (2010). Nanoscale proteomics in cancer.

42. D. W. Felsher, *Memorial Sloan Kettering Cancer Center* (2010). Oncogene addiction: inside and out.
43. D. W. Felsher, *Columbia University* (2010). Modeling oncogene addiction inside out.
44. D. W. Felsher, *Stanford Cancer Center CCRTP Course* (2010). Molecular therapies that target oncogenes.
45. D. W. Felsher, *Bio-X/Novartis Meeting* (2010). Modeling oncogene addiction for the development of new treatments for cancer.
46. A. C. Fan *et al., AACR 100th Annual Meeting* (2009). Nanoscale quantification of phosphorylated and unphosphorylated ERK and MEK isoforms differentiates tumor and non-tumor clinical specimens.
47. L. Xu *et al., Stanford Oncology and Hematology Research Retreat* (2009). Nanoscale proteomic analysis of signaling protein changes in myelodysplastic syndrome (MDS).
48. D. W. Felsher, *Keystone Symposia on Molecular and Cellular Biology* (2009). Targeted cancer therapies.
49. D. W. Felsher, *AACR 100th Annual Meeting* (2009). Tumor dormancy and oncogene addiction
50. D. W. Felsher, *Annual Conference of the Chinese-American Bio/Pharmaceutical Society (CABS)* (2009). Reversing cancer through targeted oncogene inactivation.
51. D. W. Felsher, *First Annual Center for Cancer Nanotechnology Excellence Symposium* (2009). Mouse models of human cancers.
52. D. W. Felsher, *Molecular Therapeutics Research Association Meeting* (2009). Modeling oncogene addiction.
53. D. W. Felsher, *The EMBO Meeting* (2009). The expanding role of Tet-controlled expression models to understand oncogene addiction and malignant progression.
54. D. W. Felsher, *Gordon Research Conference: Stem Cells and Cancer* (2009). MYC, self-renewal and senescence.
55. D. W. Felsher, *ADAPT Congress* (2009). Protein biomarkers.
56. D. W. Felsher, *The Third Comprehensive Cancer Research Training Program at Stanford University (CCRTP-3)* (2009). Oncogene addiction: Cell regulation and cancer.
57. D. W. Felsher, *Cancer Models and Mechanisms Symposium* (2009). Modeling oncogene addiction: Reversing cancer from inside and out.
58. D. W. Felsher, *Lurie Cancer Center of Northwestern University* (2009). Molecular modeling oncogene addiction.

CONCLUSIONS:

We have achieved the goals of our proposed Specific Aims in our grant. Over the three-year funding period, we have made excellent progress achieving these goals. Indeed, we have exceeded our objectives as follows: 1). We have identified the molecular mechanism of a novel PLK1 inhibitor, ON01910.Na, for the treatment of MDS. 2). We have identified biomarkers that appear to predict the clinical activity of this drug for MDS. 3). We have built an independent AutoChIP instrument in the Felsher laboratory, which enables us to unlimited access to this technology. 4). We have optimized conditions for AutoChIP-seq that will enable us to understand the molecular mechanism of targeted therapeutics by profiling global changes of gene activation and inactivation. Finally, during the three years of funding period, we have generated five published papers, two

manuscripts in preparation, and we have also presented the DoD supported work in over 50 oral and poster presentations.

REFERENCES:

1. K. Strebhardt and A. Ullrich, *Nat Rev Cancer.* 6(4) 321 (2006). Targeting polo-like kinase 1 for cancer therapy.
2. P. L. Greenberg *et al., Blood.* 88(11) 4275 (2009). Altered oncoprotein expression and apoptosis in myelodysplastic syndrome marrow cells.
3. A. Prasad *et al. Oncogene.* 28 1518 (2009). Styryl sulfonyl compounds inhibit translation of cyclin D1 in mantle cell lymphoma cells.
4. K. Zeller *et al*., *Genome Biology* 4(10) R69 (2003). An integrated database of genes responsive to the Myc oncogenic transcription factor: identification of direct genomic targets.
5. S. Park *et al*., *Haematologica*. 95 819 (2010). Role of the PI3K/AKT and mTOR signaling pathways in acute myeloid leukemia.
6. K. Kawauchi *et al*., *Anticancer Agents Med Chem*. 9 550 (2009). The PI3K/Akt pathway as a target in the treatment of hematologic malignancies.
7. M.Y. Follo *et al*., *Cancer Res.* 67 4287 (2007). The Akt/mammalian target of rapamycin signal transduction pathway is activated in high-risk myelodysplastic syndromes and influences cell survival and proliferation.
8. P. Perego *et al*., *Biochem Pharmacol* 80 1459 (2010). Modulation of cell sensitivity to antitumor agents by targeting survival pathways.

APPENDICES:

SUPPORTING DATA:

LIST OF PERSONNEL RECEIVING PAY FROM THE RESEARCH EFFORT:

Dean Felsher
Jason Gotlib
David Bellovin
Tahera Zabuawala
Lowen Lee
Judy Rabano
Liwen Xu
Qiwei Yang
Alice Fan
Kavya Rakhra
Etelka Gabriel
Albert Ho
John Renschler
Yasodha Natkunam
Angela Wu

TECHNICAL REPORTS

nature medicine

Nanofluidic proteomic assay for serial analysis of oncoprotein activation in clinical specimens

Alice C Fan[1], Debabrita Deb-Basu[2], Mathias W Orban[1], Jason R Gotlib[3], Yasodha Natkunam[4], Roger O'Neill[2], Rose-Ann Padua[5], Liwen Xu[1], Daryl Taketa[2], Amy E Shirer[1], Shelly Beer[1], Ada X Yee[1], David W Voehringer[2] & Dean W Felsher[1]

Current methods of protein detection are insensitive to detecting subtle changes in oncoprotein activation that underlie key cancer signaling processes. The requirement for large numbers of cells precludes serial tumor sampling for assessing a response to therapeutics. Therefore, we have developed a nanofluidic proteomic immunoassay (NIA) to quantify total and low-abundance protein isoforms in nanoliter volumes. Our method can quantify amounts of MYC oncoprotein and B cell lymphoma protein-2 (BCL2) in Burkitt's and follicular lymphoma; identify changes in activation of extracellular signal–related kinases-1 (ERK1) and ERK2, mitogen-activated kinase-1 (MEK), signal transducer and activator of transcription protein-3 (STAT3) and STAT5, c-Jun N-terminal kinase (JNK) and caspase-3 in imatinib-treated chronic myelogeneous leukemia (CML) cells; measure an unanticipated change in the phosphorylation of an ERK2 isomer in individuals with CML who responded to imatinib; and detect a decrease in STAT3 and STAT5 phosphorylation in individuals with lymphoma who were treated with atorvastatin. Therefore, we have described a new and highly sensitive method for determining oncoprotein expression and phosphorylation in clinical specimens for the development of new therapeutics for cancer.

Cancer is frequently associated with the abnormal expression and phosphorylation of oncogenes[1–4]. Specific hematopoietic tumors are frequently characterized by the discrete activation of specific oncogenes such as *MYC*[5–7], *BCL2*[8,9] and *BCR-ABL* (encoding breakpoint cluster region-Abelson)[10–13]. Targeted inactivation of oncoproteins is emerging as a specific and effective therapy for cancer[14,15]. The best known example of a targeted therapy is imatinib mesylate, a small molecule that inactivates several tyrosine kinases, including the BCR-ABL tyrosine kinase in CML[16–18]. Imatinib treatment results in tumor cell signaling changes *in vitro*, leading to cell death[19,20]. In general, the ability to detect specific oncoproteins and their activation state is likely to be highly useful toward the development of new therapeutics as well as in monitoring the effectiveness of these treatments and in evaluating apparent therapeutic resistance[13,21].

To accurately measure oncoprotein expression and activation in limited clinical specimens, we have developed the NIA detection method, which combines isoelectric protein focusing and antibody detection. Here we show that we can use this new technique to quantify oncoprotein expression and phosphorylation in clinical specimens to precisely measure specific changes in phosphoisomers of oncoproteins *in vitro* and *in vivo*.

RESULTS

NIA detection of oncoprotein expression in clinical specimens

NIA incorporates isoelectric focusing of proteins followed by antibody detection of specific epitopes with chemiluminescence[22]. The chemiluminescent signal is rendered as a chemiluminescence isoelectropherogram (trace) of relative luminescence units (RLU) on the *y* axis versus isoelectric point (pI) on the *x* axis (**Fig. 1a**). As little as 2 pg of recombinant MYC protein could be detected in 4 nl of sample per capillary (final capillary concentration 0.004–0.12 pg nl^{-1}) at the expected pI of 5.6 with a linear response (**Fig. 1b**, $R^2 = 0.9984$). Concentrations of BCL2 could be detected over up to a three-log dynamic range at pI 6.7 (**Fig. 1c**, $R^2 = 0.9647$). Therefore, NIA is highly quantitative and sensitive over a large dynamic range.

Next, we assessed the ability to detect oncoproteins in tumor cell lines both *in vitro* and *in vivo*. Previously, we described the generation of a conditional transgenic lymphoma model that uses the Tet-off system to regulate oncoprotein expression[23–25]. Briefly, the Tet-off system was used to conditionally regulate the expression of a human *MYC* or *BCL2* transgene in lymphocytes. In the absence of doxycycline, the transgene is expressed, and in the presence of doxycycline, the transgene is turned off. In our tumor-derived cell lines, MYC and BCL2 were readily detected by NIA, comparable to western blot analysis (**Supplementary Fig. 1** online). Each oncoprotein measurement from these tumor lysates showed a characteristic peak profile defined by how post-translational modifications influence its isoelectric point. The profile obtained from mouse tumor lines was

[1]Stanford University, School of Medicine, Division of Oncology, Departments of Medicine and Pathology, Stanford, California, USA. [2]Cell Biosciences, Palo Alto, California, USA. [3]Stanford University, School of Medicine, Division of Hematology, Department of Medicine, Stanford Cancer Center, Stanford, California, USA. [4]Stanford University, School of Medicine, Department of Pathology, Stanford, California, USA. [5]Institut Universitaire d'Hematologie, Institut National de la Santé et de la Recherche Médicale U718, Hopital Saint Louis, Paris, France. Correspondence should be addressed to D.W.F. (dfelsher@stanford.edu).

Received 16 June 2008; accepted 12 November 2008; published online 12 April 2009; doi:10.1038/nm.1903

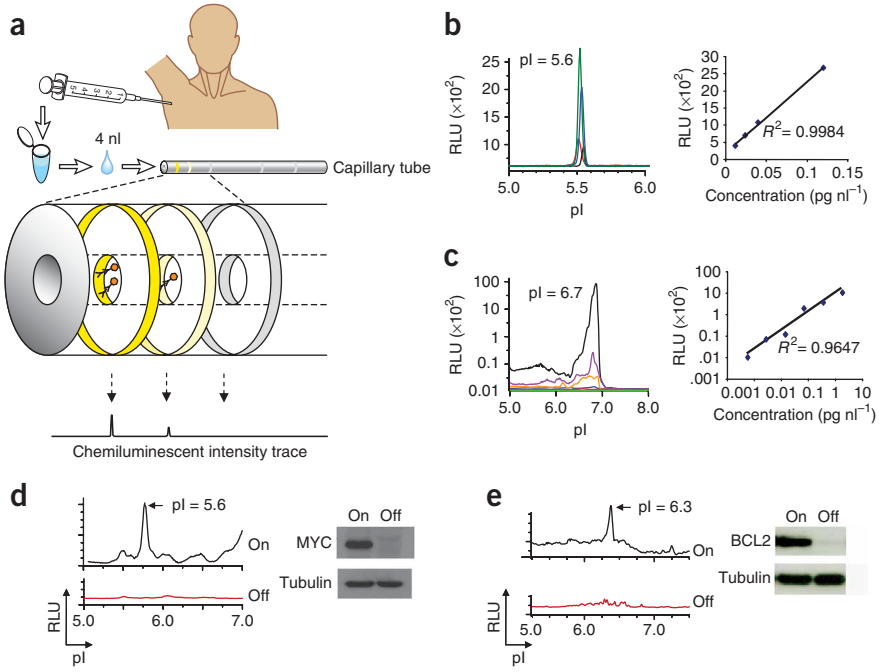

Figure 1 NIA for the quantitative analysis of oncoproteins. (**a**) Schematic of the use of NIA for the measurement of oncoproteins from clinical specimens. NIA can be used to measure oncoprotein expression and phosphorylation in clinical specimens, incorporating charge-based separation coupled to antibody detection. (**b**,**c**) Detection of recombinant MYC (**b**) or BCL2 (**c**) oncoproteins *in vitro* by NIA. Left, representative NIA traces of MYC (black, 0.004 pg nl^{-1}; red, 0.012 pg nl^{-1}; blue, 0.04 pg nl^{-1}; green, 0.12 pg nl^{-1}) or BCL2 (green, 0.0019 pg nl^{-1}; red, 0.0075 pg nl^{-1}; blue,0.03 pg nl^{-1}; orange, 0.12 pg nl^{-1}; purple, 0.47 pg nl^{-1}; black, 1.8 pg nl^{-1}). Right, the trace data are represented as the peak area versus protein concentration. The calculated correlation coefficients are shown. (**d**,**e**) Detection of MYC (**d**) or BCL2 (**e**) oncoproteins in transgenic mouse tumors obtained from serial FNAs by NIA. Serial FNAs were obtained from subcutaneous tumors in mice before (on) and after (off) the suppression of expression of MYC or BCL2. Left, representative NIA traces. Right, corresponding western blot analysis.

different from the recombinant BCL2 described above because NIA is exquisitely sensitive to the cationic charge associated with the histidine tag of the recombinant protein. Our results elaborate how NIA can distinguish and measure oncoprotein expression from tumor cell lines.

To evaluate whether we could quantitatively detect oncoprotein expression *in vivo*, we inoculated conditional mouse tumor-derived cell lines into syngeneic mice. Examination of serial tumor samples by fine needle aspiration (FNA) confirmed that both MYC and BCL2 expression could be readily detected and quantified *in vivo* by NIA with results comparable to western blot analysis (**Fig. 1d**,**e**). To determine oncoprotein expression in human tumors, we measured MYC and BCL2 abundance in four lymphomas and two benign lymph nodes. As expected, we detected increased MYC protein abundance in Burkitt's lymphoma and increased BCL2 protein abundance in follicular lymphoma compared with benign nodes (**Fig. 2a**). Thus, NIA can reproducibly detect changes in oncoprotein expression even from limited clinical biopsy specimens from mouse or human tumors.

Our results suggested that we may be able to precisely quantify the amounts of oncoproteins in clinical specimens. We analyzed a set of 27 human specimens that included Burkitt's lymphoma, follicular lymphoma and benign lymph nodes, as well as normal peripheral blood mononuclear cells (set 1; **Fig. 2b**). In this set, Burkitt's lymphoma samples expressed MYC at a level higher than all of the other sample groups (Mann-Whitney test, $P < 0.0001$). All of the Burkitt's lymphoma specimens had a MYC expression level higher than 0.2 RLU, compared with 11% of the follicular lymphoma specimens.

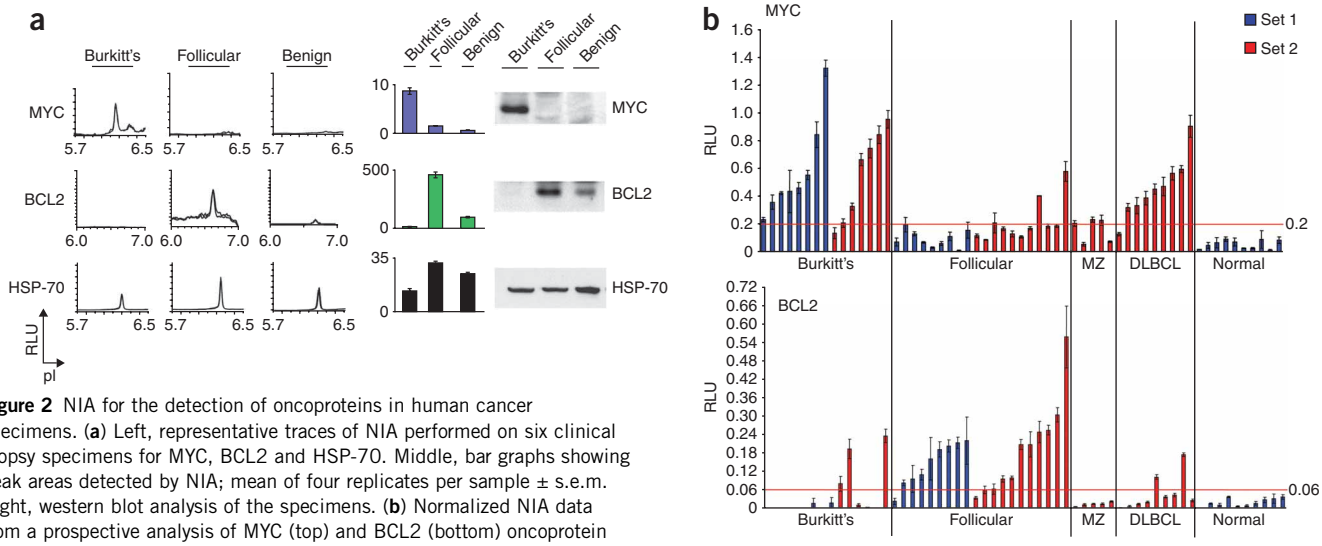

Figure 2 NIA for the detection of oncoproteins in human cancer specimens. (**a**) Left, representative traces of NIA performed on six clinical biopsy specimens for MYC, BCL2 and HSP-70. Middle, bar graphs showing peak areas detected by NIA; mean of four replicates per sample ± s.e.m. Right, western blot analysis of the specimens. (**b**) Normalized NIA data from a prospective analysis of MYC (top) and BCL2 (bottom) oncoprotein expression in two sets of clinical specimens. Set 1 included eight Burkitt's lymphoma, nine follicular lymphoma and ten normal samples (the first four normal specimens were benign lymph nodes and the last six normal specimens were control peripheral mononuclear cell samples). Set 2 included seven Burkitt's lymphoma, eleven follicular lymphoma, five marginal zone (MZ) lymphoma and nine DLBCL specimens. Data are represented as the normalized peak areas detected by NIA; mean of four replicates per sample ± s.e.m.

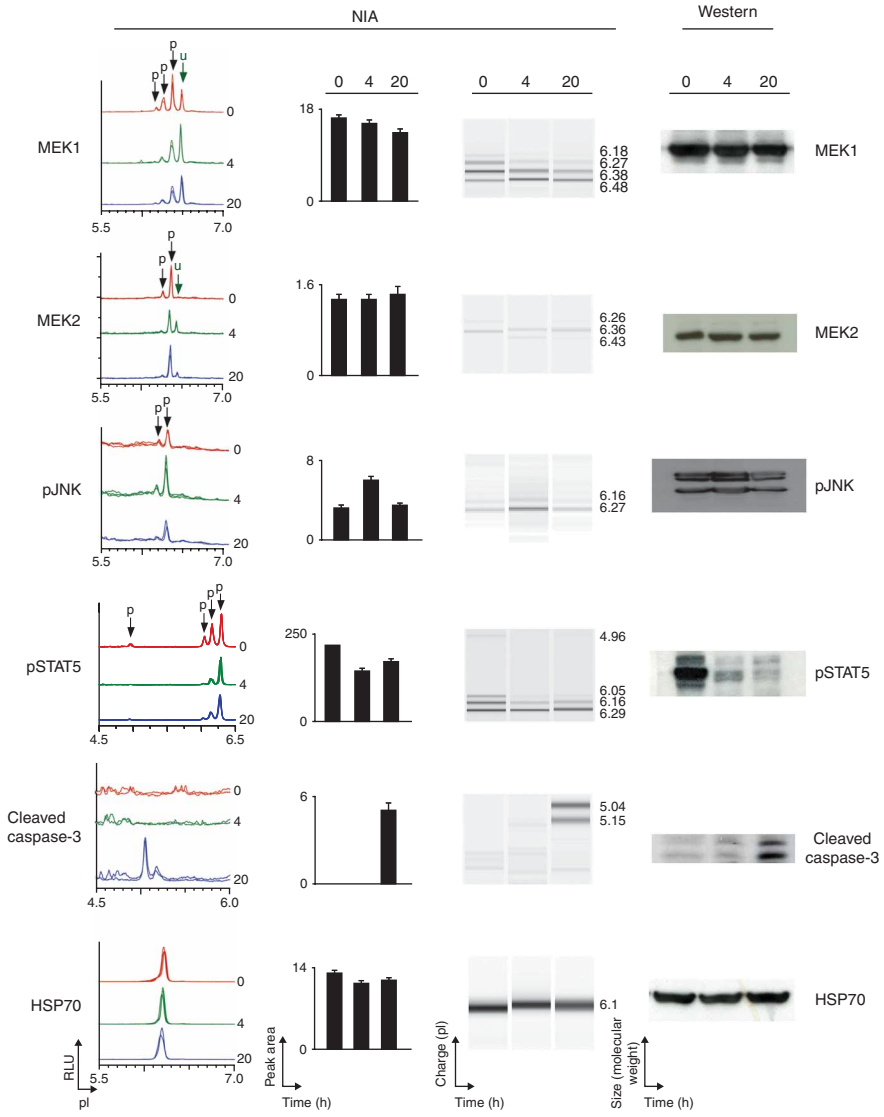

Figure 3 NIA detection of changes in oncoprotein activation in CML cells treated with imatinib. NIA was used to quantify proteomic changes in the K562 cell line treated with imatinib *in vitro* for 0, 4 and 20 h. MEK1, MEK2, phospho-JNK (pJNK), pSTAT5 and activated caspase-3 were detected by NIA. From left to right: representative traces for the protein of interest, bar graph of NIA quantification of each protein, NIA pseudoblot representation and western blot data. Peaks on the traces that represent phosphorylated isoforms are indicated with black arrows. All measurements were performed in six replicates, and bar graph data are represented as the mean peak area ± s.e.m.

Follicular lymphoma samples expressed significantly more BCL2 than all other sample groups (Mann-Whitney test, $P < 0.0001$); 89% of the individuals with follicular lymphoma had a BCL2 level higher than 0.06 RLU, compared with none of the individuals with Burkitt's lymphoma. BCL2 was detectable and quantifiable even in normal specimens (**Fig. 2a**,**b**). NIA was quantitative enough to distinguish statistically significant differences in oncoprotein expression between lymphomas.

To validate our results, we next quantified MYC and BCL2 abundance in a new series of clinical specimens including seven Burkitt's lymphoma, eleven follicular lymphoma, nine diffuse large B cell lymphoma (DLBCL) and five marginal zone lymphoma specimens (set 2; **Fig. 2b**). We confirmed that the MYC threshold of 0.2 RLU and the BCL2 threshold of 0.06 RLU were statistically significant for distinguishing Burkitt's from follicular lymphoma (Fisher's exact test, two-tailed: $P = 0.0498$ and $P = 0.0474$, respectively). We observed that two of nine DLBCL tumors overexpressed BCL2, and many tumors expressed high amounts of MYC (**Fig. 2a**,**b**). In contrast, marginal zone lymphomas expressed a low mean level of 0.18 RLU MYC (**Fig. 2a**,**b**). Hence, we found that in 44 of 49 tumor specimens the MYC and BCL2 expression differed when compared with normal controls.

NIA of oncoprotein phosphorylation in clinical specimens

A key feature of NIA is that it can be used to identify phosphorylated isoforms of a protein[22]. We detected ERK and distinct patterns of phosphoisomers in the normal and lymphoma specimens (**Supplementary Fig. 2a** online). Next, we identified mitogen-activated protein kinase kinase-1 (MEK1) and MEK2 isomers (**Supplementary Figs. 2b** and **3** online). We performed the experiments in quadruplicate, and they were highly reproducible. We could detect as little as a 10% difference in abundance of specific phosphorylated isoforms of either ERK or AKT across the panel of specimens. Our results show that NIA is highly sensitive, reproducible and quantitative.

Next, we evaluated whether we could detect specific protein signaling changes in human tumors in response to targeted therapy. Treatment of the K562 human CML cell line with imatinib *in vitro* resulted in changes in the phosphorylation of STAT3, STAT5, JNK, MEK1 and MEK2 and an expected increase in activated caspase-3 associated with apoptosis (**Fig. 3** and **Supplementary Fig. 4** online). To facilitate a comparison with western blot results, we converted the data into a 'pseudo-blot' representation. In a pseudo-blot, the area under each NIA peak is represented as a band at the corresponding isoelectric point. By visualizing different isoforms we were able to identify that imatinib treatment was associated with a decrease in the expression of a specific ERK2 phosphoisomer (**Supplementary Fig. 5a** online). Thus, NIA seemed to detect a unique signaling change in response to the targeted therapeutic agent, imatinib.

To evaluate whether we could identify changes in protein signaling *in vivo* in clinical specimens, we measured changes in oncoprotein signaling in the tumor cells in the peripheral blood of individuals with CML treated with tyrosine kinase inhibitors. All seven subjects who responded to tyrosine kinase inhibitor therapy showed a 54–100% decrease in a monophosphorylated ERK2 isoform (**Fig. 4a** and **Supplementary Fig. 5b**,**c**), whereas two subjects who were resistant to tyrosine kinase inhibitor therapy did not (**Fig. 4b**,**c** and **Supplementary Table 1** online). Although basal ERK2 expression was not different (**Supplementary Fig. 6** online), the relative fold change in ERK2 phosphorylation was different between subjects with CML who responded to therapy versus those who did not (unpaired

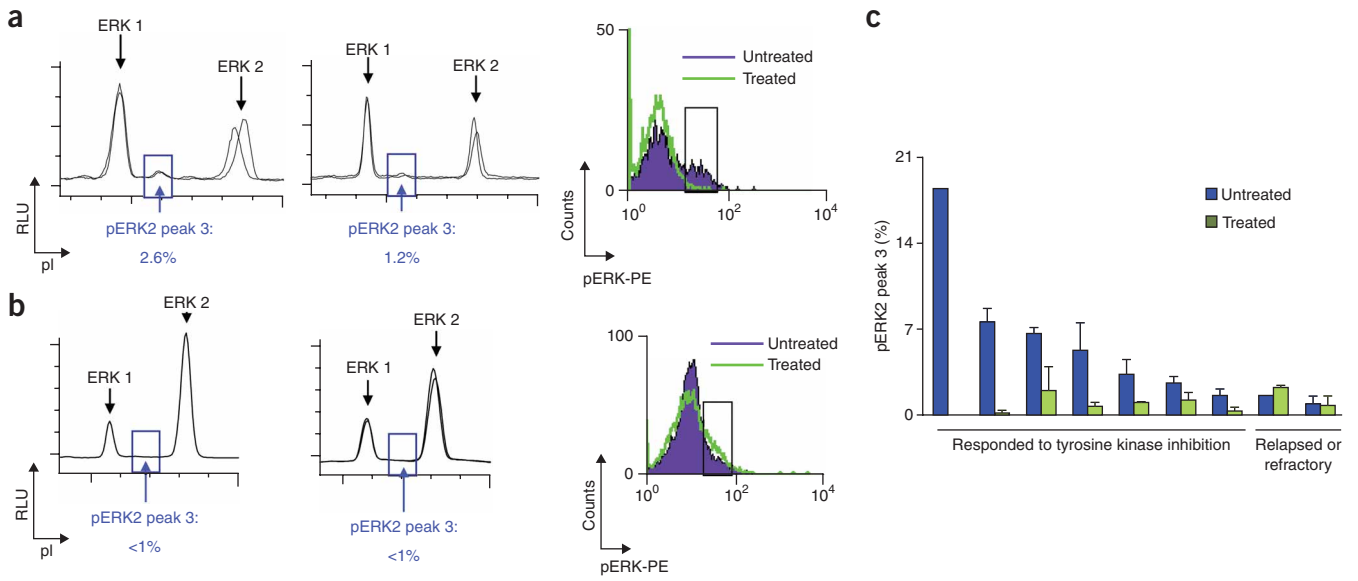

Figure 4 NIA detected changes in pERK in individuals with CML who responded to imatinib treatment. (**a**) Representative NIA traces of total ERK for a subject who responded to treatment. Traces before initiating treatment (left) and during treatment (middle) are shown. The blue box highlights a specific change in the abundance of pERK2 (peak 3). Right, similar results obtained by FACS analysis of clinical specimens. The black box highlights pERK changes detected by FACS. PE, phycoerythrin. (**b**) Representative NIA traces of total ERK for a subject who failed to respond to treatment, analyzed as in **a**. (**c**) Quantification of NIA pERK2 peak 3 analysis of eight subjects before and after initiating treatment. Results are represented as the percentage of pERK2 peak 3 divided by the sum of total phosphorylated and unphosphorylated ERK peaks. Experiments were performed in triplicate.

t test, two-tailed $P = 0.0007$). Thus, NIA may have identified a specific change in ERK phosphorylation that seems to be associated with a clinical response to effective therapy.

Finally, we determined whether NIA could be used to serially monitor the response of a patient's tumor to a potential biologic response modifier *in vivo*. Recently, we described that atorvastatin treatment causes tumor regression associated with specific changes in oncoprotein signaling in a mouse model of lymphoma[26]. We have investigated whether atorvastatin has biological activity in humans with lymphoma. We found that patients treated with atorvastatin showed detectable decreases in phosphorylation of STAT3 and STAT5 after 8 d of treatment (**Fig. 5**). Thus, we found that atorvastatin has unanticipated *in vivo* biologic activity against human lymphoma cells.

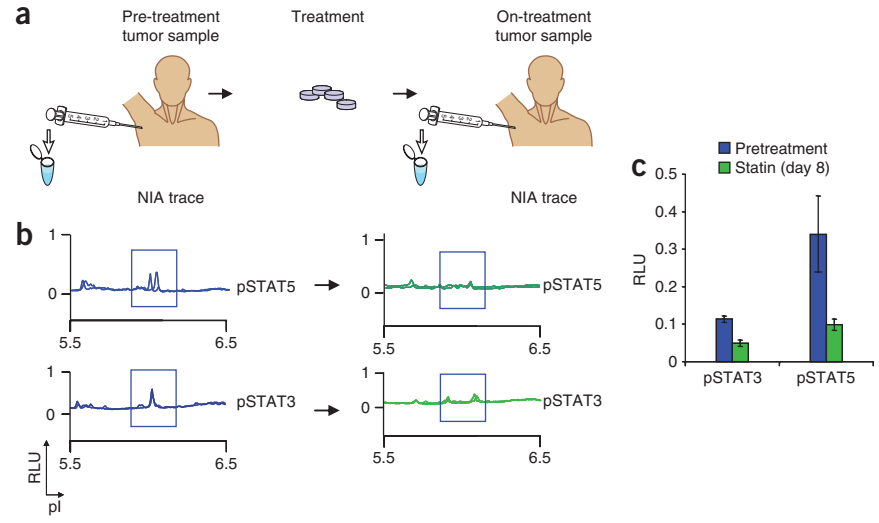

Figure 5 NIA detected decrease in oncoproteins upon treatment with biologic response modifying therapeutic agent. (**a**) Schematic for the use of NIA to assess proteomic changes in clinical tumor specimens. Patients undergo pretreatment tumor sampling at baseline and again after 8 d of treatment with atorvastatin. (**b**) NIA analysis of tumor cells for changes in pSTAT3 and pSTAT5. (**c**) NIA quantification of pSTAT3 and pSTAT5 ± s.e.m. Samples were run in triplicate.

DISCUSSION

We have developed a highly sensitive and reproducible nanoscale technology to measure oncoprotein expression and phosphorylation and to identify the biological response to therapeutics. Our method detected as little as 2 pg of protein in as few as 4 nl of material over a three-log dynamic range. We quantified MYC and BCL2 oncoproteins as well as changes in cancer signaling proteins including ERK, MEK, JNK, STAT3 and STAT5 and apoptotic proteins such as caspase-3. The requirement of only a small amount of material enabled us to analyze serial samples of the same tumor *in vivo*, as we demonstrated in mouse models of lymphoma and in human tumor specimens; oncoprotein phosphorylation decreased in samples obtained from subjects with lymphoma before and after initiating treatment with imatinib or atorvastatin. We have shown that our method may have utility both for preclinical and clinical studies.

Our method enables the analysis of solid tissue specimens such as from tumor biopsies, as we illustrate through the analysis of lymphoma specimens. Thus, we could quantify differences in MYC and BCL2 oncoprotein expression in normal lymph tissue and different non-Hodgkin's lymphoma subtypes, including Burkitt's and follicular lymphomas. DLBCL and marginal zone lymphomas were not as readily distinguished, underlining that

lymphomas can have complex patterns of oncoprotein overexpression, and single proteomic measurements are not sufficient to distinguish most subtypes[27–38]. The pathological diagnosis of lymphoma as well as of other tumor subtypes requires the combination of a number of analytical methods, including histological, biochemical and genetic techniques. Our approach has unique features that may complement these existing methodologies.

We were able to precisely measure oncoprotein isoforms that may be useful in the analysis of the therapeutic response in clinical tumor specimens. Previously, *in vitro* studies had suggested that treatment of CML tumor lines with imatinib results in decreased ERK phosphorylation[19,20]. With our approach, we were able to identify specific and rare ERK isoforms *in vivo* in subjects with CML that would only be detectable with large amounts of tumor tissue for alternative techniques such as two-dimensional blots or mass spectrometry. Charge-based separation via isoelectric focusing of each protein isoform on the basis of its unique pI allowed simultaneous quantification of multiple isoforms of the same protein in relative proportions that could not have been detected *a priori* by western blot or FACS techniques. Our results would have been missed by conventional immunoassay or flow cytometric techniques, as commercially available immunoreagents for activated ERK are raised against dually phosphorylated ERK epitopes. Unlike FACS samples, NIA samples did not require processing into a single cell suspension, fixation or permeabilization. Furthermore, the decreased ERK2 phosphorylation correlated with the clinical response to tyrosine kinase inhibitors. Future studies will determine whether ERK2 phosphorylation will identify the 15% of patients in whom imatinib will eventually lose its effectiveness.

In addition, we were able to serially sample tumors in subjects with lymphoma for a biologic response to a therapeutic agent, atorvastatin. Our observations are consistent with our previous description that atorvastatin decreases STAT3 and STAT5 phosphorylation in mouse models of lymphoma[26]. One possible explanation for these findings is that atorvastatin treatment leads to the inhibition and activation of signaling molecules upstream of STAT3 and STAT5 (ref. 26). Our observations illustrate that NIA could be similarly used to determine the protein signature of and identify biomarkers for response to known and new therapeutic agents.

Our results demonstrate how a nanoscale proteomic technology can be used to uncover unanticipated changes in protein signaling *in vivo*. Small perturbations in the equilibrium between active and inactive protein isoforms may have marked effects on the biologic state of a cell[39]. Our approach provides a new technique that could be incorporated into preclinical and clinical studies to evaluate subtle shifts in protein abundance and modification that may be useful for the discovery of new drugs that target protein pathways and the identification of biomarkers of therapeutic efficacy.

METHODS

Nanofluidic proteomic immunoassay. We performed NIA experiments with a Firefly instrument (Cell Biosciences)[22]. Briefly, for each capillary analysis, we diluted 4 nl of 10 mg ml^{-1} lysate to 0.2 mg ml^{-1} in 200 nl HNG (20 mM HEPES pH 7.5, 25 mM NaCl, 0.1%, 10% glycerol, Sigma Phosphatase Inhibitor Cocktail 1 diluted 1 in 100 and Calbiochem Protease Inhibitor diluted 1 in 100). We added 200 nl sample mix containing internal pI standards. The Firefly system first performed a charge-based separation (isoelectric focusing) in a 5-cm-long, 100-micron-inner-diameter capillary. We calculated predicted pIs with Scansite[40]. We ran each sample on a panel of different pH gradients (pH 3–10 and pH 2–11) to optimize the resolution of different peak patterns. After separation and photo-activated in-capillary immobilization, we detected proteins with antibodies. We detected MYC protein with the 9E10, OP-10 mouse monoclonal antibody that recognizes human MYC (Calbiochem). We detected BCL2 protein with the clone 124 mouse monoclonal antibody that recognizes human BCL2 (Dako Laboratories) and the clone 6C8 monoclonal hamster antibody that recognizes human BCL2 (Becton-Dickinson). We detected total ERK1 and ERK2 protein with a rabbit polyclonal antibody that recognizes mouse and human ERK1 and ERK2 (Upstate). We detected phospho-ERK1 and phospho-ERK2 protein with a mouse monoclonal antibody that recognizes both mouse and human phospho-ERK1 and phospho-ERK2 (Cell Signaling). We also used antibodies to activated caspase-3 (Cell Signaling), MEK1 (Upstate), phospho-MEK1 (Novus), MEK2 (Abcam), phospho-STAT3 (Cell Signaling), phospho-STAT5 (Cell Signaling), phospho-JNK (Cell Signaling) and heat shock protein-70 (HSP-70; Novus).

Nanofluidic proteomic immunoassay peak area quantification. We quantified the peaks with peak analysis software. We manually selected the start and end of each peak and a flat baseline. We calculated the area of each peak by dropping verticals to the baseline at the peak start and end and summing the area between the start and endpoints. NIA has previously been shown to be able to discriminate between and to quantify phosphorylated and unphosphorylated isoforms of ERK in a single sample with a total ERK antibody[22]. The areas under different peaks within a single tracing represented various ERK isoforms. To calculate the percentage of monophosphorylated ERK2 (identified here as peak 3), we divided the area under peak 3 by the sum of the area under the total ERK peaks. We ran samples in duplicate.

Nanofluidic proteomic immunoassay pseudoblot generation. We created the pseudoblots by a linear mapping of the signal intensity to a grayscale image. Each pseudoblot lane is representative of a single capillary and consists of horizontal bands corresponding proportionally to the signal present. Absence of signal is white, whereas increasing signal is seen as an increasing dark band. It should be noted that what is seen as a single band of protein in a size-based western blot can appear as either a single band on an NIA pseudoblot or, when multiple charged isomers of the protein are present, as multiple bands on an NIA pseudoblot.

Human tumor samples. We obtained tissues from subjects and banked them per Stanford University Institutional Review Board–approved protocols. We obtained informed consent from all subjects. We isolated CML and CLL cells from total blood by Ficoll separation, resuspended them in heat-inactivated FBS plus 10% DMSO and stored them in liquid nitrogen. We thawed tumor cells stored in liquid nitrogen at 37 °C into prewarmed PBS and washed them once in PBS immediately before use. We obtained four previously banked follicular lymphomas viably cryopreserved in a single cell suspension. We also obtained previously banked Burkitt's lymphomas, follicular lymphomas, marginal zone lymphomas, T cell acute lymphoblastic leukemia and nonmalignant lymph nodes frozen in optimal tissue-cutting blocks from the Stanford Hematology Division Tissue Bank.

Data and statistical analyses. We did NIA Multipeak fitting and peak area calculations with Peak Fit version 4.11 (Systat Software), using Gaussian peaks with variable widths, as previously described[22]. To obtain R^2 correlation coefficients, we calculated the best-fit line by linear regression with IGOR Pro version 5.03 (Wavemetrics). We compared NIA quantifications of MYC and BCL2 abundance to the relative intensity of respective quantified western blot bands by Pearson correlation. We used the paired *t* test (two-tailed) to analyze the percentage of phospho-ERK2 peak 3 before and during treatment. We performed the Mann-Whitney rank-sum test on the panels of clinical specimens with Prism version 4.0 (GraphPad). We also used Prism version 4.0 for Fisher's exact test (two-tailed) analysis of contingency table data for MYC and BCL2.

Normalization of nanofluidic proteomic immunoassay data. We normalized NIA data in a similar fashion to normalization of traditional western blots or other molecular biology assays. We used HSP-70 as a 'housekeeping' protein for NIA normalization. We calculated RLU by dividing the measured peak area for the protein of interest by the measured peak area for HSP-70 and expressed it

as a percentage. Across different experiments, we used a standardized lysate control for calibration of instruments and runs.

Additional methods. Detailed methodology is described in the **Supplementary Methods** online.

Note: Supplementary information is available on the Nature Medicine website.

ACKNOWLEDGMENTS

This manuscript is dedicated to the memory of Roger O'Neill. This work was supported, in part, by the US National Cancer Institute grants CA89305, CA034233, P01 CA034233, NIH/NCI ICMIC P50, Burroughs Welcome Fund, the Damon Runyon Foundation (to D.W.F.), and the Leukemia and Lymphoma Society (to D.W.F. and A.C.F.). We thank the members of the Felsher laboratory for their helpful suggestions. We thank W.-K. Weng (Stanford Bone Marrow Transplantation Division) for providing access to previously banked tumor samples and the Stanford Hematology Division Tissue Bank for the use of samples.

COMPETING INTERESTS STATEMENT

The authors declare competing financial interests: details accompany the full-text HTML version of the paper at http://www.nature.com/naturemedicine/.

Published online at http://www.nature.com/naturemedicine/
Reprints and permissions information is available online at http://npg.nature.com/reprintsandpermissions/

1. Futreal, P.A. *et al.* Cancer and genomics. *Nature* **409**, 850–852 (2001).
2. Harris, H. Tumour suppression: putting on the brakes. *Nature* **427**, 201 (2004).
3. Sharpless, N.E. & DePinho, R.A. Cancer: crime and punishment. *Nature* **436**, 636–637 (2005).
4. Vogelstein, B. & Kinzler, K.W. Cancer genes and the pathways they control. *Nat. Med.* **10**, 789–799 (2004).
5. Dalla-Favera, R. *et al.* Human c-myc onc gene is located on the region of chromosome 8 that is translocated in Burkitt lymphoma cells. *Proc. Natl. Acad. Sci. USA* **79**, 7824–7827 (1982).
6. Ferry, J.A. Burkitt's lymphoma: clinicopathologic features and differential diagnosis. *Oncologist* **11**, 375–383 (2006).
7. Dang, C.V., O'Donnell, K.A. & Juopperi, T. The great MYC escape in tumorigenesis. *Cancer Cell* **8**, 177–178 (2005).
8. Tsujimoto, Y., Cossman, J., Jaffe, E. & Croce, C.M. Involvement of the bcl-2 gene in human follicular lymphoma. *Science* **228**, 1440–1443 (1985).
9. Bordeleau, L. & Berinstein, N.L. Molecular diagnostics in follicular non-Hodgkin's lymphoma: a review. *Semin. Oncol.* **27**, 42–52 (2000).
10. Lugo, T.G., Pendergast, A.M., Muller, A.J. & Witte, O.N. Tyrosine kinase activity and transformation potency of bcr-abl oncogene products. *Science* **247**, 1079–1082 (1990).
11. Melo, J.V. & Barnes, D.J. Chronic myeloid leukaemia as a model of disease evolution in human cancer. *Nat. Rev. Cancer* **7**, 441–453 (2007).
12. Weisberg, E., Manley, P.W., Cowan-Jacob, S.W., Hochhaus, A. & Griffin, J.D. Second generation inhibitors of BCR-ABL for the treatment of imatinib-resistant chronic myeloid leukaemia. *Nat. Rev. Cancer* **7**, 345–356 (2007).
13. Ghaffari, S., Daley, G.Q. & Lodish, H.F. Growth factor independence and BCR/ABL transformation: promise and pitfalls of murine model systems and assays. *Leukemia* **13**, 1200–1206 (1999).
14. Felsher, D.W. Cancer revoked: oncogenes as therapeutic targets. *Nat. Rev. Cancer* **3**, 375–380 (2003).
15. Giuriato, S., Rabin, K., Fan, A.C., Shachaf, C.M. & Felsher, D.W. Conditional animal models: a strategy to define when oncogenes will be effective targets to treat cancer. *Semin. Cancer Biol.* **14**, 3–11 (2004).
16. Druker, B.J. *et al.* Efficacy and safety of a specific inhibitor of the BCR-ABL tyrosine kinase in chronic myeloid leukemia. *N. Engl. J. Med.* **344**, 1031–1037 (2001).
17. Kantarjian, H. *et al.* Hematologic and cytogenetic responses to imatinib mesylate in chronic myelogenous leukemia. *N. Engl. J. Med.* **346**, 645–652 (2002).
18. Weisberg, E. *et al.* Characterization of AMN107, a selective inhibitor of native and mutant Bcr-Abl. *Cancer Cell* **7**, 129–141 (2005).
19. Brozik, A. *et al.* Reduction of Bcr-Abl function leads to erythroid differentiation of K562 cells via downregulation of ERK. *Ann. NY Acad. Sci.* **1090**, 344–354 (2006).
20. Kohmura, K., Miyakawa, Y., Kawai, Y., Ikeda, Y. & Kizaki, M. Different roles of p38 MAPK and ERK in STI571-induced multi-lineage differentiation of K562 cells. *J. Cell. Physiol.* **198**, 370–376 (2004).
21. Solit, D.B. *et al.* BRAF mutation predicts sensitivity to MEK inhibition. *Nature* **439**, 358–362 (2006).
22. O'Neill, R.A. *et al.* Isoelectric focusing technology quantifies protein signaling in 25 cells. *Proc. Natl. Acad. Sci. USA* **103**, 16153–16158 (2006).
23. Felsher, D.W. & Bishop, J.M. Reversible tumorigenesis by MYC in hematopoietic lineages. *Mol. Cell* **4**, 199–207 (1999).
24. Karlsson, A. *et al.* Genomically complex lymphomas undergo sustained tumor regression upon MYC inactivation unless they acquire novel chromosomal translocations. *Blood* **101**, 2797–2803 (2003).
25. Giuriato, S. *et al.* Sustained regression of tumors upon MYC inactivation requires p53 or thrombospondin-1 to reverse the angiogenic switch. *Proc. Natl. Acad. Sci. USA* **103**, 16266–16271 (2006).
26. Shachaf, C.M. *et al.* Inhibition of HMGcoA reductase by atorvastatin prevents and reverses MYC-induced lymphomagenesis. *Blood* **110**, 2674–2684 (2007).
27. Mitani, S., Sugawara, I., Shiku, H. & Mori, S. Expression of c-myc oncogene product and ras family oncogene products in various human malignant lymphomas defined by immunohistochemical techniques. *Cancer* **62**, 2085–2093 (1988).
28. Wennborg, A.D., Altiok, E., Moore, J.P., Ernberg, I. & Klein, G. Differential c-myc protein expression in Burkitt's lymphomas and EBV-transformed lymphoblastoid lines. *Eur. J. Cancer* **27**, 1643–1645 (1991).
29. Johnson, N.A. *et al.* Prognostic significance of secondary cytogenetic alterations in follicular lymphomas. *Genes Chromosom. Cancer* **47**, 1038–1048 (2008).
30. Hann, S.R. & Eisenman, R.N. Proteins encoded by the human c-myc oncogene: differential expression in neoplastic cells. *Mol. Cell. Biol.* **4**, 2486–2497 (1984).
31. Ramsay, G., Evan, G.I. & Bishop, J.M. The protein encoded by the human proto-oncogene c-myc. *Proc. Natl. Acad. Sci. USA* **81**, 7742–7746 (1984).
32. Barrans, S.L. *et al.* Germinal center phenotype and bcl-2 expression combined with the International Prognostic Index improves patient risk stratification in diffuse large B-cell lymphoma. *Blood* **99**, 1136–1143 (2002).
33. Colomo, L. *et al.* Clinical impact of the differentiation profile assessed by immunophenotyping in patients with diffuse large B-cell lymphoma. *Blood* **101**, 78–84 (2003).
34. Gascoyne, R.D. *et al.* Prognostic significance of Bcl-2 protein expression and Bcl-2 gene rearrangement in diffuse aggressive non-Hodgkin's lymphoma. *Blood* **90**, 244–251 (1997).
35. Calvo, K.R. *et al.* IL-4 protein expression and basal activation of Erk *in vivo* in follicular lymphoma. *Blood* **112**, 3818–3826 (2008).
36. Camacho, F.I. *et al.* Nodal marginal zone lymphoma: a heterogeneous tumor: a comprehensive analysis of a series of 27 cases. *Am. J. Surg. Pathol.* **27**, 762–771 (2003).
37. Dierlamm, J. *et al.* Marginal zone B-cell lymphomas of different sites share similar cytogenetic and morphologic features. *Blood* **87**, 299–307 (1996).
38. Irish, J.M., Czerwinski, D.K., Nolan, G.P. & Levy, R. Altered B-cell receptor signaling kinetics distinguish human follicular lymphoma B cells from tumor-infiltrating non-malignant B cells. *Blood* **108**, 3135–3142 (2006).
39. Lee, T., Yao, G., Nevins, J. & You, L. Sensing and integration of Erk and PI3K signals by Myc. *PLOS Comput. Biol.* **4**, e1000013 (2008).
40. Obenauer, J.C., Cantley, L.C. & Yaffe, M.B. Scansite 2.0: Proteome-wide prediction of cell signaling interactions using short sequence motifs. *Nucleic Acids Res.* **31**, 3635–3641 (2003).

Lab on a Chip c2lc21290k

PAPER

High throughput automated chromatin immunoprecipitation as a platform for drug screening and antibody validation

Angela R. Wu, Tiara L.A. Kawahara Shiell, Nicole A. Rapicavoli, Jan van Riggelen, Emelyn H. Shroff, Liwen Xu, Dean W. Felsher, Howard Y. Chang and Stephen R. Quake

An automated microfluidic-based, high-throughput platform for chromatin immunoprecipitation screening that is sensitive enough to detect cytokine-induced cellular epigenetic changes over a fine temporal resolution.

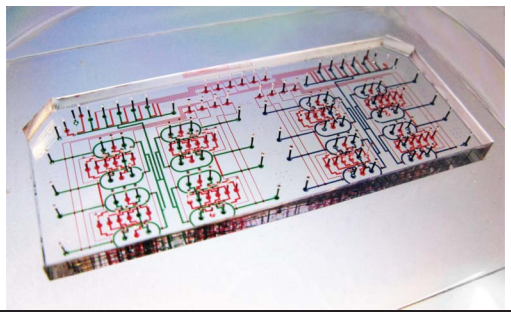

Please check this proof carefully. Our staff will not read it in detail after you have returned it.
Translation errors between word-processor files and typesetting systems can occur so the whole proof needs to be read. Please pay particular attention to: tabulated material; equations; numerical data; figures and graphics; and references. If you have not already indicated the corresponding author(s) please mark their name(s) with an asterisk. Please e-mail a list of corrections or the PDF with electronic notes attached — do not change the text within the PDF file or send a revised manuscript.

Please bear in mind that minor layout improvements, e.g. in line breaking, table widths and graphic placement, are routinely applied to the final version.

We will publish articles on the web as soon as possible after receiving your corrections; no late corrections will be made.

Please return your **final** corrections, where possible within **48 hours** of receipt, by e-mail to: advances@rsc.org

Electronic (PDF) reprints will be provided free of charge to the corresponding author. Enquiries about purchasing paper reprints should be addressed via: http://www.rsc.org/publishing/journals/guidelines/paperreprints. Costs for reprints are below:

Reprint costs

No of pages	Cost for 50 copies	Cost for each additional 50 copies
2–4	£225	£125
5–8	£350	£240
9–20	£675	£550
21–40	£1250	£975
>40	£1850	£1550

Cost for including cover of journal issue:
£55 per 50 copies

Authors Queries

Journal: **Lab On A Chip**

Paper: **c2lc21290k**

Title: **High throughput automated chromatin immunoprecipitation as a platform for drug screening and antibody validation**

Editor's queries are marked like this... 1, and for your convenience line numbers are indicated like this... 5.

Query Reference	Query	Remarks
1	[INFO-1] Please carefully check the spelling of all author names. This is important for the correct indexing and future citation of your article. No late corrections can be made. FOR YOUR INFORMATION: You can cite this paper before the page numbers are assigned with: (authors), Lab Chip, DOI: 10.1039/c2lc21290k.	

Cite this: DOI: 10.1039/c2lc21290k

www.rsc.org/loc

PAPER

High throughput automated chromatin immunoprecipitation as a platform for drug screening and antibody validation†‡

Angela R. Wu,[a] Tiara L.A. Kawahara Shiell,[b] Nicole A. Rapicavoli,[b] Jan van Riggelen,[c] Emelyn H. Shroff,[c] Liwen Xu,[c] Dean W. Felsher,[c] Howard Y. Chang[bd] and Stephen R. Quake[ad]

Received 23rd December 2011, Accepted 19th March 2012
DOI: 10.1039/c2lc21290k

Chromatin Immunoprecipitation (ChIP) is an assay for interrogating protein–DNA interactions that is increasingly being used for drug target discovery and screening applications. Currently the complexity of the protocol and the amount of hands-on time required for this assay limits its use to low throughput applications; furthermore, variability in antibody quality poses an additional obstacle in scaling up ChIP for large scale screening purposes. To address these challenges, we report HTChIP, an automated microfluidic-based platform for performing high-throughput ChIP screening measurements of 16 different targets simultaneously, with potential for further scale-up. From chromatin to analyzable PCR results only takes one day using HTChIP, as compared to several days up to one week for conventional protocols. HTChIP can also be used to test multiple antibodies and select the best performer for downstream ChIP applications, saving time and reagent costs of unsuccessful ChIP assays as a result of poor antibody quality. We performed a series of characterization assays to demonstrate that HTChIP can rapidly and accurately evaluate the epigenetic states of a cell, and that it is sensitive enough to detect the changes in the epigenetic state induced by a cytokine stimulant over a fine temporal resolution. With these results, we believe that HTChIP can introduce large improvements in routine ChIP, antibody screening, and drug screening efficiency, and further facilitate the use of ChIP as a valuable tool for research and discovery.

Introduction

Chromatin immunoprecipitation (ChIP) is an assay used to study protein-DNA interactions in the cell.[1] In a typical ChIP assay, antibodies against the proteins of interest are used to purify these proteins along with the DNA they bind to. Subsequently this DNA can be released, identified and quantified, giving information about where the protein binds across the genome.[2,3]

Gene transcription, a critical cellular process, is directly controlled by transcription factor protein-DNA interactions, and also indirectly regulated by histone protein-DNA interactions.[4] These epigenetic control mechanisms have increasingly been shown to play an important role in human diseases, for example in cancer[5–7] and diabetes.[8,9] ChIP has been used extensively to further our understanding of such disease mechanisms, to elucidate genomic locations of abnormal transcriptional activity,[9] as well as to compare normal and abnormal histone modification profiles in the cell.[7,10,11] With the decreasing cost of microarrays and high throughput sequencing technologies, genome wide studies of protein-DNA interactions using ChIP-chip (ChIP followed by microarray) and ChIP-Seq (ChIP followed by high throughput sequencing) are becoming more accessible to researchers. In addition to being used to investigate specific cellular mechanisms in depth by basic science researchers, ChIP is also being used in screening applications to identify feasible epigenetic drug targets,[11–13] or to evaluate the effect of drugs on cell epigenetics by the biotech industry.[14,15]

Unfortunately, the conventional ChIP methodology is not amenable to industrial scale-up and automation, due to the amount of hands-on time, total experiment time, and the prohibitively high quantity of sample and reagents required. Efforts to improve ChIP methodology have largely been successful in reducing sample and reagent requirements to thousands of cells per assay,[16–20] but have not provided any scalable, automatable solutions. Flanagin *et al.* have increased the throughput of ChIP by adapting it to a 96-well microplate platform called Matrix-ChIP,[21] but this method still requires 100 000 cells per well, which implies 10 million cells that must be manually processed from culture for each plate of assays. It can

[a]*Department of Bioengineering, Stanford University, Stanford, CA 94305, United States of America. E-mail: quake@stanford.edu; Fax: (650) 736-1961; Tel: (650) 724-8890*
[b]*Program in Epithelial Biology, Stanford University School of Medicine, Stanford, California*
[c]*Division of Medical Oncology, Departments of Medicine and Pathology, Stanford University School of Medicine, Stanford, California*
[d]*Howard Hughes Medical Institute, Chevy Chase, MD 20815-6789*
† Published as part of a LOC themed issue dedicated to research from the USA: Guest Editors Don Ingber and George Whitesides
‡ Electronic supplementary information (ESI) available. See DOI: 10.1039/c2lc21290k

thus be concluded that existing techniques, although improvements on traditional ChIP, do not adequately address the need for a scalable, low consumption ChIP technique that will enable high throughput epigenetic drug target discovery in the industrial setting.

Another major bottleneck preventing ChIP being more widely used in industrial screening applications is the variability in antibody quality: the success of a ChIP experiment is largely determined by the specificity and sensitivity of the antibody.[22,23] An antibody that has high specificity will result in a good enrichment of the target protein over background, and a more confident prediction of protein binding. An antibody that has high sensitivity means that a stronger signal can be obtained in experiments that start with fewer cells, or for a low abundance protein. Although certain commercial vendors market lines of antibodies as "ChIP-grade", the variation in antibody specificity and sensitivity is still extremely problematic. This variation in quality does not occur only between antibodies targeting different epitopes; even for antibodies targeting the same epitope, there is variation between different vendors, and even between batches from the same vendor. This introduces problems of replicability in experimentation, and results in a waste of time, samples, and reagents for the researcher. Currently, antibodies are evaluated by testing them in immunohistochemistry (IHC) or western blots (WB), and top performers in these assays are labeled "ChIP-grade".[23] However, it is well known that antibodies that perform well in IHC or WB do not necessarily perform well in ChIP, and the best way to test an antibody for ChIP performance is using ChIP.[22,23] Hence, a high throughput, low consumption ChIP screening technique would also be of great value in validation of ChIP antibodies, both in an industry setting and for the individual researcher.

To address the two aforementioned major challenges in scaling up epigenetic screening, we have developed a high throughput, low consumption, automated microfluidic device for ChIP for drug screening and antibody validation (HTChIP). Previously we reported a high sensitivity microfluidic ChIP technique, AutoChIP, which allows two ChIP-qPCR and two control measurements per device run, starting from as few as 2,000 cells for each measurement.[24] Here, we describe a new microfluidic device which increases ChIP throughput by a factor of 7-fold: 14 ChIP and two control measurements can be made from a single biological sample simultaneously, or 6 ChIP and two control measurements each from two biological samples simultaneously, using only 10 000 cells' equivalent of chromatin and < 0.5 μg of antibody for each measurement. Each ChIP mixing chamber can be independently addressed such that the combination of antibodies used on each chromatin sample is completely customizable; if desired, a set of completely different antibodies can be used for the first chromatin sample than the second chromatin sample. To address the specifications of high-throughput screening ChIP applications better, HTChIP has been designed to take fragmented chromatin prepared with conventional methods, rather than to fragment the chromatin *in situ*. In addition to proof-of-concept, and characterization of the pull-down efficiency of HTChIP, we establish the utility of HTChIP in antibody screening assays by comparing multiple antibodies' performance in ChIP using our HTChIP platform. Moreover, we use HTChIP to track ex-vivo nuclear protein-DNA interactions in response to different durations of cytokine stimulation with a fine temporal resolution, demonstrating the potential of HTChIP as a tool for high-throughput drug screening.

Materials and methods

Device fabrication and operation

The main body of our device is made of polydimethylsiloxane (PDMS) containing channels and valves, fabricated as detailed previously[25,26] with some modifications. The hybrid flow master molds were fabricated out of 45 μm AZ-50XT (Mays Chemicals) and 35 μm SU8-50 photoresists (Microchem), and the control molds were cast from 35 μm SU8-2025 (Microchem). For the PDMS control layer, 20 g of uncured PDMS (20 Part A:1 Part B) was spun onto the negative mold at 1,500 rpm for 60 s. Cross-sectional dimensions of the control channels are 35 μm $\times$ 300 μm. For the PDMS flow layer, 40 g of uncured PDMS (5 Part A:1 Part B) was poured onto the negative mold, degassed for 1 h and baked for 1 h at 80 °C to cure. Cross-sectional dimensions of the flow channels are 45 μm $\times$ 300 μm at rounded valves and 35 μm $\times$ 300 μm otherwise. The ring structures of the device are in 7500 μm length and 3800 μm in width (from outer edge to outer edge). Actuation and operation of the device is also as previously described.[25] An image and labeled schematic of the device are presented in Fig. 1 and 2.

Cell culture

HeLa cells from the ATCC and were propagated in DMEM (Invitrogen) plus 10%fetal bovine serum, and grown to confluency before harvesting. Murine embryonic fibroblasts (MEF) were derived from 13.5-day-old mouse embryos using standard protocol, and propagated in DMEM (Invitrogen) plus 15% FBS, as described previously.[27]

Conventional ChIP assay

The conventional ChIP protocol used on HeLa cells to validate HTChIP is described in a previous publication.[28]

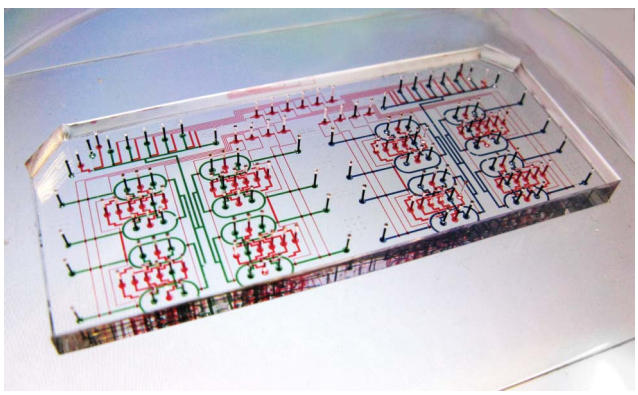

Fig. 1 Photograph of HTChIP device. Device is filled with different dye colours to demonstrate independent sample loading on the left and the right side of the device, allowing simultaneous processing of two distinct biological samples.

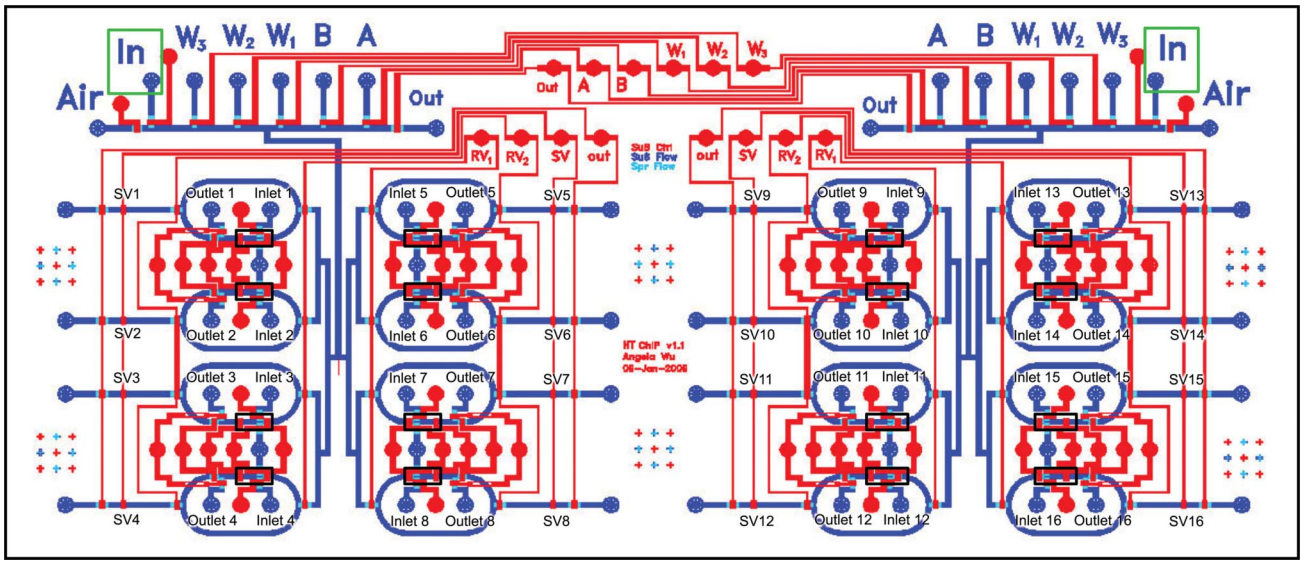

Fig. 2 Schematic of HTChIP. Reagent-containing flow channels are shown in blue shades, and valve-actuating control channels in red. Antibody-bead preparations are loaded into the black-boxed regions of rings *via* Inlets 1–16, and then mixed with sheared chromatin. After IP, samples are washed in columns stacked behind sieve valves SV1-16, and collected from the device. All fluids are driven by pneumatic, non-pulsatile pressure at 5 psi.

Microfluidic ChIP assay (HTChIP)

Fig. 2 shows a labeled schematic of the device where different stages of ChIP are performed. Figure S1 illustrates the process flow for a ChIP assay performed using HTChIP.

Cell and chromatin processing. Cells were processed as previously described.[27] Briefly, cells were treated with TNF-α (20 ng ml^{-1}) for the indicated times. DNA was cross-linked for 10 min with 1% formaldehyde and stopped in 0.125 M glycine. Purified chromatin was sonicated to ~500 bp using the Bioruptor (Diagenode, Inc). The final chromatin concentration was 25 000 cells μL^{-1} equivalent. Fragmented chromatin was snap frozen and stored at −80C in single use aliquots (20 μL each) to avoid repeated freeze/thaw cycles.

Immunoprecipitation and wash. Before each experiment, the inside surface of the device is treated with 0.2% pluronic solution (0.2% w/v cell culture grade Pluronic F127 (Sigma) in DPBS (Dulbecco's Phosphate Buffered Saline) (GIBCO)) for 15 min, followed by rinsing with DPBS and air drying. The device has dedicated inlets 'A' for flowing in Pluronic solution, and inlets 'B' for washing with DPBS. Inlets marked 'Air' are used to introduce air into the device for drying (Fig. 2).

The rings are pre-loaded with antibody-functionalized beads (Protein A Dynabeads (Invitrogen) with antibodies) between the two valves in the black-boxed regions shown in Fig. 2, by flowing beads through Inlets 1–16 to outlets 1–16 (Figure S1-i). Sieve valves trap the beads to make a bead column (Figure S1-ii). Antibodies are loaded into rings randomly, with no specific assignment of antibody to a specific ring from experiment to experiment. Roughly 2 μL of antibody-conjugated beads are loaded into each ring for each ChIP assay, which corresponds to just under 0.5 ug of antibody. 1.6 μL of chromatin is reserved as Input reference, equivalent to four times the amount of chromatin used in each ChIP measurement. The remaining chromatin is introduced into all the rings by flowing it in through inlet marked 'In' (Fig. 2, green-boxed). If two samples are to be processed simultaneously with 8 measurements each sample, then the two independent 'In' inlets are used to load different chromatin samples to the two sides of the device: Rings 1–8 loaded with one sample, Rings 9–16 loaded with another (as demonstrated in Fig. 1 by the green and blue color dyes). Alternatively, both 'In' inlets can be used to load the same sample into all of Rings 1–16 to achieve 16 measurements on a single sample. The bifurcated channels divide the chromatin into equal parts of 10 000 cell equivalents per ring: 0.4 μL volume ring filled with 25 000 cells μL^{-1} equivalent chromatin. No outlets are opened in this step, so that the rings can be "dead-end filled' with chromatin; opening outlets will result in loss of chromatin (Figure S1-iii). Dead-end filling is possible because PDMS is gas permeable; in a matter of minutes the air in the rings is expelled and replaced by liquid. During IP, the antibody-beads are mixed with the chromatin for 2 h, and the device is placed on a Peltier device set at 4 °C (Fig. S1-iv).

After IP, the beads are re-stacked in a column behind sieve valves SV1-SV16 (Fig. S1-v), and washed for 10 min with RIPA buffer (10 mM Tris-HCl pH 7.5, 1 mM EDTA, 0.5 mM EGTA, 1% Triton X-100, 0.1% SDS, 0.1% Na-deoxycholate, 140 mM NaCl) introduced through inlets 'W_1' (Fig. S1-vi). Inlets 'W_2' and 'W_3' were unused in this case, but could be used to flow in other wash buffers if a multi-buffer wash system is desired. When washing, the pneumatic pressure on the wash buffers is adjusted to 5 psi to better control wash volume. A lower pressure also prevents specifically bound materials from being stripped off the antibodies under high shear forces and lost. Following the RIPA wash, the beads were eluted into thin-walled PCR tubes with a minimal amount of TE (10 mM Tris-HCl, 1 mM EDTA pH 8.0). These PCR tubes were then immediately placed on a magnet and the DPBS removed with a pipette leaving only the magnetic beads. The DNA was then purified from the beads using the Chelex (Bio-Rad) resin extraction method described

previously.[29] An ethanol precipitation was done on the input sample by adding 250 μL of 100% ethanol (Sigma-Aldrich), 2 μL of carrier glycoblue (Invitrogen), and 16 μL of 5 M NaCl to the sample and precipitating at −80 °C for one hour. The precipitated sample was then centrifuged at 20 000 g for 15 min, and the supernatant discarded. The pellet was washed in 500 μL of freshly prepared and chilled 70% ethanol, and then centrifuged again at 20 000 g for 10 min. Finally, the supernatant was discarded and the pellet left to air dry. Once the pellet was dry, the same Chelex resin extraction was applied in parallel with the IP samples. The purified DNA was used directly in the real-time quantitative SYBR green PCR reactions (qPCR).

Real-time qPCR

Real-time qPCR reactions were performed using Taqman probes (IDT) or SYBRgreen ER (Invitrogen), in a Stratagene thermocycler (Roche). Sequences of PCR primers used were taken from Kawahara *et al.*[27,28] with the permission of the authors, and are provided in Table 1. The following thermal cycling profile was used: Hot start 95 °C for 10 min, followed by 40 cycles of 95 °C for 15 s, 57 °C for 30 s, 72 °C for 30 s. Primer concentrations were 0.5 μM. In the case of SYBRgreen assays, post-run melt curve analysis was used to confirm that all products formed were full length and not primer dimers.

Results and discussion

HTChIP demonstrates improved IP efficiency

Presently, ChIP used in screening applications is not restricted by the quantity of starting material; therefore, we designed the HTChIP to be compatible with relative larger quantities of chromatin that has been isolated and fragmented using conventional means. Previously, we reported a similar microfluidic platform, AutoChIP, which can perform ChIP measurements on as few as 2,000 cells.[24] We observed higher enrichment of target proteins in AutoChIP than in the conventional benchtop ChIP and proposed that this higher level of enrichment might be due to improved antibody-target interactions facilitated by a smaller reaction volume, leading to a higher IP efficiency. Since our previous design uses chromatin generated *in situ*, we wanted to first verify that (1) the HTChIP design still takes advantage of the smaller reaction volume to deliver similar gains in IP efficiency as reported in the AutoChIP design, and (2) while using conventionally treated chromatin as input as opposed to chromatin generated *in situ*.

Table 1 Sequences of primers and probes to promoter regions that were used in qPCR reactions to evaluate ChIP experiment enrichments

HeLa primers		
IAP2	*Forward*	CCA CGA GCA ATG AAG CAA ATG TC
	Reverse	GGG GAA CTC CAG CGG TAA TAA C
	Probe	TCC AGT AAA TGC CGC GAA G
MnSOD	*Forward*	AGGTCGGCTTACTTGCAAAGC
	Reverse	CGCCCTTCCAACCCGTAT
	Probe	TACGGCGCAAGAGT
NFkbia	*Forward*	GCAGCCCCCTAACCACAGT
	Reverse	CTGGGCGTAGGGATTTGCT
	Probe	TTCCCCTTAGAAGTCTG
IL8	*Forward*	GGCCATCAGTTGCAAATCGT
	Reverse	CCTACTAGAGAACTTATGCACCCTCAT
	Probe	ATTTCCTCTGACATAATGAA
MEF Primers		
NFKBIA	*Forward*	GCC ATG GAG CAA ACC CAT AG
	Reverse	ATT CCA TAG CGG GAG GTG TCT
NFKB2	*Forward*	CCA TGG CAG CGA CTC TTG T
	Reverse	CTG CCT TCC CCC TGC AT
CDKN1A	*Forward*	TCT TCC AGT CCT TGG AGA CC
	Reverse	GCA CCT GGA ATC CCT AGA AA
DLL1	*Forward*	GCG TGG CTG TCA TTA AGG
	Reverse	GGT GCT GTC TGC ATT ACC

To test these hypotheses we isolated and sheared chromatin from a HeLa cell line, and performed ChIP using a conventional approach as well as our HTChIP platform for a direct comparison of IP efficiency. In both approaches, different antibodies were conjugated to Protein A-covered magnetic beads, but the IP was performed either in a microcentrifuge tube for the conventional method, or in a microfluidic mixing chamber for the HTChIP (see Figure S1 for schematic of microfluidic ChIP experimental flow). 40 000 cells were used for each ChIP assay. After ChIP, qPCR against four genomic loci was used to evaluate the IP performance of each method. The genomic loci of interest lie in the promoter region of NF-κB target genes: *IAP2*, *MnSOD*, *IL8*, and *NFKBIA*.

Fig. 3 shows results for the IP using anti-H3K9Ac (antibody against acetylated-lysine-9-on-histone-3), and from these results it is evident that while preserving the patterns of relative enrichment between different genomic loci, the IP performed using HTChIP generated a significantly higher signal than that performed in a conventional microcentrifuge tube (p-values $<$ 0.01 for all loci tested). The same outcome was observed for the IP of anti-PanH3 (antibody against core histone H3), indicating that the improvement in IP efficiency is a general phenomenon and not antibody specific (Fig. S1). A slight increase in the background signal, as determined by IP using anti-IgG (antibody against non-specific IgG), was also observed (Fig. S2). This

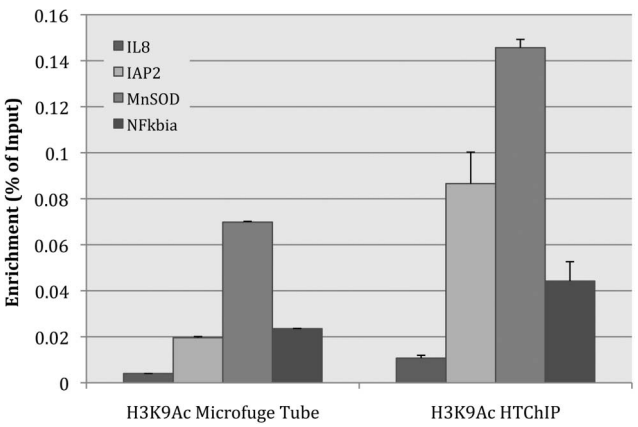

Fig. 3 Bar graph comparing IP efficiency between IP performed in a microcentrifuge tube on the benchtop, and the microfluidic environment of HTChIP. ChIP was performed using anti-acetylated-histone-3-lysine-9. The HTChIP signal was significantly higher than the signal from the microcentrifuge tube based method, with a p-value $<$ 0.01 (unpaired Student's T-test) for each genomic loci tested. Since the metric being compared is raw IP efficiency, enrichment values were not normalized to any background or control ChIP, but rather displayed as ratio to non-normalized Input values. Error bars represent standard error over three (3) PCR replicates.

is consistent with previous observations made by our group and others,[24,29–31] but the magnitude of the increase in background is much lower than the increase in signal observed in the other ChIP assays. That is, the HTChIP method resulted in a net signal increase over the conventional method. This confirms our hypothesis that simply performing the IP in a microfluidic reaction chamber results in higher IP efficiency and target enrichment, even when using the same starting amount of chromatin.

HTChIP accurately reflects protein-DNA binding patterns in the cell after stimulation

Next we demonstrate that the HTChIP can accurately capture the changes (or lack thereof) in the cell's protein-DNA interactions induced by drug treatment of the cell. HeLa cells were treated with TNF-α for 1 h, and subsequently subject to ChIP-qPCR using the same antibodies and PCR primers in order to assess changes in histone binding induced by the stimulation. In this model system, TNF-α treatment induces translocation of NF-κB into the cell nucleus, where it binds to the promoters of genes to initiate gene transcription.[32] In individual cells, NF-κB binding is highly dynamic and periodic, and for some target genes, specific histone modification patterns are incited at the target gene promoter to prevent repeated activation of that gene upon prolonged stimulation with TNF-α.[33] These histone modifications regulate chromatin structure, which can control chromatin openness and accessibility.[34] For example, H3K9Ac is a modified histone mark that is found near open chromatin in regions of active transcription.[34] Prior work in this particular cell line determined that the presence of H3K9Ac at the four promoter regions of interest is cyclic to prevent repeated NF-κB activation of the associated genes.[28] The period of this cycle was found to be 1 h, therefore if we only observe the zero and 1 h time point, we would expect to find no overall change in H3K9Ac levels at the four promoters of interest (*i.e.* any changes in H3K9Ac levels at these promoters would only be observed at intermediate time points of TNF-α stimulation).

Indeed, a Student's two-tailed T-Test with a significance level of $p = 0.01$ found that the level of H3K9Ac binding at all the tested genomic loci did not significantly differ between TNF-α stimulate cells and untreated cells, when assessed using the conventional ChIP assay (Fig. 4, Fig. S3). When we performed the same test on the ChIP results generated using HTChIP, the same trend was observed: No significant difference was found in the level of H3K9Ac binding at the genomic loci of interest (Fig. 4, Fig. S3). This result leads us to believe that the HTChIP can reliably be used to assess and compare *in vivo* protein-DNA binding events in untreated cells and cells that have been subject to external stimuli.

"ChIP-grade" antibody screening using HTChIP is fast and effective

As mentioned previously, there are now many antibodies available that are marketed as "ChIP-grade". However, due to batch variation, even the same antibody clone may generate antibody lots that produce variable ChIP results. The highly parallel nature of HTChIP is designed to address this problem, allowing users to simultaneously interrogate multiple antibody lots or antibodies from different suppliers, in order to assess and choose the best antibody for their application. To test demonstrate the utility of our microfluidic platform in this respect, we procured three different lots of anti-Sirt6 antibody at random from a single supplier (Abcam), and tested them, along with the relevant controls, on our HTChIP platform using chromatin isolated from murine embryonic fibroblasts. MEF is a primary cultured cell directly derived from mouse embryos that is more difficult to obtain and to propagate in culture; unlike HeLa cells, MEFs are not immortalized and can only be sustained for 10–15 passages before reaching scenescence.[35] We chose MEFs as a model system because of its importance in embryonic stem cell culture and studies,[36–39] and because we have previously studied the response of MEFs to TNF-α stimulation in the context of Sirt6 mediated chromatin remodeling.[27] We generated chromatin from MEFs that were stimulated for 30 min with TNF-α, and performed 6 different ChIP assays on this material: anti-FLAG, anti-PanH3, anti-H3K9Ac, anti-Sirt6 Lot 02, anti-Sirt6 Lot 14, anti-Sirt6 Lot 77. Anti-FLAG is used as a background negative control; anti-PanH3 and anti-H3K9Ac are used as positive control to ensure that the HTChIP experiment is working. Lot numbers of Sirt6 antibodies represent the last two digits of the manufacturer's lot number for each antibody. For each ChIP experiment, 10 000-cell equivalent of chromatin was used, and results were assessed by qPCR of four gene promoters: *NFKB2*, *NFKBIA*, *CDKN1A*, *DLL1*. *NFKB2*, *NFKBIA* are canonical NF-κB target genes, and based on our previous work, it is known that after 30 min of TNF-α treatment, H3K9Ac will be present at these promoters to facilitate transcription of these genes by NF-κB, and that Sirt6 will also bind to these promoters to begin H3K9 deacetylation in order to restrict continual activation of these genes in the event of sustained TNF-α stimulation. After 60 min of TNF-α stimulation, H3K9 is deacetylated to induce a closed chromatin structure at these promoters, and these promoters are devoid of both H3K9Ac and Sirt6. The *CDKN1A* promoter is occupied by Sirt6 independent of TNF-α stimulation, and was selected as a positive control. *DLL1* promoter is not bound by Sirt6, and was included as a negative control.

Fig. 5 shows the results of this ChIP antibody screening experiment. First, note that the signal for *DLL1* enrichment is low regardless of the antibody used. This suggests that the ChIP pull down was specific, and did not enrich for regions not bound by Sirt6. For other promoters, these results clearly show the amount of variability between these three lots of Sirt6 antibody in terms of sensitivity. Lot 77 signal levels in the promoter regions that should be enriched are comparable to that of *DLL1* negative control. This result indicates that Sirt6-lot 77 did not pull down any specific Sirt6 protein in the IP. Lots 02 and 14 both demonstrated superior sensitivity than lot 77, with signals much higher than background, but lot 14 is clearly the superior lot, with higher signal to background ratio than lot 02 for every promoter region that was tested.

In order to demonstrate the versatility of HTChIP with different cell and antibody systems, we performed a similar antibody screening experiment, using chromatin from an immortalized mouse lymphoma cell line (6780) that expresses MYC. Three anti-MYC antibodies from three different sources were tested for ChIP application using our HTChIP platform.

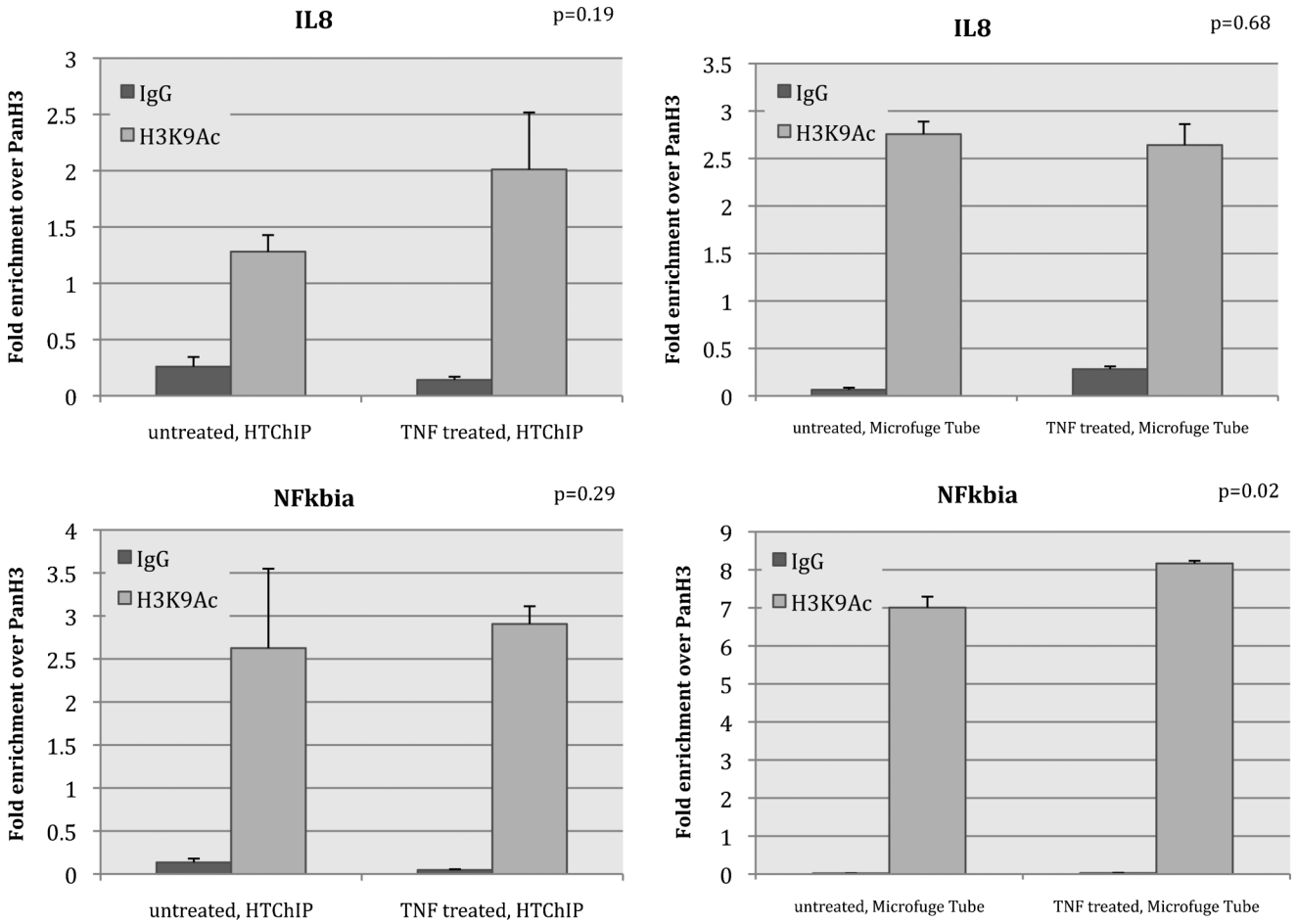

Fig. 4 Bar graphs showing ChIP enrichment of H3K9Ac of HeLa cells with and without TNF-α stimulation, measured at NFκB target promoters. Left graphs show results obtained using HTChIP; right graphs show results obtained using conventional benchtop protocol. Each graph shows H3K9Ac enrichment at the loci of interest without TNF-α stimulation on the left, and with 1 h of TNF-α treatment on the right. For benchtop ChIP, there is no significant difference between H3K9Ac levels at these gene promoters in untreated and treated cells; data from HTChIP leads to the same conclusion (Bonferroni corrected unpaired Student's T-test at $\alpha = 0.01$). Both sets of results concur with those previously reported in literature. In each ChIP, enrichments were normalized to PanH3 levels for comparability, and non-specific anti-IgG was used as background control. Error bars represent standard error over three (3) PCR replicates for both HTChIP and benchtop ChIP experiments.

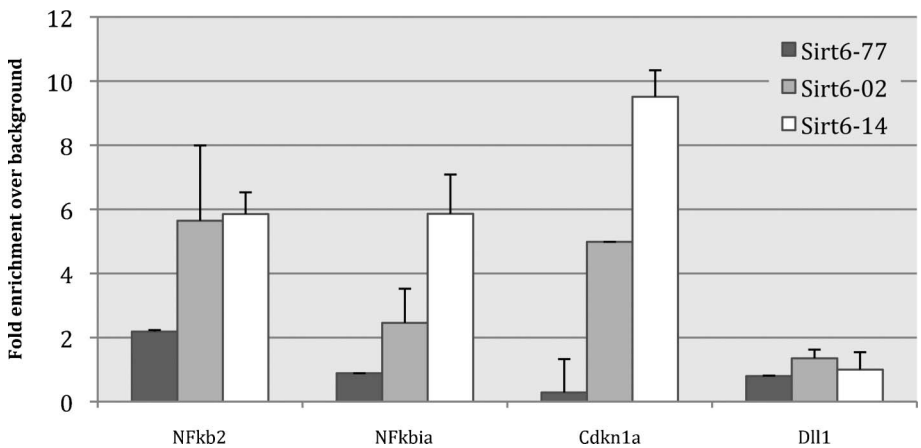

Fig. 5 Bar graph of HTChIP results comparing ChIP enrichment obtained using three different batches of an anti-Sirt6 antibodies generated from the same antibody clone. *Dll1* is included as a negative control promoter; *Cdkn1a* is a positive control promoter. From this graph, lot #14 is the Sirt6 antibody lot with highest sensitivity and specificity. ChIP enrichment is shown here as fold enrichment over background control to highlight the difference in specificity between antibody lots. Error bars represent standard error over three (3) technical replicates.

The ODC1 promoter was the genomic loci of interest as it is a known site for MYC binding. The ODC1 E-box region contains a transcription factor binding motif and serves as the MYC binding site where enrichment for MYC should be high. A control region 1 kbp upstream of the E-box motif, ODC1 upstream, was used as the negative control region where MYC enrichment should be low. Once again, results in Fig. 6 reveals the high degree of variation between antibodies, this time procured from different sources. The anti-MYC from Epitomics gave the greatest amount of signal, and is therefore the most sensitive antibody, however it is lacking specificity, as it appears to have enriched the non-specific upstream region as well. The Abcam anti-MYC was the worst performer, giving almost no signal at all. The Santa Cruz antibody was intermediate, with a much lower E-box enrichment than Epitomics, but also a much lower upstream non-specific enrichment, thus it has the highest signal to background ratio. Depending on the purpose of the ChIP assay that will be performed, one may either prefer the Epitomics anti-MYC for its sensitivity (for example when interrogating endogenous MYC, which occurs at relatively low levels), or choose the Santa Cruz anti-MYC for its specificity (for example when the sample is over-expressing MYC, and false positives are undesirable).

The experiments described above highlight the advantages of using HTChIP for antibody screening applications: since only 10 000 cells were used for each ChIP, very little cell sample is consumed when using HTChIP for antibody screening. In addition, < 0.5 μg of antibody was used for each ChIP. For low throughput research studies, this means that most of the valuable sample and now ChIP-validated antibody can be reserved for meaningful high quality ChIP experiments, instead of being wasted on failed ChIP experiments due to poor antibody quality. For high throughput industrial screening applications, this means that the same biological sample can be used to screen more antibodies, and the same antibody batch used to screen more drugs, rather than having to compare results generated from different antibody batches or pooled biological samples that may have introduce heterogeneity, and lead to confounding results.

Tracking dynamic transcription factor and chromatin remodeling with HTChIP

After identifying a Sirt6 antibody with good sensitivity and specificity, we used HTChIP to track the interaction of Sirt6 and H3K9Ac at canonical NF-κB target promoters over a high-resolution time course (Fig. 7-data for untreated cells was previously published[27]). Our results confirm previous findings that Sirt6 binds quickly to NF-κB target promoters after stimulation with TNF-α, and subsequently leads to H3K9 deacetylation and thus transcriptional repression at that site.[27] Both NF-κB target promoters show no occupancy by Sirt6 or H3K9Ac prior to TNF-α stimulation. After 30 min of TNF-α treatment, H3K9 is acetylated to allow an open chromatin structure and gene transcription by NF-κB at these promoters, as indicated by high levels of enrichment for H3K9Ac. At the same time, Sirt6 is found poised at these promoters. After 60 min of treatment, Sirt6 localization to these promoters has led to H3K9 deacetylation and transcriptional repression, and because H3K9 is no longer acetylated, Sirt6 also no longer occupies these promoter regions, and we observe enrichment for both Sirt6 and H3K9Ac at a level that is similar to that of untreated MEFs. We simultaneously interrogated two other histone marks, H3K9m2 (histone-3-lysine-9-dimethylated) and H3K9m3 (histone-3-lysine-9-trimethylated). H3K9m2 is a mark of transcriptional repression, and H3K9m3 is a mark of constitutive heterochromatin.[34] Interestingly, in our data H3K9m2 binding trends over time also confirms the pattern of periodic transcriptional activation that was observed with H3K9Ac and Sirt6. Untreated cells and cells stimulated for 60 min show a higher level of H3K9m2 binding at NF-κB target promoters, confirming that these regions are in

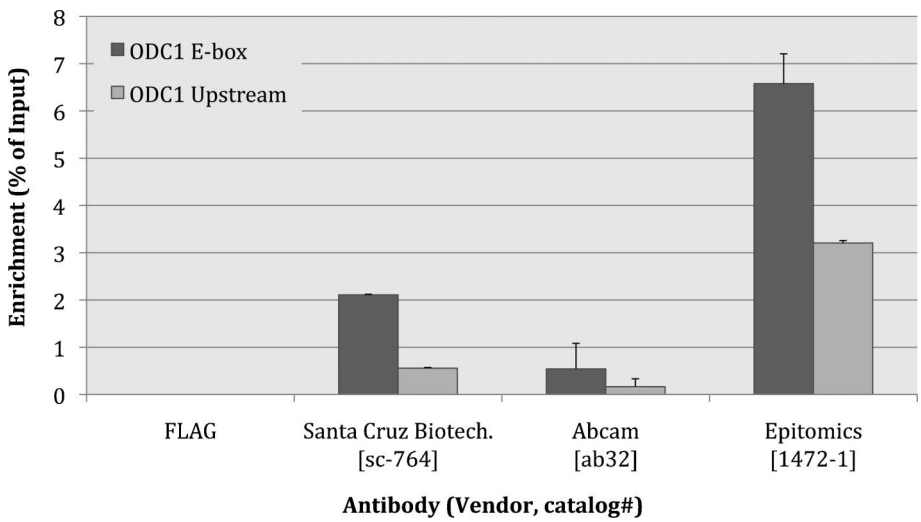

Fig. 6 Bar graph of HTChIP results comparing ChIP enrichment obtained using three different anti-MYC antibodies from different vendors. *Odc1 Upstream* is the negative control region; *Odc1 E-box* is the positive control *Odc1* promoter. From this graph, sc-764 has the best signal to noise, but Epitomics 1472-1 has higher sensitivity and higher signal. Note that *anti*-FLAG was used as the non-specific background control. Since enrichment for FLAG is zero (no PCR C(t) value), it is mathematically not possible to calculate the fold enrichment over background. Therefore here ChIP enrichment is shown as a ratio over Input without any normalization. Error bars represent standard error over three (3) technical replicates.

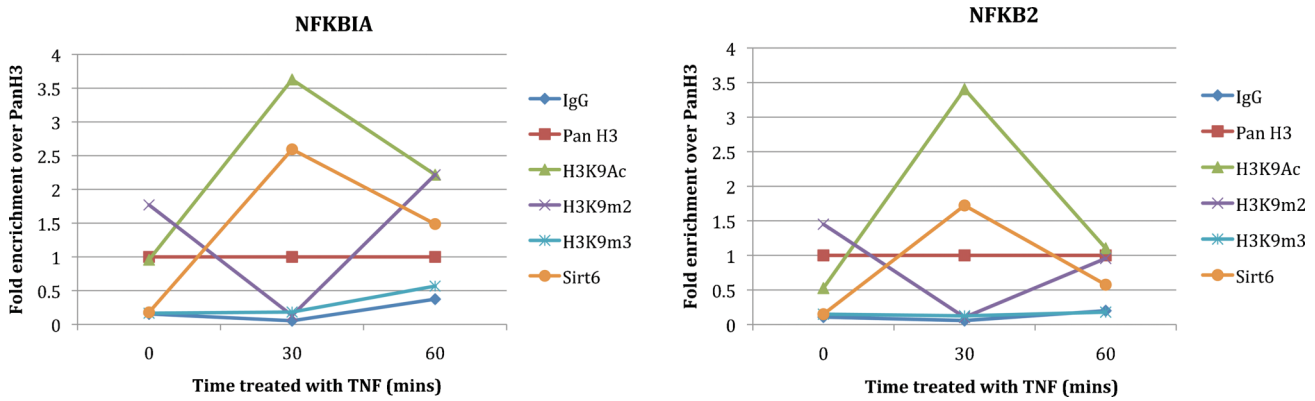

Fig. 7 Line graph of HTChIP results showing ChIP enrichment of various histone marks and Sirt6 at canonical NFκB promoters in MEF cells after stimulation with TNF-α for different amounts of time. Sirt6 is recruited to NFκB promoters after 30 min of stimulation and leads to deacetylation of H3K9. This demonstrates that HTChIP is sensitive enough to track changes in enrichment levels over a fine temporal resolution, and allows tracing of many protein simultaneously, generating a holistic picture of dynamic intracellular protein-DNA interaction.

heterochromatin form and transcription is repressed. Whereas at 30 min of stimulation, H3K9m2 levels decrease while H3K9Ac levels increase, again validating our finding that these promoter regions are transcriptionally active at this time. To the best of our knowledge, these findings on the modulation of H2K9m2 in the context of SIRT6 and NF-κB activity were previously unreported in the literature. H3K9m3 levels at these promoters are low, independent of TNF-α stimulation, indicating that these regions are not constitutively silenced; instead transcription at these sites is active but dynamically regulated by protein-DNA interactions.

Importantly, this set of tracking assays used only one biological sample for each time point, and there was no need to pool any samples, even though 6 ChIP assays were performed for each time point. A conventional bench-top ChIP protocol would have needed 500 000 cells for each ChIP, requiring a total of 3.5 million cells for each time point, whereas the HTChIP can perform several replicate assays at each time point using the same number of cells. Particularly for cells that are difficult to obtain or culture, this is an advantage that saves time and resources.

Conclusions

We have presented a high throughput, low consumption, automated microfluidic device for ChIP for drug screening and antibody validation, HTChIP. This device has a 7-fold throughput improvement over our previously reported microfluidic ChIP device, and the design can be easily scaled up to accommodate even more assays in parallel. To make the device fully automatable, and to take advantage of existing front-end research infrastructure and practices, HTChIP has been designed to take as input fragmented chromatin that was prepared in bulk using conventional methods, as opposed to fixed whole cells. We believe that with these design considerations, the HTChIP platform will be an effective and efficient tool for researchers in both industry and academic settings, particularly in antibody screening, drug screening, and epigenetic characterization studies.

In this report, we have detailed the design, fabrication and method of use for the HTChIP platform, which are amenable to both scaled commercialization and individual use. Proof-of-concept experimental data were presented to demonstrate significantly superior IP efficiency using HTChIP as compared to conventional benchtop methods, and despite slight increases in background, using HTChIP produces a net increase in ChIP signal. Next we show that HTChIP is able to faithfully reproduce results of an epigenetic study. In testing whether a specific histone-DNA binding increased in certain genomic regions upon inflammatory stimulation of the cell, data generated using HTChIP leads to the same conclusion as data generated using conventional ChIP protocols. The conclusion that there is no change in specific histone-DNA binding levels at the loci of interest is substantiated by the literature.[28] This microfluidic ChIP platform was also tested for antibody screening capability by performing ChIP with a large number of antibodies in parallel and evaluating antibody specificity by qPCR, and was able to distinguish good ChIP antibodies from poor ones. Finally, we demonstrate the use of HTChIP in tracking TNF-α induced transcription factor binding events in MEF cells. We successfully measured the effect of the transcription factor Sirt6 binding on the levels of H3K9Ac binding at specific genomic loci with a fine temporal resolution. The results of this study were in concordance with previous findings about the regulatory mechanism of Sirt6,[27] again showing the robustness of HTChIP in producing reliable ChIP data.

Overall, this data from a series of characterization assays confirm that this HTChIP platform can rapidly and accurately evaluate the epigenetic states of a cell. It is sensitive enough to detect the changes in the epigenetic state induced by a cytokine stimulant over a fine temporal resolution, and allows tracing of many protein simultaneously, generating a holistic picture of dynamic intracellular protein-DNA interaction. With these results, we believe that HTChIP can introduce large improvements in routine ChIP, antibody screening, and drug screening efficiency, and given its ease of manufacturing, scalability, and automation it will be a valuable tool in the biotechnology research space.

Acknowledgements

The authors thank J. Wang, Dr C. H. Fan, Dr N. Jiang, Dr M. Meiers, and W. Gu for helpful discussion and advice. W. Koh

for fruitful dialogue on data analysis. A. Adams, G. Su, and P. Nazh for device fabrication. This work has been funded by NCI, DoD, Pioneer, and Ellison Medical Foundation grants; the author also thanks the Bio-X Foundation Fellowship and Siebel Foundation Scholarship for their support.

References

1 M. J. Solomon, P. L. Larsen and A. Varshavsky, *Cell*, 1988, **53**, 937–947.
2 P. C. Dedon, J. A. Soults, C. D. Allis and M. A. Gorovsky, *Anal. Biochem.*, 1991, **197**, 83–90.
3 P. C. Dedon, J. A. Soults, C. D. Allis and M. A. Gorovsky, *Mol Cell Biol*, 1991, **11**, 1729–1733.
4 S. I. Grewal and D. Moazed, *Science*, 2003, **301**, 798–802.
5 M. Esteller, *Nat. Rev. Genet.*, 2007, **8**, 286–298.
6 E. N. Gal-Yam, Y. Saito, G. Egger and P. A. Jones, *Annu. Rev. Med.*, 2008, **59**, 267–280.
7 M. Esteller, *N. Engl. J. Med.*, 2008, **358**, 1148–1159.
8 F. Miao, I. G. Gonzalo, L. Lanting and R. Natarajan, *J. Biol. Chem.*, 2004, **279**, 18091–18097.
9 F. Miao, D. D. Smith, L. Zhang, A. Min, W. Feng and R. Natarajan, *Diabetes*, 2008, **57**, 3189–3198.
10 M. F. Fraga, E. Ballestar, A. Villar-Garea, M. Boix-Chornet, J. Espada, G. Schotta, T. Bonaldi, C. Haydon, S. Ropero, K. Petrie, N. G. Iyer, A. Perez-Rosado, E. Calvo, J. A. Lopez, A. Cano, M. J. Calasanz, D. Colomer, M. A. Piris, N. Ahn, A. Imhof, C. Caldas, T. Jenuwein and M. Esteller, *Nat. Genet.*, 2005, **37**, 391–400.
11 J. C. Wang, M. K. Derynck, D. F. Nonaka, D. B. Khodabakhsh, C. Haqq and K. R. Yamamoto, *Proc. Natl. Acad. Sci. U. S. A.*, 2004, **101**, 15603–15608.
12 A. Testa, G. Donati, P. Yan, F. Romani, T. H. Huang, M. A. Vigano and R. Mantovani, *J. Biol. Chem.*, 2005, **280**, 13606–13615.
13 J. M. Hearnes, D. J. Mays, K. L. Schavolt, L. Tang, X. Jiang and J. A. Pietenpol, *Mol. Cell. Biol.*, 2005, **25**, 10148–10158.
14 Y. Wang, H. R. Krishnan, A. Ghezzi, J. C. Yin and N. S. Atkinson, *PLoS Biol.*, 2007, **5**, e265.
15 J. Comley, in *SBS 16th Annual Conference & Exhibition*, Phoenix, Arizona, 2010.
16 L. P. O'Neill, M. D. VerMilyea and B. M. Turner, *Nat. Genet.*, 2006, **38**, 835–841.
17 L. G. Acevedo, A. L. Iniguez, H. L. Holster, X. Zhang, R. Green and P. J. Farnham, *BioTechniques*, 2007, **43**, 791–797.
18 J. D. Nelson, O. Denisenko and K. Bomsztyk, *Nat. Protoc.*, 2006, **1**, 179–185.
19 J. A. Dahl and P. Collas, *Front. Biosci.*, 2007, **12**, 4925–4931.
20 J. A. Dahl and P. Collas, *Stem Cells*, 2007, **25**, 1037–1046.
21 S. Flanagin, J. D. Nelson, D. G. Castner, O. Denisenko and K. Bomsztyk, *Nucleic Acids Res.*, 2008, **36**, e17.
22 P. J. Park, *Nat. Rev. Genet.*, 2009, **10**, 669–680.
23 Making The ChIP Grades, http://www.epigenie.com/Insights/Making-The-ChIP-Grades-Millipore-ChIP-AbPlus.html..
24 A. R. Wu, J. B. Hiatt, R. Lu, J. L. Attema, N. A. Lobo, I. L. Weissman, M. F. Clarke and S. R. Quake, *Lab Chip*, 2009, **9**, 1365–1370.
25 J. S. Marcus, W. F. Anderson and S. R. Quake, *Anal. Chem.*, 2006, **78**, 3084–3089.
26 J. S. Marcus, W. F. Anderson and S. R. Quake, *Anal. Chem.*, 2006, **78**, 956–958.
27 T. L. Kawahara, N. A. Rapicavoli, A. R. Wu, K. Qu, S. R. Quake and H. Y. Chang, *PLoS Genet.*, 2011, **7**, e1002153.
28 T. L. Kawahara, E. Michishita, A. S. Adler, M. Damian, E. Berber, M. Lin, R. A. McCord, K. C. Ongaigui, L. D. Boxer, H. Y. Chang and K. F. Chua, *Cell*, 2009, **136**, 62–74.
29 J. A. Dahl and P. Collas, *Nat. Protoc.*, 2008, **3**, 1032–1045.
30 J. A. Dahl and P. Collas, *Nucleic Acids Res.*, 2008, **36**, e15.
31 J. L. Attema, P. Papathanasiou, E. C. Forsberg, J. Xu, S. T. Smale and I. L. Weissman, *Proc. Natl. Acad. Sci. U. S. A.*, 2007, **104**, 12371–12376.
32 M. S. Hayden and S. Ghosh, *Genes Dev.*, 2004, **18**, 2195–2224.
33 S. L. Foster, D. C. Hargreaves and R. Medzhitov, *Nature*, 2007, **447**, 972–978.
34 T. Kouzarides, *Cell*, 2007, **128**, 693–705.
35 J. Xu, *Curr Protoc Mol Biol*, 2005, **Chapter 28, Unit 28 21.**
36 B. E. Reubinoff, M. F. Pera, C. Y. Fong, A. Trounson and A. Bongso, *Nat. Biotechnol.*, 2000, **18**, 399–404.
37 G. Schatten, J. Smith, C. Navara, J. H. Park and R. Pedersen, *Nat. Methods*, 2005, **2**, 455–463.
38 J. A. Thomson, J. Itskovitz-Eldor, S. S. Shapiro, M. A. Waknitz, J. J. Swiergiel, V. S. Marshall and J. M. Jones, *Science*, 1998, **282**, 1145–1147.
39 J. A. Thomson and V. S. Marshall, *Curr. Top. Dev. Biol.*, 1998, **38**, 133–165.

Published OnlineFirst January 24, 2011; DOI:10.1158/0008-5472.CAN-10-3367

Cancer Research

MYC Phosphorylation, Activation, and Tumorigenic Potential in Hepatocellular Carcinoma Are Regulated by HMG-CoA Reductase

Zhongwei Cao, Hua Fan-Minogue, David I. Bellovin, et al.

Cancer Res 2011;71:2286-2297. Published OnlineFirst January 24, 2011.

Published OnlineFirst January 24, 2011; DOI:10.1158/0008-5472.CAN-10-3367

Therapeutics, Targets, and Chemical Biology

Cancer Research

MYC Phosphorylation, Activation, and Tumorigenic Potential in Hepatocellular Carcinoma Are Regulated by HMG-CoA Reductase

Zhongwei Cao[1], Hua Fan-Minogue[2], David I. Bellovin[1], Aleksey Yevtodiyenko[1], Julia Arzeno[1], Qiwei Yang[1], Sanjiv Sam Gambhir[2], and Dean W. Felsher[1]

Abstract

MYC is a potential target for many cancers but is not amenable to existing pharmacologic approaches. Inhibition of 3-hydroxy-3-methylglutaryl-coenzyme A reductase (HMG-CoA reductase) by statins has shown potential efficacy against a number of cancers. Here, we show that inhibition of HMG-CoA reductase by atorvastatin (AT) blocks both MYC phosphorylation and activation, suppressing tumor initiation and growth *in vivo* in a transgenic model of MYC-induced hepatocellular carcinoma (HCC) as well as in human HCC-derived cell lines. To confirm specificity, we show that the antitumor effects of AT are blocked by cotreatment with the HMG-CoA reductase product mevalonate. Moreover, by using a novel molecular imaging sensor, we confirm that inhibition of HMG-CoA reductase blocks MYC phosphorylation *in vivo*. Importantly, the introduction of phosphorylation mutants of MYC at Ser62 or Thr58 into tumors blocks their sensitivity to inhibition of HMG-CoA reductase. Finally, we show that inhibition of HMG-CoA reductase suppresses MYC phosphorylation through Rac GTPase. Therefore, HMG-CoA reductase is a critical regulator of MYC phosphorylation, activation, and tumorigenic properties. The inhibition of HMG-CoA reductase may be a useful target for the treatment of MYC-associated HCC as well as other tumors. *Cancer Res; 71(6); 2286–97. ©2011 AACR.*

Introduction

Hepatocellular carcinoma (HCC) is one of the most common and generally incurable malignancies with an estimated 9% 5-year survival rate (1). Hepatocellular carcinogenesis is strongly associated with hepatitis B and C virus (HBV and HCV) infection and other pathologic conditions resulting in liver regeneration (2), which, in turn, facilitates the activation of specific oncogenes, most notably *MYC* (c-MYC; 3). Thus, targeted inactivation of MYC may be an effective therapy for HCC (4–6). Indeed, we have reported recently that the conditional inactivation of MYC can be sufficient to induce sustained regression of HCC (7). However, there is no existing therapy that targets MYC for the treatment of any cancer.

Authors' Affiliations: [1]Division of Medical Oncology, Departments of Medicine and Pathology and [2]Departments of Radiology, Bioengineering and Materials Sciences and Engineering, Molecular Imaging Program at Stanford, Stanford University, Stanford, California

Note: Supplementary data for this article are available at Cancer Research Online (http://cancerres.aacrjournals.org/).

Z. Cao, H. Fan-Minogue, D.I. Bellovin, and A. Yevtodiyenko have contributed equally to this work.

Corresponding Author: Dean W. Felsher, Stanford University School of Medicine, 269 Campus Drive, CCSR 1105, Stanford, CA 94305. Phone: 650-498-5269; Fax: 650-725-1420; E-mail: dfelsher@stanford.edu

doi: 10.1158/0008-5472.CAN-10-3367

The *MYC* protooncogene family is composed of *c-MYC, N-MYC*, and *L-MYC* and has been shown to impact almost every aspect of tumorigenesis, including promoting unrestricted cell proliferation, inhibiting cell differentiation, reducing cell adhesion, and enhancing metastasis, genomic instability, and angiogenesis (8, 9). *MYC* functions as an oncogene upon overexpression, either due to increased expression of the *myc* gene or due to increased stability of the MYC protein. MYC protein stability is regulated as follows (10): through the ubiquitin/26S proteasome pathway and the sequential phosphorylation of MYC at serine 62 (S62) and threonine 58 (T58). The phosphorylation of S62 is mediated by the MAPK/ERK (mitogen activated protein kinase/extracellular signal regulated kinase) pathway and contributes to the stabilization of MYC. Subsequent phosphorylation of T58, mediated by GSK3β, promotes ubiquitin-dependent MYC degradation once S62 is dephosphorylated (11–13). Mutations in these phosphorylation sites that stabilize MYC protein have been identified in human cancers, thereby highlighting the importance of S62 and T58 phosphorylation as regulators of MYC in tumorigenesis (14, 15). Hence, targeting MYC phosphorylation could be useful as an anticancer therapy.

The enzyme 3-hydroxy-3-methylglutaryl-coenzyme A reductase (HMG-CoA reductase) controls the rate-limiting step in the mevalonate (MV) pathway that is essential for cholesterol biosynthesis (16). Statins were initially utilized to inhibit HMG-CoA reductase as a means to reduce the serum cholesterol level (16). However, many studies have shown that inhibition of

Published OnlineFirst January 24, 2011; DOI:10.1158/0008-5472.CAN-10-3367

HMG-CoA reductase also has antitumor efficacy both *in vitro* and *in vivo* in multiple tumor types (17–20), including colorectal cancer (21, 22), breast cancer (23), melanoma (24), and lymphoma (25). Statins have been suggested to block tumor cell growth through the inhibition of proliferation and angiogenesis, induction of apoptosis, and repression of tumor metastasis (26).

Statins may mediate their anticancer properties through inhibition of the synthesis of lipid isoprenoid intermediates, including farnesyl pyrophosphate (FPP) and geranylgeranyl pyrophosphate (GGPP), which are produced downstream of the MV pathway (19). Generally, FPP activates the Ras GTPase family whereas GGPP activates the Rho/Rac family by prenylating and anchoring them on the cell membrane (27). Both Ras (12, 27) and Rho/Rac family members (28) are required to phosphorylate MYC. Hence, we speculated that by inhibiting these pathways, statins might therefore block MYC activation.

Here we show that the inhibition of HMG-CoA reductase by atorvastatin (AT) inhibits MYC phosphorylation and activation and thereby blocks MYC-induced HCC onset and tumor maintenance. Moreover, by using a novel molecular imaging sensor that noninvasively detects MYC phosphorylation, we found, both *in vitro* in human HCC cells and *in vivo* in mice, that AT inhibits MYC phosphorylation. Furthermore, the introduction of mutant *MYC* alleles that cannot be phosphorylated on S62 or T58 prevented AT from inhibiting the *in vivo* tumor growth of HCC. Finally, we provide evidence suggesting that AT may mediate these effects on MYC phosphorylation and activation by inhibiting Rac GTPase. Therefore, HMG-CoA reductase seems to be a critical regulator of MYC activation and may have potent activity against MYC-induced cancers.

Materials and Methods

Antibodies

The antibody to Ki67 was obtained from BD Biosciences; c-MYC, Cdk4, E2F1, and Rac1 antibodies were obtained from Santa Cruz Biotechnology; phospho-c-MYC was obtained from Cell Signaling Technology; antibodies to Tubulin and HA were from Sigma-Aldrich. Horseradish peroxidase–conjugated sheep anti-mouse IgG and sheep anti-rabbit IgG were obtained from GE Healthcare and biotinylated anti-mouse IgG was from BD Biosciences.

Cell lines

The Huh7 and HepG2 cell lines were obtained from the American Type Culture Collection originally characterized by DNA profile and cytogenetic analysis and were passaged for less than 6 months *in vitro*.

Transgenic mice

The Tet System was used previously to generate transgenic mice that conditionally express human c-MYC cDNA in hepatocytes, as described (7). MYC expression was induced by removing doxycycline (Dox, 100 μg/mL) from the drinking water of mice. All animals were maintained and treated in accordance with the policies of Stanford University.

AT treatment

AT (prescription formulation; Pfizer Inc.) was resuspended in PBS. It was administered orally in 100 mg/kg doses with or without 20 mg/kg MV 3 times a week, using 20-mm feeding needles (Popper and Sons). PBS was administered as a negative control. Purified AT (Sequoia Research Products) resuspended in 100% DMSO was used for *in vitro* studies.

Histology and immunohistochemistry

Tissues were fixed in 10% buffered formalin and embedded in paraffin. Sections of 5 μm were stained with hematoxylin-eosin (H&E) or analyzed by immunohistochemistry using the antibody to Ki67. DAB (3,3′-diaminobenzidine; Vector Laboratories) was used to achieve color development.

Proliferation assay

Cells were seeded in 24-well plates (5,000 cells/well) and incubated overnight. Next, cells were treated with PBS, AT (0.5, 1.0, 2.5, 5.0, 10, or 25 μmol/L), 10 or 25 μmol/L AT and 100 μmol/L MV, 10 or 25 μmol/L AT and 10 μmol/L FPP, or 10 or 25 μmol/L AT and 10 μmol/L GGPP for 96 hours. Cell proliferation was evaluated using the MTT assay. Data were from 6 replicated experiments.

Quantitative real-time PCR

HCC cells were treated with PBS, 20 ng/mL Dox, 10 μmol/L AT, or 10 μmol/L AT and 100 μmol/L MV for 24 hours. Total mRNA from HCC cells was extracted and purified using the RNeasy Mini Kit from Qiagen and quantified by spectrophotometer (Beckman Coulter). cDNA was reverse-transcribed from 2 μg of total mRNA using oligo-d(T) primers. Real-time PCR analysis was done in an ABI PRIZM analyzer (Applied Biosystems).

Cell membrane fractionation and protein isolation

Cells (2×10^8) were washed 3 times with PBS and extracted in lysis buffer (50 mmol/L Tris, 50 mmol/L NaCl, 2 mmol/L EDTA, 1 mmol/L $MgCl_2$, 10 mmol/L NaF, 1 mmol/L DTT, pH 7.4). Lysates were centrifuged at 36,000 rpm for 40 minutes, using Beckman L8-70M ultracentrifuge. The membrane pellet was solubilized in immunoprecipitation buffer (0.15 mol/L NaCl, 1% Triton X-100, 0.1% SDS, 0.5% sodium deoxycholate, 10 mmol/L Tris-HCl, pH 7.4) and incubated at 4°C for 30 minutes. The solution was centrifuged at 15,000 rpm for 10 minutes, and the supernatant was collected as the membrane protein fraction.

Viral infection

Ad-c-MYC^{WT}, Ad-c-MYC^{S62A}, and Ad-c-MYC^{T58A} viruses were kindly provided as a gift from Dr. Rosalie C. Sears (Oregon Health & Science University, Portland, OR). Briefly, Ad-c-MYC^{WT}, Ad-c-MYC^{S62A}, and Ad-c-MYC^{T58A} adenovirus were cloned by inserting c-MYC^{WT} (Ad-c-MYC^{WT}), c-MYC^{S62A} (Ad-c-MYC^{S62A}), and c-MYC^{T58A} (Ad-c-MYC^{T58A}) cDNA into the pADEasy-1 backbone (Stratagene). Transplanted tumor cells were infected as previously described (29). Briefly, SCID mice were injected with hepatocellular

Published OnlineFirst January 24, 2011; DOI:10.1158/0008-5472.CAN-10-3367

carcinoma cells isolated from LAP-tTA/TRE-MYC transgenic mice. Tumor masses were injected at 3 sites with Ad-c-MYC^{WT} or Ad-c-MYC^{T58A} once every week. Successful infection was confirmed by green fluorescent protein (GFP) coexpression in tumors (Supplementary Information, Fig. S9). Mice were treated with 100 μg/mL Dox to inactivate transgenic MYC expression. Tumor growth was measured using calipers 3 times a week for 3 weeks after viral injection.

Immunoprecipitation and immunoblotting

Cells were lysed in immunoprecipitation buffer (0.15 mol/L NaCl, 1% Triton X-100, 0.1% SDS, 0.5% sodium deoxycholate, 10 mmol/L Tris-HCl, pH 7.4) and cleared lysates were immunoprecipitated with 2 μg HA antibody. The precipitated proteins were resolved by SDS-PAGE, transferred to nitrocellulose, and blotted with the antibodies indicated in the figures. Total MYC and phospho-MYC level were detected by immunoblotting, and their optical density (OD) was measured and normalized to actin band OD. The MYC phosphorylation level was determined by the ratio between phospho-MYC and total MYC.

Molecular imaging of MYC phosphorylation

A bioluminescent sensor system that can noninvasively detect c-MYC phosphorylation was utilized to detect the AT inhibitory effect in intact cells and living mice. The sensor system utilizes the fact that S62 phosphorylation of MYC is required for its interaction with GSK3β and detects the protein interaction between GSK3β and MYC to indirectly report the MYC phosphorylation, using a split Firefly luciferase (FL) complementation system (30). Specific GSK3β and MYC fragments are fused with the inactive C-terminal and N-terminal fragment of the split FL, respectively (GSK35-433-CFL/NFL-c-Myc). Phosphorylation-induced interaction between GSK3β and MYC brings the 2 split fragments into close proximity and recovery of the luciferase activity.

The sensor system has been validated both in intact cells and in mouse xenograft model, which is described in an independent article (31). For *in vitro* imaging, the sensor plasmids were transiently transfected into HuH7 and HepG2 cells, using Superfect (Qiagen) and Lipofectamine 2000 (Invitrogen) reagent, respectively. Renilla luciferase (*RL*) gene was cotransfected for the control of the transfection efficiency. Twenty-four hours after transfection, cells were treated with AT with different concentration as indicated for 18 hours. Bioluminescent imaging (BLI) was conducted in IVIS 50 (Caliper Life Science) after adding 45 μg/mL D-Luciferin (Promega) to the cells. Cells were lysed for RL assay (Promega) and Western blotting analysis after imaging. For *in vivo* liver tumor imaging, we used a hydrodynamic injection method as previously described (32). Briefly, 2 mL of saline solution containing 25 μg of the MYC sensor plasmid with CMV promoter was injected into the tail vein within 8 seconds. Mice were imaged in IVIS 200, 22 hours after injection, based on time course of the sensor expression as determined in control experiments (Supplementary Information, Figs. S6 and S7).

Results

Inhibition of HMG-CoA reductase by AT suppresses MYC-induced HCC

The effects of inhibition of HMG-CoA reductase were examined on HCC growth *in vitro* and *in vivo* by administering AT to multiple HCC tumor cell lines derived from the LAP-tTA/TRE-MYC transgenic mice, a previously described conditional transgenic model of MYC-induced HCC, using the Tet-system (7), in addition to human HCC cell lines. The murine cell lines were all generated from HCC isolated from dual transgenic animals. These cell lines are dependent upon high levels of human MYC expression, which can be inactivated upon treatment with Dox. Hence, in these transgenic tumor-derived cell lines, as a positive control for MYC inactivation, we used Dox to induce the suppression of transgenic MYC. Doses of AT used for our experiments were comparable with previously published studies (33, 34). Moreover, as control for nonspecific effects of statins, we confirmed that effects were reversed with cotreatment with the enzyme product of HMG-CoA reductase MV. Note that because of marked differences in the pharmacokinetics between mouse and human, AT doses in mice are approximately 50-fold higher than the pharmacologically equivalent dose in humans (35, 36).

First, AT inhibited the *in vitro* proliferation of the MYC-induced murine cell line HCC 3-4 as measured by the MTT assay (Fig. 1A and Supplementary Information, Fig. S2A; 75% decrease at 10 μmol/L and 92% decrease at 25 μmol/L AT at 96 hours of AT treatment, $P < 0.0001$ each). Also, AT decreased the number of cells in S and G_2/M phases from 38% to 26%, as assessed by propidium iodide (PI) staining (Fig. 1B, $P = 0.01$), and reduced Ki67 immunofluorescence from 81.4% to 31.2% following 48 hours of 10 μmol/L AT treatment (Fig. 1C, $P < 0.0001$). Importantly, the effects of AT on proliferation and cell-cycle arrest were rescued by cotreatment with MV, the immediate downstream target of HMG-CoA reductase (Fig. 1A–C), confirming these effects are specific to inhibition of the cholesterol biosynthesis pathway. Moreover, AT was found to similarly inhibit proliferation and induce cell-cycle arrest and apoptosis in 2 independently derived murine HCC cell lines, EC4 and HCC 4-4, in a dose-dependent manner (Supplementary Information, Figs. S1–S3). Thus, AT inhibits proliferation and induces apoptosis of murine HCC tumor cells *in vitro*.

Second, AT inhibited the growth of the murine HCC 3-4 cell line transplanted into syngeneic mice by up to 80% compared with treatment by PBS or AT and MV (Fig. 1D and E, $P = 0.0003$). Note, that FVB/N mice treated with 100 mg/kg AT did not exhibit any general toxicity and, in particular, had normal liver histology and serum bilirubin levels, showing that the clinical effects are not secondary nonspecific hepatotoxicity (Supplementary Information, Fig. S4). Therefore, inhibition of HMG-CoA reductase by AT has potent *in vivo* antitumor activity against murine MYC-induced HCC.

Third, we interrogated the ability of AT to suppress growth in Huh7 cells, a human HCC cell line. AT blocked the *in vitro* growth of Huh7 cells over a 96-hour time course (Fig. 2A and Supplementary Information, Fig. S2B; 69% decrease at 10

Published OnlineFirst January 24, 2011; DOI:10.1158/0008-5472.CAN-10-3367

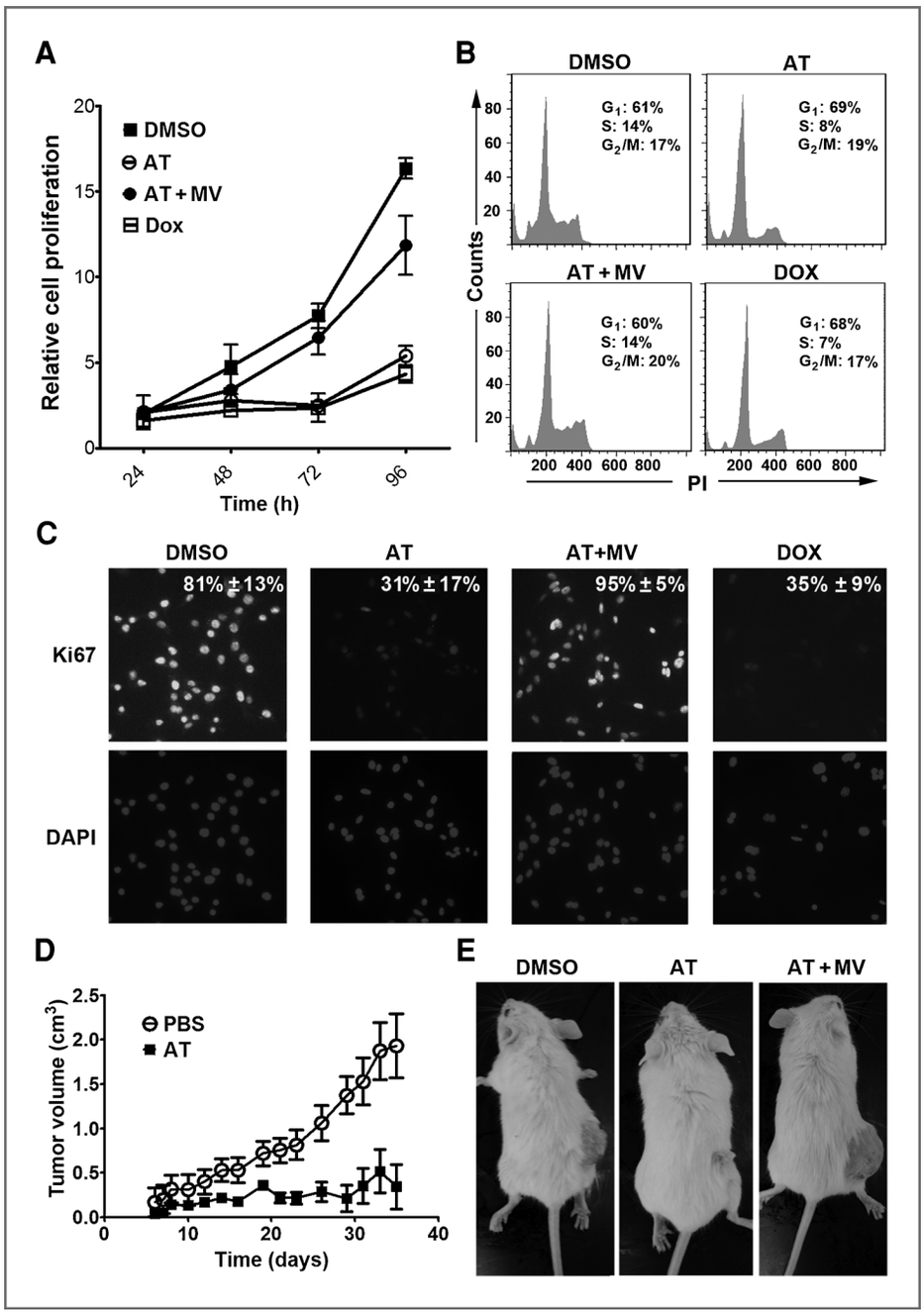

Figure 1. Inhibition of HMG-CoA reductase by AT suppresses growth of MYC-induced HCC *in vitro* and *in vivo*. A, AT inhibits the proliferation of a MYC-induced tumor-derived cell line, HCC 3-4. MTT assay was conducted every 24 hours for 4 days on HCC cells treated with 10 μmol/L AT, AT plus 100 μmol/L MV, or DMSO as a vehicle control. Cells were also treated with Dox to inactivate transgenic MYC as a positive control. All experiments were repeated 3 times ($P < 0.0001$). Error bars, SD. B, AT induces cell-cycle arrest in murine HCC as assessed by fluorescence-activated cell-sorting analysis of PI-stained cells ($P = 0.01$). Cells were treated with 10 μmol/L AT, AT plus MV, DMSO, or Dox for 48 hours. C, immunofluorescence for Ki67 on HCC cells treated with 10 μmol/L AT for 48 hours shows that statin treatment inhibits HCC proliferation ($P < 0.0001$). D, AT inhibits growth of MYC-induced HCC cells *in vivo*. Murine HCC cells were subcutaneously transplanted into FVB/N mice treated with PBS ($n = 5$) or AT ($n = 5$). $P = 0.0003$. Error bars, SD. E, representative images of mice treated with PBS (left), AT (middle), or AT plus MV (right) show that AT suppresses growth of MYC-induced HCC *in vivo*.

μmol/L and 86% decrease at 25 μmol/L AT, $P < 0.0001$ each) while inhibiting cell-cycle progression (Fig. 2B; 75% reduction in S phase, $P = 0.003$) and reducing Ki67 positivity (Fig. 2C; 58% reduction, $P < 0.0001$) following 48 hours of 10 μmol/L AT treatment. Moreover, AT suppressed the *in vivo* growth of Huh7 cells (Fig. 2D; PBS vs. AT, $P = 0.03$; AT vs. AT + MV, $P = 0.04$; PBS vs. AT + MV, $P = 0.8$). Cotreatment with MV blocked the effects of statin treatment, confirming that the inhibition of human HCC by AT is specific to the suppression of HMG-CoA reductase (Fig. 2A–D).

Finally, we evaluated the ability of HMG-CoA reductase inhibition to block the initiation of MYC-induced HCC growth *in vivo* in the LAP-tTA/TRE-MYC transgenic mice treated with PBS, AT, or AT with MV (Fig. 3A, left). Treatment with 100 mg/kg AT versus PBS significantly delayed tumor onset and increased survival (Fig. 3A; median survival increased from 80 to 147 days, $P < 0.005$). Importantly, MV treatment prevented AT from inhibiting tumorigenesis (Fig. 3A). Gross pathology revealed that AT markedly reduced the size and frequency of tumor nodules (Fig. 3B, left). H&E staining

Published OnlineFirst January 24, 2011; DOI:10.1158/0008-5472.CAN-10-3367

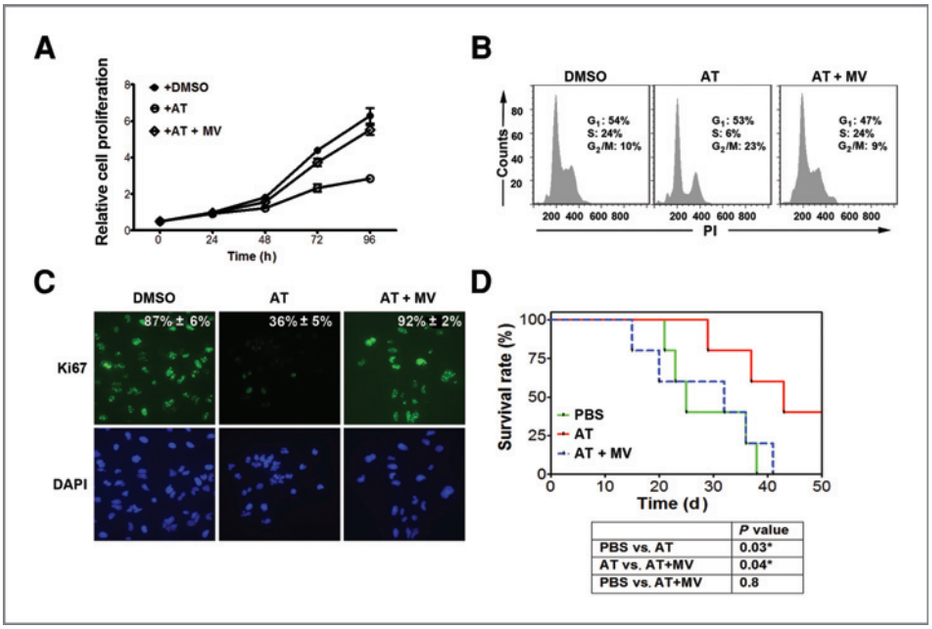

Figure 2. Blocking HMG-CoA reductase via AT inhibits growth of human HCC cells *in vitro* and *in vivo*. A, MTT analysis of the human HCC cell line Huh7 treated with 10 μmol/L AT shows significant inhibition of growth *in vitro* ($P < 0.0001$). Error bars, SD. B, fluorescence-activated cell-sorting analysis of PI-stained Huh7 cells reveals that AT suppresses cell-cycle progression ($P = 0.0003$). Cells were treated with 10 μmol/L AT for 48 hours. C, Huh7 cells treated with 10 μmol/L AT for 48 hours were examined by immunofluorescence for Ki67, showing statin-induced reduction in proliferative cells ($P < 0.0001$). D, Huh7 cells were transplanted intraperitoneally into SCID mice, and host animals were treated with PBS, AT, or AT with MV. A Kaplan–Meier curve shows a significant increase in survival of animals treated with AT (PBS vs. AT, $P = 0.03$; AT vs. AT + MV, $P = 0.04$; PBS vs. AT + MV, $P = 0.8$).

revealed histologically normal liver tissue in AT-treated mice, suggesting a robust inhibition of disease onset (Fig. 3B, middle). AT-treated animals also exhibited evidence of inhibited cell proliferation, as indicated by reduced Ki67 staining compared with PBS-treated mice (Fig. 3B, right; 8 ± 3 positive cells vs. 422 ± 23 positive cells per field, $P < 0.02$). Hence, inhibition of HMG-CoA reductase by AT is potent at inhibiting MYC-induced liver tumorigenesis.

Inhibition of HMG-CoA reductase suppresses MYC phosphorylation, stability, and transactivation

MYC activation has been shown to be regulated by phosphorylation (12). Thus, we considered that AT might exert its antineoplastic effects by inhibiting MYC phosphorylation. Indeed, AT, but not AT with MV, was found to induce a dose-dependent downregulation of MYC phosphorylation *in vitro* upon 24 hours treatment (Fig. 4A; 29% reduction at 0.5 μmol/L, 34% at 1.0 μmol/L, 79% at 2.5 μmol/L, 83% at 5.0 μmol/L, 94% at 10 μmol/L, and 97% at 25 μmol/L AT; $P = 0.004$) as well as *in vivo* (Fig. 4B; 93% reduction). Moreover, AT blocked MYC phosphorylation in MYC-induced murine lymphoma, osteosarcoma, and lung cancer, as well as in human breast cancer cell lines (data not shown). In turn, the dephosphorylation was associated with a reduction in MYC protein levels *in vitro* (Fig. 4A; 17% reduction at 0.5 μmo/L, 40% at 1.0 μmol/L, 9% at 2.5 μmol/L, 41% at 5.0 μmol/L, 69% at 10 μmol/L, and 91% at 25 μmol/L AT, $P = 0.002$) and *in vivo* (Fig. 4B; 57% reduction, $P = 0.04$). Importantly, the inhibition of MYC phosphorylation by AT not only reduced MYC levels but also seemed to dramatically inhibit MYC transcriptional activation, as illustrated by the reduced mRNA expression of canonical target genes *ODC* and *nucleolin*, both in murine (Fig. 4C; 72% reduction for *ODC*, $P = 0.003$; 76% reduction for *nucleolin*, $P = 0.03$) and in human HCC upon 24 hours of 10 μmol/L AT treatment (Fig. 4D; 64% reduction for *ODC*, $P = 0.016$; 59% reduction for *nucleolin*, $P = 0.008$; Supplementary Information, Fig. S8B). Thus, the inhibition of HMG-CoA reductase blocks MYC phosphorylation, reduces MYC protein levels, and inhibits MYC transactivation.

Noninvasive molecular imaging to measure *in vivo* MYC phosphorylation

To evaluate the effects of inhibition of HMG-CoA reductase on MYC phosphorylation *in situ* in a living host, we utilized a novel molecular imaging sensor system (31). The sensor system consists of 2 parts: (i) a peptide corresponding to the phosphoregulated domain of MYC fused to the N-terminal domain of FL and (ii) the C-terminal domain of FL fused to a peptide fragment of GSK3β that recognizes phospho-MYC (Fig. 5A). When coexpressed in an intact cell, MYC phosphorylation can be detected via interaction between the MYC and GSK3β peptides, thereby localizing the N- and C-termini of FL in close proximity, conferring luciferase activity. RL is cotransfected as a control for transfection efficiency. The full-length FL was also transfected independently into these cells as a control for the direct effect of AT on luciferase activity. We confirmed that this imaging method could detect the dose-dependent

Published OnlineFirst January 24, 2011; DOI:10.1158/0008-5472.CAN-10-3367

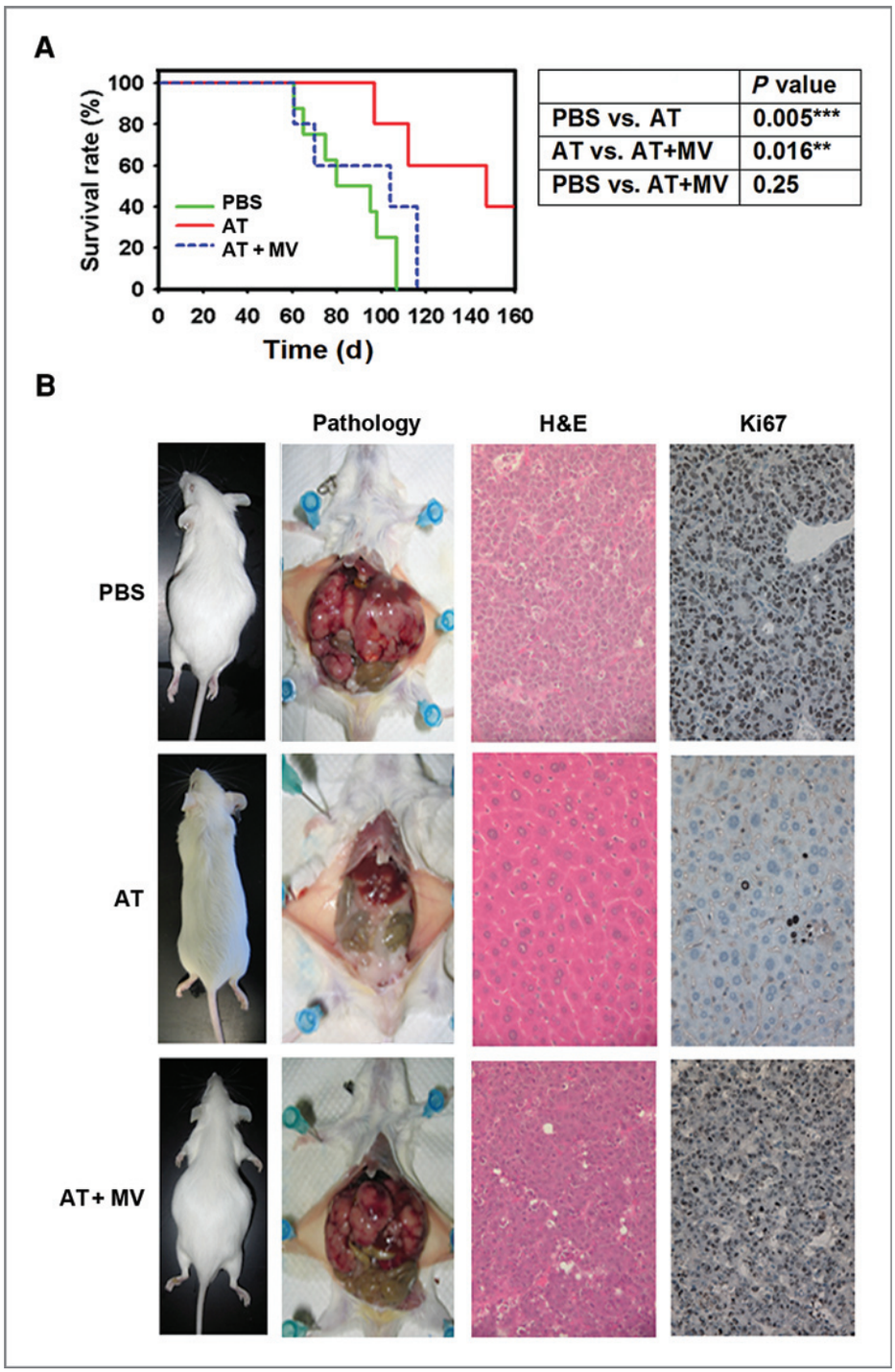

Figure 3. AT inhibition of HMG-CoA reductase suppresses MYC-induced hepatocellular tumorigenesis. A, Kaplan–Meier survival curves of adult LAP-tTA/TRE-MYC mice treated with PBS ($n = 8$), 100 mg/kg AT ($n = 5$), or AT with MV ($n = 5$) 3 times per week show a significant increase in survival of animals treated with AT (PBS vs. AT, $P = 0.005$; AT vs. AT/MV, $P = 0.016$; PBS vs. AT/MV, $P = 0.25$). B, representative photographs from each treatment group are shown. Gross anatomy reveals inhibition of tumor onset due to AT treatment. H&E staining shows that normal hepatic structure is maintained by AT treatment (middle), which was reversed by MV treatment (bottom). Immunohistochemistry for Ki67 shows a significant inhibition of proliferation due to AT (right, 8 ± 3 positive cells vs. 422 ± 23 positive cells per hpf; $P < 0.02$).

reduction of MYC phosphorylation in human Huh7 and HepG2 cells upon 18 hours of AT treatment (Fig. 6B and C and Supplementary Information, Fig. S5, $P < 0.0001$).

Next, this imaging sensor was used to monitor MYC phosphorylation *in vivo*. The sensor system was introduced in liver cells of LAP-tTA/TRE-MYC mice by hydrodynamic injection. Two groups of transgenic mice ($n = 3$ each) had MYC activated at the same time and were treated with either AT or PBS. The MYC sensor was imaged at days 0 and 15 posttreatment. The PBS-treated group showed no significant change of the sensor signal, whereas the AT-treated group showed 72% reduction of the sensor signal at day 15 of treatment (Fig. 5D and E; AT-treated mice day 0 vs. day 15, $P = 0.038$; PBS-treated day 0 vs. day 15, $P = 0.638$). Notably,

Published OnlineFirst January 24, 2011; DOI:10.1158/0008-5472.CAN-10-3367

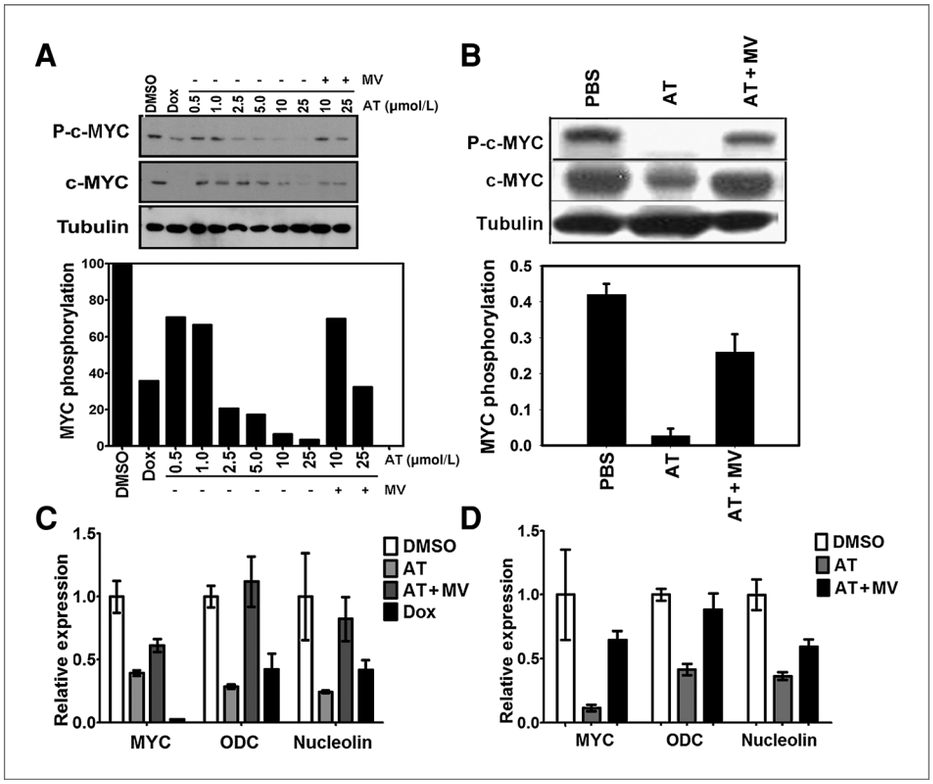

Figure 4. Inhibition of HMG-CoA reductase blocks MYC activity by reducing its phosphorylation. A, murine HCC cells were treated with indicated concentrations of AT with or without MV for 24 hours. MYC phosphorylation and expression are suppressed by AT treatment in a dose-dependent manner ($P = 0.002$). Values are normalized to the DMSO control. Representative immunoblots are shown. B, primary liver tissue of transgenic animals shows an AT-dependent suppression of MYC phosphorylation ($P = 0.04$). Representative immunoblots are shown. Error bars, SD. C, quantitative PCR analysis of MYC and MYC target gene mRNA expression in murine HCC cells. Treatment of cells with 10 μmol/L AT for 24 hours results in reduced MYC transcriptional activity as shown by 72% and 76% reduction in expression of *ODC* and *nucleolin* ($P = 0.003$, $P = 0.03$), respectively. Expression is normalized to ubiquitin and values are relative to DMSO control. Error bars, SD. D, quantitative PCR analysis of MYC and MYC target gene mRNA expression in human Huh7 cells. Cells were treated with 10 μmol/L AT for 24 hours and show suppression of MYC transcriptional activity as assessed by reductions of 64% for *ODC* and 59% for *nucleolin* expression ($P = 0.016$, $P = 0.008$), respectively. Expression is normalized to ubiquitin and values are relative to DMSO control. Error bars, SD.

AT-mediated inhibition of MYC phosphorylation *in vivo* was associated with a 44% and 56% downregulation in the expression of downstream target genes, *E2F1* and *Cdk4* (Supplementary Information, Fig. S8A), further showing the inhibition of MYC activity. Hence, a novel imaging sensor was used to show that the inhibition of HMG-CoA reductase by AT inhibits MYC phosphorylation *in vivo*.

MYC phosphomutants confer resistance to the inhibition of HMG-CoA reductase

To examine whether inhibition of MYC phosphorylation mediates the anticancer effect of AT, we introduced phosphomutants of MYC into HCC tumor cell lines. First, recombinant adenovirus was used to express MYC that is mutated with either an alanine substitution at either S62 or T58 (Ad-MYC^{S62A} and Ad-MYC^{T58A}) and hence cannot be regulated by phosphorylation at these sites (37). AT treatment at 10 μmol/L for 24 hours dramatically suppressed WT MYC but failed to significantly inhibit protein levels of either S62A MYC or T58A MYC (Fig. 6A; MYC^{S62A} vs. MYC^{S62A} + AT, $P = 0.09$; MYC^{T58A} vs. MYC^{T58A}+AT, $P = 0.06$). Thus, we concluded that phosphoregulation through either S62 or T58 is necessary for AT to suppress MYC expression.

Using an antibody specific for phospho-S62 and -T58, we show that AT inhibits phosphorylation in T58A MYC similar to wild-type MYC (Fig. 6A, 62% reduction for MYC^{WT}, $P = 0.01$; 68% reduction for MYC^{T58A}, $P = 0.008$). These data show that the reduction of phospho-MYC by AT seems to occur by preventing S62 phosphorylation. However, the reduction of total MYC protein cannot occur without T58 phosphorylation. In addition, HCC cells expressing the S62A MYC mutant were less sensitive whereas cells expressing T58A MYC were completely insensitive to the inhibition of proliferation upon AT treatment (Fig. 6B, 26% reduction for WT, $P < 0.001$; 17% reduction for S62, $P < 0.0001$; no reduction for T58, $P = 0.8$). Thus, inhibition of HMG-CoA reductase suppresses MYC activation in a phosphorylation-dependent manner.

Next, we investigated whether the MYC phosphomutants could suppress the ability of the inhibition of HMG-CoA reductase to block HCC tumor growth *in vivo*. Syngeneic hosts were transplanted with MYC-induced HCC cells that were then injected with Ad-MYC^{WT}, Ad-MYC^{S62A}, or Ad-MYC^{T58A}. Tumor

Published OnlineFirst January 24, 2011; DOI:10.1158/0008-5472.CAN-10-3367

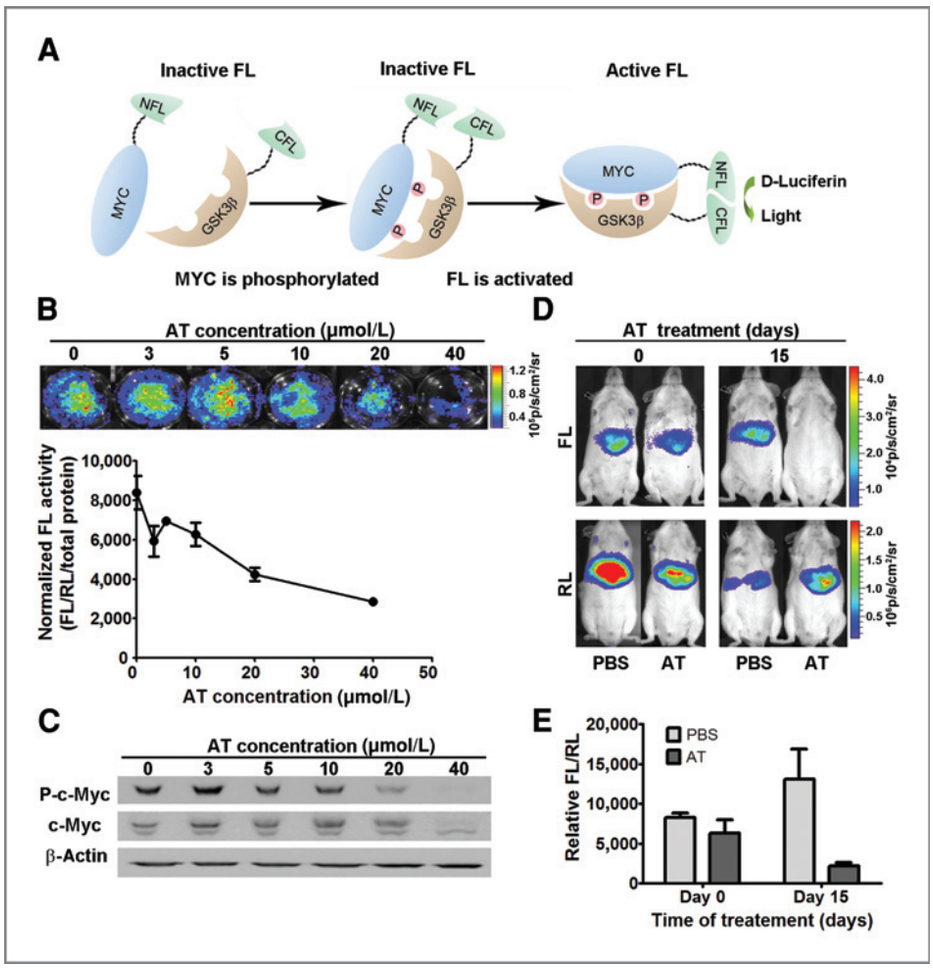

Figure 5. A novel bioluminescence c-MYC phosphosensor noninvasively shows AT-dependent inhibition of MYC phosphorylation. A, the N- and C-termini of split FL were fused to the phosphoregulated domain of MYC and the corresponding domain of GSK3β, respectively. Phosphorylation of the MYC peptide results in FL enzymatic activity. B, Huh7 cells were transfected with the MYC phosphorylation sensor and treated with AT. BLI shows a dose-dependent inhibition of phospho-MYC ($P < 0.0001$). FL activity was normalized to RL activity and plotted against AT concentration. Error bars, SD. C, Western blotting confirms AT-dependent suppression of phospho-MYC in transfected Huh7 cells. D, LAP-tTA/TRE-MYC transgenic mice were treated with AT or PBS ($n = 3$), and hydrodynamic injection of the phosphosensor followed by BLI shows AT-dependent inhibition of MYC phosphorylation *in vivo* (AT-treated mice day 0 vs. day 15, $P = 0.038$; PBS-treated mice day 0 vs. day 15, $P = 0.638$). E, FL activity was normalized to RL activity and plotted against days of AT treatment.

growth was monitored in response to AT, PBS, or AT with MV treatment (Fig. 6C). The adenoviral delivery of the MYC phosphomutants was confirmed by coexpression of GFP (Supplementary Information, Fig. S9). To suppress the conditional transgenic MYC expression, mice were treated with Dox, thereby resulting in the effective knock-in of the Ad-MYC^{WT}, Ad-MYC^{S62A}, or Ad-MYC^{T58A} constructs into the HCC cells. HCC growth upon injection of Ad-MYC^{WT} showed 66% inhibition by 100 mg/kg AT but not by PBS or AT and MV treatment (Fig. 6D, left, PBS vs. AT, $P = 0.01$; AT vs. AT + MV, $P = 0.007$). However, HCC tumors that were injected with Ad-MYC^{S62A} exhibited only 44% inhibition of tumor growth upon treatment with AT (Fig. 6D, middle, PBS vs. AT, $P = 0.02$; AT vs. AT + MV, $P = 0.03$). Tumors that were injected with Ad-MYC^{T58A} showed complete rescue from sensitivity to AT treatment (Fig. 6D, right, PBS vs. AT, $P = 0.56$; AT vs. AT + MV, $P = 0.03$). Therefore, MYC phosphorylation is necessary for AT to inhibit MYC-induced HCC tumor growth.

Inhibition of HMG-CoA reductase may block MYC activity through Rac GTPase

We examined whether the inhibition of HMG-CoA reductase blocks MYC activation through Rac GTPases. Statins block production of the isoprenoids farnesyl pyrophosphate and geranylgeranyl pyrophosphate (23, 38, 39). FPP prenylates the Ras, Rheb, and PTP4A3 family whereas GGPP prenylates the Rac, Rho, and Cdc42 family of small GTPases (16). Previous studies suggest that Ras and Rac/Rho families of GTPases may contribute to the regulation of MYC phosphorylation (25). Thus, the inhibition of HMG-CoA reductase is likely to prevent MYC phosphorylation through these GTPases

To explore the role of GTPases in mediating inhibition of MYC phosphorylation, we conducted several experiments. First, to control GTPase activity, we supplemented growth media with either FPP or GGPP before 96 hours AT treatment of MYC-induced murine HCC cells *in vitro*. Both MV and GGPP restored HCC cell proliferation to levels similar to those of DMSO controls (Fig. 7A; DMSO vs. AT + MV, $P = 0.07$; DMSO vs. GGPP, $P = 0.053$), whereas FPP showed significantly less reduction in AT-mediated growth inhibition (DMSO vs. FPP, $P < 0.002$). Similarly, in Huh7 cells, GGPP was more potent than FPP in abrogating the effect of 96 hours of 10 μmol/L AT on proliferation (Fig. 7B; 16% reduction for DMSO vs. AT + MV, $P < 0.01$; 16% reduction for DMSO vs. GGPP, $P < 0.01$; 32% reduction for DMSO vs. FPP, $P < 0.001$). In addition, GGPP was more efficient in rescuing the transcription of multiple MYC

Published OnlineFirst January 24, 2011; DOI:10.1158/0008-5472.CAN-10-3367

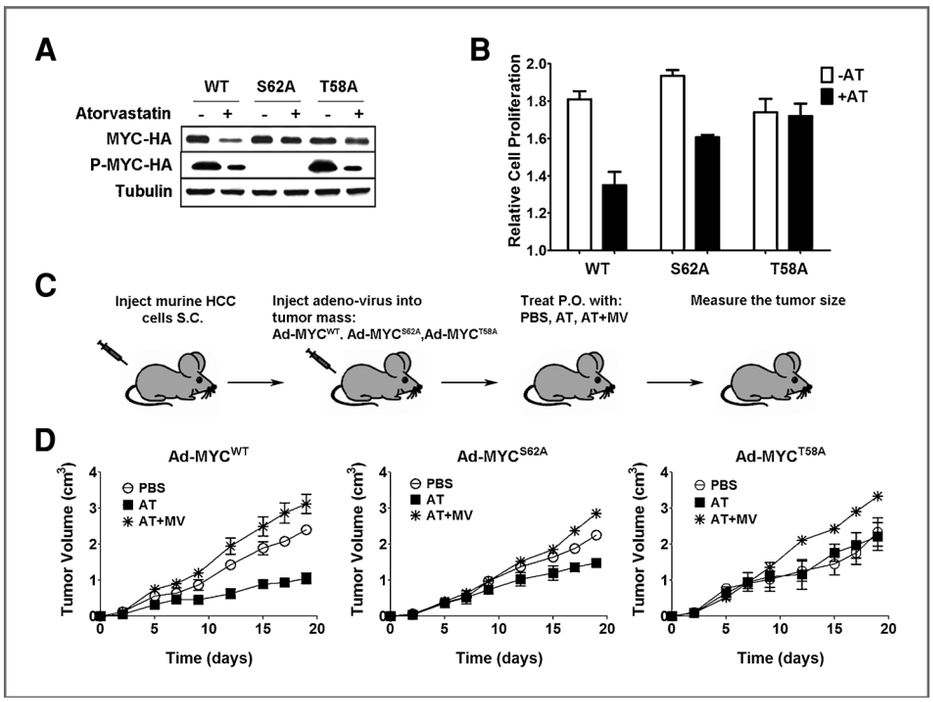

Figure 6. HCC transduced with S62A or T58A MYC phosphomutants show reduced sensitivity to HMG-CoA reductase inhibition. A, murine HCC cells were infected with Ad-MYC^{WT} (WT), Ad-MYC^{S62A} (S62A), or Ad-MYC^{T58A} (T58A) adenovirus, and HA-tagged MYC was immunoprecipitated using an antibody to the HA tag. Immunoblot analysis suggests that AT-dependent phosphoregulation of MYC is via S62. However, the inhibition of protein stability requires both S62 and T58 phosphoregulation. Cells were treated with 10 μmol/L AT for 24 hours. B, S62A partially and T58A completely abrogated AT inhibition of cell proliferation (S62A: PBS vs. AT, $P < 0.0001$; T58A: PBS vs. AT, $P = 0.8$). Error bars, SD. C, HCC cells isolated from transgenic animals were transplanted into SCID mice, injected with Ad-MYC^{WT}, Ad-MYC^{S62A}, or Ad-MYC^{T58A} once every week, and orally treated with PBS ($n = 6$), AT ($n = 5$), or AT with MV ($n = 5$) together with Dox. Tumor growth was measured 3 times per week. D, *in vivo* growth kinetics of HCC infected with Ad-MYC^{WT} show that AT inhibits tumor growth *in vivo* (left, PBS vs. AT, $P = 0.01$; AT vs. AT + MV, $P = 0.007$). Error bars, SD. Infection with Ad-MYC^{S62A} partially rescues growth inhibition due to AT (middle, PBS vs. AT, $P = 0.02$; AT vs. AT + MV, $P = 0.03$). Error bars, SD. Ad-MYC^{T58A} completely rescues AT-mediated growth inhibition of HCC (right, PBS vs. AT, $P = 0.56$; AT vs. AT + MV, $P = 0.03$). Error bars, SD.

target genes, including *Cdk4* and *E2F1*, than FPP following 24 hours of 10 μmol/L AT treatment (Supplementary Information, Fig. S10, 40%–45% reduction for FPP, $P < 0.001$; 25%–60% increase for GGPP, $P < 0.03$). MYC phosphorylation was restored to levels similar to PBS-treated controls when media containing 10 μmol/L AT was supplemented with GGPP but not with FPP (Fig. 7C; 76% reduction for FPP, $P = 0.001$; 21% reduction for GGPP, $P = 0.02$). Therefore, inhibition of HMG-CoA reductase seems to inactivate MYC through the inhibition of the Rho/Rac pathway.

Finally, we examined the potential role of the Rac/Rho/Cdc42 pathway as a mechanism by which AT suppresses MYC activation. First, we investigated whether AT was influencing the membrane localization of Rac1. Indeed, 24-hour treatment with 10 μmol/L AT resulted in the delocalization of Rac1 from the plasma membrane (Fig. 7D; 83% reduction for AT, $P < 0.001$). As a control, we showed that treatment with MV blocked these effects, as did treatment with GGPP (Fig. 7D; no change for PBS vs. AT + MV, $P = 0.08$; 37% increase for PBS vs. GGPP, $P < 0.03$). Notably, AT had little effect on Ras localization (data not shown). Second, using a Rac pull-down assay, 24 hours of 10 μmol/L AT treatment was shown to reduce Rac1 activity by 77% (Fig. 7E). Thus, the inhibition of HMG-CoA reductase by AT seems to suppress activation of the Rac pathway, suggesting that AT in blocks MYC phosphorylation and activation via inhibition of Rac.

Discussion

Here, we show that MYC phosphorylation, activation, and thereby tumorigenic potential are regulated by HMG-CoA reductase. In particular, the inhibition of HMG-CoA reductase by statins suppresses MYC phosphorylation and activation. The consequences of these effects on MYC include preventing HCC initiation as well as inhibiting the *in vivo* growth of established murine and human HCC tumors. Moreover, statins, by blocking HMG-CoA reductase, inhibit GTPase activity, thereby resulting in MYC dephosphorylation and inactivation, which is essential for their anticancer therapeutic effect (Fig. 7F). Hence, the inhibition of HMG-CoA reductase by AT may be an effective strategy for the inhibition of MYC in the treatment and prevention of HCC.

Importantly, we confirmed the antitumor effects of statins that we observed both *in vitro* and *in vivo* were specific to HMG-CoA reductase because they could be readily reversed by cotreatment with MV. We note that the AT doses we used in

Published OnlineFirst January 24, 2011; DOI:10.1158/0008-5472.CAN-10-3367

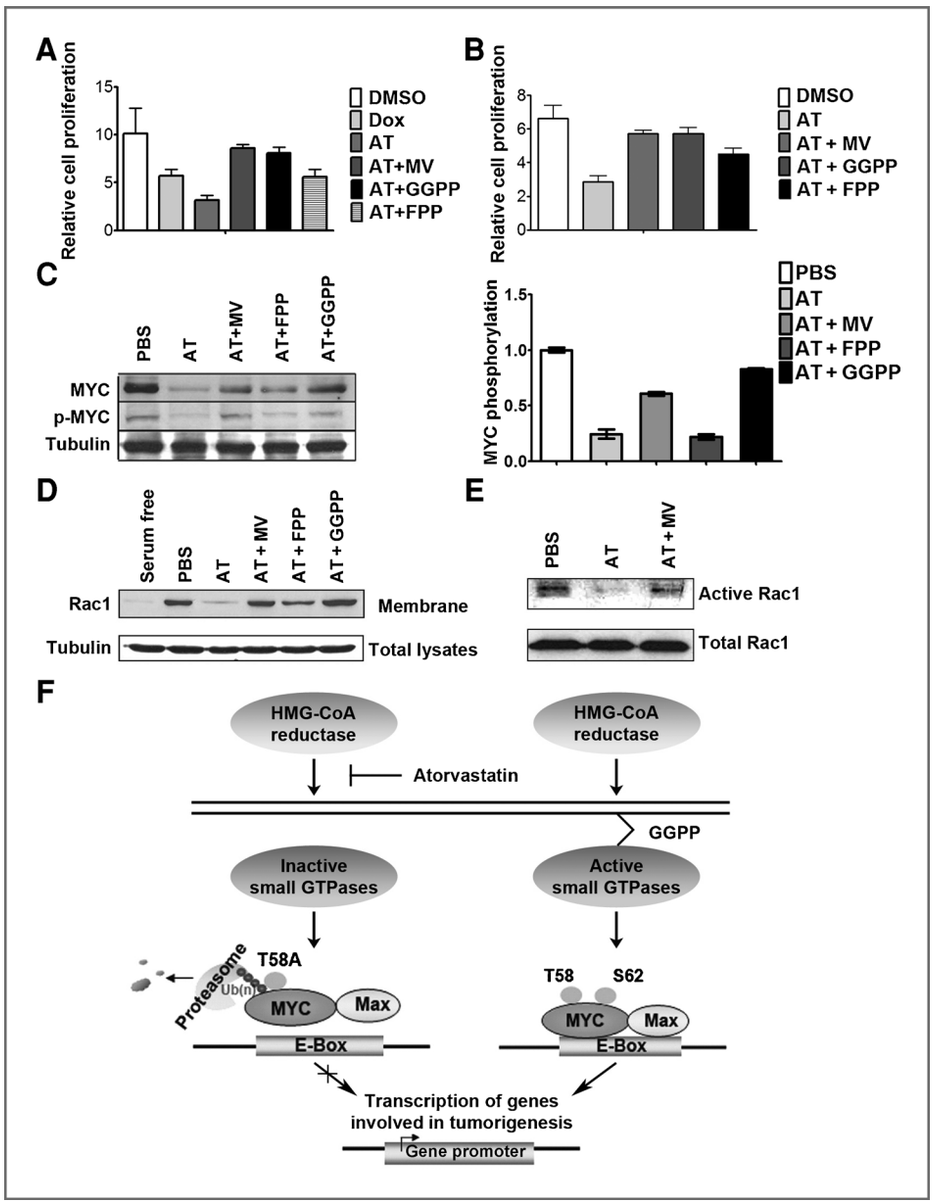

Figure 7. HMG-CoA reductase influences MYC phosphorylation through a Rac GTPase–dependent mechanism. A, suppression of murine HCC growth *in vitro* upon 10 μmol/L AT treatment for 96 hours is rescued by GGPP treatment, as assessed by MTT (DMSO vs. AT + MV, $P = 0.07$; DMSO vs. GGPP, $P = 0.053$, DMSO vs. FPP, $P = 0.002$). Error bars, SD. B, GGPP treatment rescues the AT-dependent suppression in human HCC cell growth upon 10 μmol/L AT treatment (DMSO vs. AT + MV, $P = 0.01$; DMSO vs. GGPP, $P = 0.01$, DMSO vs. FPP, $P < 0.001$). Error bars, SD. C, GGPP treatment rescues AT-dependent inhibition of MYC phosphorylation. Representative immunoblots are shown. Error bars, SD. D, GGPP treatment prevents the decrease in the membrane accumulation of Rac induced by 24 hours of 10 μmol/L AT. E, AT treatment inhibits Rac activity, which was reduced by 77% as measured by pull-down assay. F, our results suggest a model in which inhibition of HMG-CoA reductase by AT blocks prenylation and activation of small GTPases, specifically including Rac. AT-mediated inhibition of Rac likely results in reduction of phospho-S62 MYC. Dephosphorylation at S62 in the context of phospho-T58 thereby results in the ubiquitin-mediated degradation of MYC. As such, AT treatment ultimately results in the inhibition of MYC oncogenic activity and suppressed hepatocellular carcinogenesis.

mice seem to be higher than generally used in humans. However, it is well known that, because of differences in the pharmacokinetics, murine doses have to be 50-fold higher than in humans (35, 36). Moreover, we confirmed that the antitumor dose of AT did not exhibit *in vivo* toxicity (Supplementary Information, Fig. S4) and hence is likely to be achievable in humans.

The inhibition of HMG-CoA reductase was found to block MYC phosphorylation. First, AT treatment blocks MYC phosphorylation in murine and human HCC cells both *in vitro* and *in vivo*. Concomitant treatment with MV abrogates the ability of AT to block MYC phosphorylation and activation and mediate its suppressive effect on HCC growth, indicating that the antineoplastic effect of AT is *via* the inhibition of HMG-CoA reductase (Fig. 4). Second, a novel phosphorylation sensor was used to show *in situ* in human HCC cells and *in vivo* in living mice (Fig. 5). This phosphosensor may be a useful approach to develop therapies that target MYC phosphorylation. Third, mutations in 2 MYC phosphorylation sites, specifically S62 and T58, blocks the ability of AT to inhibit tumor growth *in vivo*. Therefore, HMG-CoA reductase activity is important to the regulation of MYC phosphorylation.

We infer that MYC phosphorylation is an essential component of the mechanism by which statins mediate their antineoplastic properties. The introduction of mutant MYC alleles in HCC tumor cells reduced their sensitivity to statins *in vitro* and *in vivo*. Specifically, the differential ability of S62A and T58A MYC to block the effect of AT *in vitro* and *in vivo* (Fig. 6)

Published OnlineFirst January 24, 2011; DOI:10.1158/0008-5472.CAN-10-3367

suggests that AT-mediated reduction in phospho-S62 would therefore result in MYC phosphorylated at only T58, which is rapidly degraded in a ubiquitin-dependent manner (12, 13). Our results are consistent with a role of S62 and T58 phosphorylation in MYC stability and transcriptional activity and, most important, their role in tumorigenesis (12). However, we note that S62/T58 phosphorylation has not always been found to regulate MYC stability (40). We conclude that the inhibition of MYC phosphorylation may be important to the mechanism by which the inhibition of HMG-CoA reductase by statins exerts its antineoplastic properties.

Many reports suggest that statins have antineoplastic properties (25, 41–44). Many mechanisms have been proposed including the inhibition of the ErbB2 pathway (45), the blocking of the interaction between the lymphocyte function–associated antigen and intercellular cell adhesion molecule-1 (46), the suppression of geranylgeranylation of the Rho family proteins (47), and the prevention of the prenylation of RhoA and downstream activation of focal adhesion kinase, AKT, and β-catenin (23). Although we cannot preclude any of these possibilities, our results are consistent with the notion that the inhibition of HMG-CoA reductase by AT in HCC cells blocks MYC phosphorylation likely through the inhibition of small GTPases in the Rac pathway (Fig. 7).

Our results are the first to suggest that HMG-CoA reductase regulates MYC activation via Rac. We are currently investigating the signaling intermediates that may function between Rac and MYC to mediate the antineoplastic effect of AT. Previously, it has been suggested that Rac regulates MYC (28). Rac1 can inhibit protein phosphatase PP2A (48), which has been shown to dephosphorylate MYC at S62 (13). One possible mechanism suggested by our work is that AT inhibition of Rac can result in activation of PP2A, which subsequently dephosphorylates MYC at S62 and induces the ubiquitin-dependent degradation of T58-phosphorylated MYC (Fig. 7F).

Our results illustrate that the inhibition of HMG-CoA reductase by statins may be useful in the treatment and prevention of human HCC. HCC is increasing in incidence, has a generally dismal prognosis, and there are few treatment options (49). Statins were developed to inhibit HMG-CoA reductase in the liver to reduce cholesterol. Hence, they may be aptly suited for treating cancers of the liver. Moreover, statins are well tolerated in humans and may be useful in the prevention of HCC in patients at high risk (49). Notably, some clinical studies have suggested that that the statin pravastatin may have clinical activity in patients with HCC (50, 51), whereas other studies have not found clinical benefit (52). A possible explanation for this possible discrepancy in the benefit from statins is that clinical activity could depend upon the activation status of MYC. Also, AT may be a more effective statin for the treatment of HCC.

We conclude that MYC phosphorylation is a critical mechanism by which the inhibition of HMG-CoA reductase by statins mediates their antineoplastic effects. We have shown that a novel molecular imaging sensor may be useful for the identification through high-throughput methods of new therapeutic agents that inhibit MYC phosphorylation and activation. Importantly, statins may be effective agents to inhibit MYC function as a treatment for HCC.

Disclosure of Potential Conflicts of Interest

No potential conflicts of interest were disclosed.

Acknowledgments

We dedicate this article in memory of Julie Do. We thank Dr. Rosalie C. Sears (Oregon Health & Science University, Portland, OR) for kindly providing us with mutant MYC constructs. We also value the helpful comments provided by Dr. Stacey Adam and the members of the Felsher, Sylvester, and Gambhir laboratories.

Grant Support

This work was supported by NIH grants CA89305-01A1, CA89305-0351, CA105102, and CA112973; Department of Defense grant PR080163, the Burroughs Wellcome Fund; the Leukemia and Lymphoma Society; the Damon Runyon Foundation (D.W. Felsher); and the *in vivo* cancer molecular image center (ICMIC P50) at Stanford grant CA114747 (S.S. Gambhir, D.W. Felsher). Z. Cao was supported by an American Liver Foundation fellowship. H. Fan-Minogue is supported by an NIH R25T training grant. D.I. Bellovin is supported by the NIH under NRSA fellowship F32-CA132312.

The costs of publication of this article were defrayed in part by the payment of page charges. This article must therefore be hereby marked *advertisement* in accordance with 18 U.S.C. Section 1734 solely to indicate this fact.

Received September 15, 2010; revised January 2, 2011; accepted January 5, 2011; published OnlineFirst January 24, 2011.

References

1. Farazi PA, DePinho RA. Hepatocellular carcinoma pathogenesis: from genes to environment. Nat Rev Cancer 2006;6:674–87.
2. Fausto N, Campbell JS, Riehle KJ. Liver regeneration. Hepatology 2006;43:S45–53.
3. Riehle KJ, Campbell JS, McMahan RS, Johnson MM, Beyer RP, Bammler TK, et al. Regulation of liver regeneration and hepatocarcinogenesis by suppressor of cytokine signaling 3. J Exp Med 2008;205:91–103.
4. Coleman WB. Mechanisms of human hepatocarcinogenesis. Curr Mol Med 2003;3:573–88.
5. Lee JS, Chu IS, Mikaelyan A, Calvisi DF, Heo J, Reddy JK, et al. Application of comparative functional genomics to identify best-fit mouse models to study human cancer. Nat Genet 2004;36:1306–11.
6. Thorgeirsson SS, Factor VM, Snyderwine EG. Transgenic mouse models in carcinogenesis research and testing. Toxicol Lett 2000;112–113:553–5.
7. Shachaf CM, Kopelman AM, Arvanitis C, Karlsson A, Beer S, Mandl S, et al. MYC inactivation uncovers pluripotent differentiation and tumour dormancy in hepatocellular cancer. Nature 2004;431:1112–7.
8. Adhikary S, Eilers M. Transcriptional regulation and transformation by Myc proteins. Nat Rev Mol Cell Biol 2005;6:635–45.
9. Kaposi-Novak P, Libbrecht L, Woo HG, Lee YH, Sears NC, Coulouarn C, et al. Central role of c-Myc during malignant conversion in human hepatocarcinogenesis. Cancer Res 2009;69:2775–82.
10. Salghetti SE, Kim SY, Tansey WP. Destruction of Myc by ubiquitin-mediated proteolysis: cancer-associated and transforming mutations stabilize Myc. EMBO J 1999;18:717–26.

Published OnlineFirst January 24, 2011; DOI:10.1158/0008-5472.CAN-10-3367

11. Gregory MA, Qi Y, Hann SR. Phosphorylation by glycogen synthase kinase-3 controls c-myc proteolysis and subnuclear localization. J Biol Chem 2003;278:51606–12.
12. Sears R, Nuckolls F, Haura E, Taya Y, Tamai K, Nevins JR. Multiple Ras-dependent phosphorylation pathways regulate Myc protein stability. Genes Dev 2000;14:2501–14.
13. Yeh E, Cunningham M, Arnold H, Chasse D, Monteith T, Ivaldi G, et al. A signalling pathway controlling c-Myc degradation that impacts oncogenic transformation of human cells. Nat Cell Biol 2004;6:308–18.
14. Bhatia K, Huppi K, Spangler G, Siwarski D, Iyer R, Magrath I. Point mutations in the c-Myc transactivation domain are common in Burkitt's lymphoma and mouse plasmacytomas. Nat Genet 1993;5:56–61.
15. Smith-Sorensen B, Hijmans EM, Beijersbergen RL, Bernards R. Functional analysis of Burkitt's lymphoma mutant c-Myc proteins. J Biol Chem 1996;271:5513–8.
16. Demierre MF, Higgins PD, Gruber SB, Hawk E, Lippman SM. Statins and cancer prevention. Nat Rev Cancer 2005;5:930–42.
17. Shibata MA, Ito Y, Morimoto J, Otsuki Y. Lovastatin inhibits tumor growth and lung metastasis in mouse mammary carcinoma model: a p53-independent mitochondrial-mediated apoptotic mechanism. Carcinogenesis 2004;25:1887–98.
18. Feleszko W, Mlynarczuk I, Balkowiec-Iskra EZ, Czajka A, Switaj T, Stoklosa T, et al. Lovastatin potentiates antitumor activity and attenuates cardiotoxicity of doxorubicin in three tumor models in mice. Clin Cancer Res 2000;6:2044–52.
19. Goldstein JL, Brown MS. Regulation of the mevalonate pathway. Nature 1990;343:425–30.
20. Wong WW, Dimitroulakos J, Minden MD, Penn LZ. HMG-CoA reductase inhibitors and the malignant cell: the statin family of drugs as triggers of tumor-specific apoptosis. Leukemia 2002;16:508–19.
21. Narisawa T, Morotomi M, Fukaura Y, Hasebe M, Ito M, Aizawa R. Chemoprevention by pravastatin, a 3-hydroxy-3-methylglutaryl-coenzyme A reductase inhibitor, of *N*-methyl-*N*-nitrosourea-induced colon carcinogenesis in F344 rats. Jpn J Cancer Res 1996;87:798–804.
22. Agarwal B, Rao CV, Bhendwal S, Ramey WR, Shirin H, Reddy BS, et al. Lovastatin augments sulindac-induced apoptosis in colon cancer cells and potentiates chemopreventive effects of sulindac. Gastroenterology 1999;117:838–47.
23. Denoyelle C, Albanese P, Uzan G, Hong L, Vannier JP, Soria J, et al. Molecular mechanism of the anti-cancer activity of cerivastatin, an inhibitor of HMG-CoA reductase, on aggressive human breast cancer cells. Cell Signal 2003;15:327–38.
24. He L, Mo H, Hadisusilo S, Qureshi AA, Elson CE. Isoprenoids suppress the growth of murine B16 melanomas *in vitro* and *in vivo*. J Nutr 1997;127:668–74.
25. Shachaf CM, Perez OD, Youssef S, Fan AC, Elchuri S, Goldstein MJ, et al. Inhibition of HMGCoA reductase by atorvastatin prevents and reverses MYC-induced lymphomagenesis. Blood 2007;110:2674–84.
26. Hindler K, Cleeland CS, Rivera E, Collard CD. The role of statins in cancer therapy. Oncologist 2006;11:306–15.
27. Jackson SM, Ericsson J, Edwards PA. Signaling molecules derived from the cholesterol biosynthetic pathway. Subcell Biochem 1997;28:1–21.
28. Chiariello M, Marinissen MJ, Gutkind JS. Regulation of c-myc expression by PDGF through Rho GTPases. Nat Cell Biol 2001;3:580–6.
29. Mesri M, Wall NR, Li J, Kim RW, Altieri DC. Cancer gene therapy using a survivin mutant adenovirus. J Clin Invest 2001;108:981–90.
30. Paulmurugan R, Gambhir SS. Monitoring protein-protein interactions using split synthetic Renilla luciferase protein-fragment-assisted complementation. Anal Chem 2003;75:1584–9.
31. Fan-Minogue H, Cao Z, Paulmurugan R, Chan CT, Massoud TF, Felsher DW, et al. Noninvasive molecular imaging of c-Myc activation in living mice. Proc Natl Acad Sci U S A 107:15892–7.
32. Liu F, Song Y, Liu D. Hydrodynamics-based transfection in animals by systemic administration of plasmid DNA. Gene Ther 1999;6:1258–66.
33. Black AE, Sinz MW, Hayes RN, Woolf TF. Metabolism and excretion studies in mouse after single and multiple oral doses of the 3-hydroxy-3-methylglutaryl-CoA reductase inhibitor atorvastatin. Drug Metab Dispos 1998;26:755–63.
34. Lubet RA, Boring D, Steele VE, Ruppert JM, Juliana MM, Grubbs CJ. Lack of efficacy of the statins atorvastatin and lovastatin in rodent mammary carcinogenesis. Cancer Prev Res (Phila) 2009;2:161–7.
35. Pinkel D. The use of body surface area as a criterion of drug dosage in cancer chemotherapy. Cancer Res 1958;18:853–6.
36. Reagan-Shaw S, Nihal M, Ahmad N. Dose translation from animal to human studies revisited. FASEB J 2008;22:659–61.
37. Lutterbach B, Hann SR. Hierarchical phosphorylation at N-terminal transformation-sensitive sites in c-Myc protein is regulated by mitogens and in mitosis. Mol Cell Biol 1994;14:5510–22.
38. Denoyelle C, Vasse M, Körner M, Mishal Z, Ganné F, Vannier JP, et al. Cerivastatin, an inhibitor of HMG-CoA reductase, inhibits the signaling pathways involved in the invasiveness and metastatic properties of highly invasive breast cancer cell lines: an *in vitro* study. Carcinogenesis 2001;22:1139–48.
39. Jakobisiak M, Bruno S, Skierski JS, Darzynkiewicz Z. Cell cycle-specific effects of lovastatin. Proc Natl Acad Sci U S A 1991; 88:3628–32.
40. Henriksson M, Bakardjiev A, Klein G, Luscher B. Phosphorylation sites mapping in the N-terminal domain of c-myc modulate its transforming potential. Oncogene 1993;8:3199–209.
41. Gniadecki R. Depletion of membrane cholesterol causes ligand-independent activation of Fas and apoptosis. Biochem Biophys Res Commun 2004;320:165–9.
42. Kureishi Y, Luo Z, Shiojima I, Bialik A, Fulton D, Lefer DJ, et al. The HMG-CoA reductase inhibitor simvastatin activates the protein kinase Akt and promotes angiogenesis in normocholesterolemic animals. Nat Med 2000;6:1004–10.
43. Weis M, Heeschen C, Glassford AJ, Cooke JP. Statins have biphasic effects on angiogenesis. Circulation 2002;105:739–45.
44. Tilkin-Mariamé AF, Cormary C, Ferro N, Sarrabayrouse G, Lajoie-Mazenc I, Faye JC, et al. Geranylgeranyl transferase inhibition stimulates anti-melanoma immune response through MHC Class I and costimulatory molecule expression. FASEB J 2005;19:1513–5.
45. Mueck AO, Seeger H, Wallwiener D. Effect of statins combined with estradiol on the proliferation of human receptor-positive and receptor-negative breast cancer cells. Menopause 2003;10:332–6.
46. Chan KK, Oza AM, Siu LL. The statins as anticancer agents. Clin Cancer Res 2003;9:10–9.
47. Agarwal B, Halmos B, Feoktistov AS, Protiva P, Ramey WG, Chen M, et al. Mechanism of lovastatin-induced apoptosis in intestinal epithelial cells. Carcinogenesis 2002;23:521–8.
48. ten Klooster JP, Leeuwen I, Scheres N, Anthony EC, Hordijk PL. Rac1-induced cell migration requires membrane recruitment of the nuclear oncogene SET. EMBO J 2007;26:336–45.
49. Altekruse SF, McGlynn KA, Reichman ME. Hepatocellular carcinoma incidence, mortality, and survival trends in the United States from 1975 to 2005. J Clin Oncol 2009;27:1485–91.
50. Graf H, Jüngst C, Straub G, Dogan S, Hoffmann RT, Jakobs T, et al. Chemoembolization combined with pravastatin improves survival in patients with hepatocellular carcinoma. Digestion 2008;78:34–8.
51. Kawata S, Yamasaki E, Nagase T, Inui Y, Ito N, Matsuda Y, et al. Effect of pravastatin on survival in patients with advanced hepatocellular carcinoma. A randomized controlled trial. Br J Cancer 2001;84:886–91.
52. Lersch C, Schmelz R, Erdmann J, Hollweck R, Schulte-Frohlinde E, Eckel F, et al. Treatment of HCC with pravastatin, octreotide, or gemcitabine—a critical evaluation. Hepatogastroenterology 2004; 51:1099–103.

Cancer Cell
Article

CD4+ T Cells Contribute to the Remodeling of the Microenvironment Required for Sustained Tumor Regression upon Oncogene Inactivation

Kavya Rakhra,[1,6] Pavan Bachireddy,[1,6,7] Tahera Zabuawala,[1] Robert Zeiser,[2] Liwen Xu,[1] Andrew Kopelman,[1] Alice C. Fan,[1] Qiwei Yang,[1] Lior Braunstein,[3] Erika Crosby,[4] Sandra Ryeom,[5] and Dean W. Felsher[1,*]
[1]Division of Oncology, Departments of Medicine, Pathology and Molecular Imaging, Stanford University School of Medicine, Stanford, CA 94305, USA
[2]Division of Bone Marrow Transplant, Department of Medicine, Stanford University School of Medicine, Stanford, CA 94305, USA
[3]Vascular Biology Program, Children's Hospital/Harvard Medical School, Boston, MA 02115, USA
[4]Department of Cancer Biology, Immunology Graduate Group, University of Pennsylvania School of Medicine, Philadelphia, PA 19104, USA
[5]Department of Cancer Biology University of Pennsylvania School of Medicine, Philadelphia, PA 19104, USA
[6]These authors contributed equally to this work
[7]Present address: Department of Medicine, Brigham & Women's Hospital/Harvard Medical School, Boston, MA 02115, USA
*Correspondence: dfelsher@stanford.edu
DOI 10.1016/j.ccr.2010.10.002

SUMMARY

Oncogene addiction is thought to occur cell autonomously. Immune effectors are implicated in the initiation and restraint of tumorigenesis, but their role in oncogene inactivation-mediated tumor regression is unclear. Here, we show that an intact immune system, specifically CD4+ T cells, is required for the induction of cellular senescence, shutdown of angiogenesis, and chemokine expression resulting in sustained tumor regression upon inactivation of the *MYC* or *BCR-ABL* oncogenes in mouse models of T cell acute lymphoblastic lymphoma and pro-B cell leukemia, respectively. Moreover, immune effectors knocked out for thrombospondins failed to induce sustained tumor regression. Hence, CD4+ T cells are required for the remodeling of the tumor microenvironment through the expression of chemokines, such as thrombospondins, in order to elicit oncogene addiction.

INTRODUCTION

The inactivation of a single oncogene is sufficient to induce sustained tumor regression in vivo through the phenomenon of oncogene addiction, as has been demonstrated experimentally in many conditional transgenic mouse model systems (Felsher, 2008; Sharma and Settleman, 2007; Weinstein and Joe, 2008) and through the development of targeted therapeutics such as Gleevec (Weinstein and Joe, 2006). Oncogene addiction is associated with proliferative arrest, apoptosis, differentiation, and cellular senescence as well as the shutdown of host programs such as angiogenesis (Felsher, 2003; Felsher and Bishop, 1999; Giuriato et al., 2006; Jain et al., 2002; Shachaf et al., 2004; Wu et al., 2007). To date, it has been presumed that oncogene inactivation induces tumor regression through cell autonomous mechanisms, independent of host effector cells.

The host immune system plays an important role in tumorigenesis. Both antigen-dependent and -independent mechanisms are implicated through multiple cellular effectors and effects on inflammation and the tumor microenvironment (Crowe et al., 2002; Shankaran et al., 2001). Indeed, it is well documented that CD8+ T cells contribute to antigen-dependent and NK cell-mediated tumor elimination (Shanker et al., 2007; van der Bruggen et al., 1991). Additionally, CD4+ T cells may also contribute to

Significance

Through transgenic mouse models of conditional oncogene inactivation, we show that the absence of an intact immune system results in a 10- to 1000-fold reduction in the rate, extent, and duration of tumor regression upon oncogene inactivation. We uncovered an unanticipated role for CD4+ T cell effectors in mediating cellular senescence and the shutdown of tumor angiogenesis and discovered a critical role for the expression of thrombospondin-1 in immune effectors. Most strategies to identify therapeutic agents utilize in vitro models or in vivo xenograft models overlooking the effect of the immune system. Our results argue for the necessity of models that include an intact host immune system to properly evaluate the potential efficacy of targeted therapeutics for maximum clinical impact.

tumor regression (Corthay et al., 2005; Qin and Blankenstein, 2000). Chemokines produced by the immune system have been shown to play an important role during tumor evolution and therapeutic response (Rossi and Zlotnik, 2000; Smyth et al., 2004).

In general, tumors coevolve with host immune effectors and chemokines through a process that has been described as immune editing (Dougan and Dranoff, 2009; Dunn et al., 2002; Dunn et al., 2006; Reiman et al., 2007; Swann et al., 2008). Immune editing has been dramatically illustrated in several models of carcinogenesis (Bui et al., 2006; Shankaran et al., 2001; Willimsky and Blankenstein, 2005). Host immune effectors also contribute to the initiation of tumorigenesis through profound effects on the tumor microenvironment (Coussens and Werb, 2002; de Visser et al., 2006). Thus, the immune system appears to play a complex role in both the initiation and restraint of tumorigenesis.

The role of the immune system in mediating tumor regression upon targeted oncogene inactivation is not known. Hosts that are immune compromised have a markedly increased incidence of many different types of cancers (Birkeland et al., 1995; Dunn et al., 2002; Pham et al., 1995). The host immune system is intimately involved not only in the promotion and prevention of neoplasia but also in determining the therapeutic response to treatment of cancer (Andreu et al., 2010; Boshoff and Weiss, 2002; Dave et al., 2004; Galon et al., 2006; Gatti and Good, 1971; Kohrt et al., 2005; Zitvogel et al., 2008). However, experimental study of therapeutics for cancer is usually performed in vitro or in vivo in immune compromised hosts, circumstances in which immune effectors are necessarily absent. These models do not account for the role of host-tumor interactions and the role of the immune system.

The *MYC* oncogene has been implicated in the pathogenesis of many human tumors (Meyer and Penn, 2008). *MYC* is involved in the etiology of many types of lymphoma including Burkitt's large cell and T cell acute lymphoblastic lymphoma (T-ALL) (Boxer and Dang, 2001; Pelengaris et al., 2002). We have previously described our conditional transgenic mouse models of *MYC*-induced T cell acute lymphoblastic lymphoma (T-ALL) (Felsher and Bishop, 1999). The inactivation of *MYC* is sufficient to induce sustained tumor regression associated with proliferative arrest, apoptosis, differentiation, cellular senescence and the shutdown of angiogenesis (Felsher and Bishop, 1999; Giuriato et al., 2006; Wu et al., 2007). Here, we show that defects in the host immune system have a profound influence on the ability of oncogene inactivation to elicit oncogene addiction.

RESULTS

Immune System Is Required for Rapid, Complete, and Sustained Tumor Regression

To interrogate if the immune system is required to elicit oncogene addiction upon *MYC* inactivation, we transplanted luciferase labeled tumors from our conditional transgenic mouse model of *MYC*-induced hematopoietic tumorigenesis into wild-type hosts and in hosts with specific defects in immune compartments: SCID, RAG2$^{-/-}$cγc$^{-/-}$, RAG2$^{-/-}$, CD4$^{-/-}$CD8$^{-/-}$, CD4$^{-/-}$CD8$^{+/+}$, CD4$^{+/+}$CD8$^{-/-}$ (Figures 1A and 1B). By using bioluminescence imaging, we could measure the kinetics of tumor regression upon *MYC* inactivation.

Tumors initially exhibited regression regardless of the host immune status (Figures 1A, 1B, and 1C). However, severely immune compromised hosts (SCID and RAG2$^{-/-}$cγc$^{-/-}$ mice deficient in the adaptive immune system and NK cells) demonstrated significantly delayed kinetics of tumor regression upon *MYC* inactivation compared with wild-type (WT) hosts (Figure 1D, SCID versus WT, $p < 0.001$) and failed to execute complete tumor elimination with up to 1000-fold more minimal residual disease (MRD) after *MYC* inactivation (Figure 1E, SCID versus WT, $p < 0.0001$; RAG2$^{-/-}$ cγc$^{-/-}$ versus WT, $p = 0.01$ at the nadir of luciferase activity upon *MYC* inactivation). Similarly, less severely immune compromised hosts also exhibited delayed kinetics (Figures 1B and 1D, RAG2$^{-/-}$ versus WT, $p = 0.02$; CD4$^{-/-}$CD8$^{-/-}$ versus WT, $p = 0.02$) and a significantly increased MRD (Figure 1E, RAG2$^{-/-}$ versus WT, $p = 0.01$; CD4$^{-/-}$CD8$^{-/-}$ versus WT, $p < 0.01$). Hence, an intact immune system is required for rapid and complete tumor regression.

To determine if host immune status influenced the frequency of tumor recurrence, we continued to observe mice for 80 days after *MYC* inactivation noting that tumors recurred at a statistically significant higher frequency in SCID, RAG2$^{-/-}$cγc$^{-/-}$, RAG2$^{-/-}$, and CD4$^{-/-}$CD8$^{-/-}$ hosts (87.5%, 100%, 100%, and 80%, respectively) compared with WT hosts (9%) (immune compromised hosts versus WT, $p < 0.0001$, also see Figure 1F). CD4$^{-/-}$ but not CD8$^{-/-}$ deficient hosts exhibited a significant influence on tumor recurrence (28.5%, 0%, respectively) (Figure 1F). Correspondingly, CD4^{+}, but not CD8^{+} T cell deficiency alone was sufficient to impede sustained tumor regression compared to WT mice (Figure 1F, WT versus CD4$^{-/-}$, $p = 0.02$). Similar results could be obtained using nonluciferase labeled tumors (Figure S1A). By qPCR analysis it was confirmed that doxycycline treatment resulted in similar suppression of transgenic *MYC* expression regardless of host immune status (Figure S1B). Hence, defects in the host immune system prevented sustained tumor regression upon *MYC* inactivation.

Immune System Is Not Required to Induce Proliferative Arrest or Apoptosis

Previously, we have shown that upon *MYC* inactivation in a transgenic model of T-ALL, tumor cells undergo proliferative arrest and apoptosis (Felsher and Bishop, 1999). We determined if the mechanism by which immune cells were contributing to the process of tumor regression was through effects on proliferation and apoptosis of tumor cells before and after *MYC* inactivation (Figures 2A and 2B). After 4 days of *MYC* inactivation, tumors from wild-type and immunodeficient hosts exhibited an overall loss of pleomorphic characteristics evidenced by a similarly marked reduction in cell size and nuclear to cytoplasmic ratio in both cohorts. Importantly, upon *MYC* inactivation, we observed marked changes in the total number of cells per field and carefully controlled for these changes in our quantification of TUNEL and Ki67 staining.

To measure apoptosis, TUNEL staining was performed. Apoptosis occurred similarly upon *MYC* inactivation regardless of host immune status (Figure 2A), suggesting that initial tumor regression occurs similarly regardless of the presence or

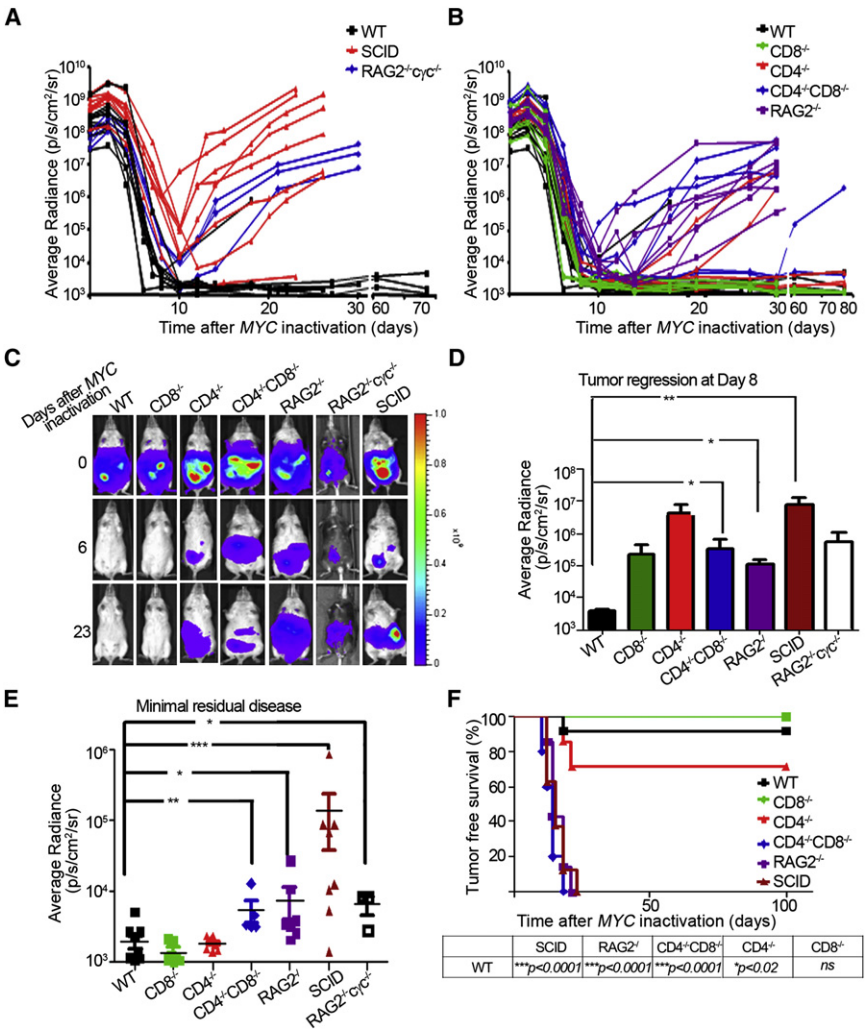

Figure 1. An Intact Immune System Is Required for Sustained Tumor Regression

(A and B) Graphical representation of tumor regression and relapse kinetics as measured by bioluminescence imaging. Luciferase-labeled tumor cell lines from our conditional mouse T-ALL model were injected s.c. into different cohorts of mice (WT, n = 11; $CD8^{-/-}$, n = 7; $CD4^{-/-}$, n = 6; $CD4^{-/-}CD8^{-/-}$, n = 5; SCID, n = 8; $RAG2^{-/-}$, n = 7; $RAG2^{-/-}c\gamma c^{-/-}$, n = 3). *MYC* was inactivated by administering doxycycline (dox) to the mice when tumors reached a comparable bioluminescence signal (10^8p/s/sr/cm^2).

(C) Bioluminescence images of tumors regressing in the different immunodeficient hosts. Data are representative of three experiments.

(D) Quantitative analysis of tumor regression in the indicated hosts, 8 days after *MYC* inactivation.

(E) Quantification of minimum residual disease in the indicated hosts. Data are presented as the minimum bioluminescence signal after *MYC* inactivation.

(F) Kaplan Meier curves of tumor-free survival in the various immunodeficient genotypes. A mouse was scored as a relapse when its tumor bioluminescence signal first began to increase after tumor regression. The log-rank test was used to compare survival curves. Data are representative of three experiments using two cell lines and one primary tumor. Statistical significance was analyzed by pooling data from all experiments (WT, n = 43; $CD8^{-/-}$, n = 20; $CD4^{-/-}$, n = 24; $CD4^{-/-}CD8^{-/-}$, n = 15; SCID, n = 15; $RAG2^{-/-}$, n = 46) (p value evaluated by unpaired Student's t test) is shown.

*p < 0.01, **p < 0.001, ***p < 0.0001. Error bars are ± SEM. See also Figure S1.

absence of an immune system. Quantification of TUNEL staining revealed a 2-fold increase in the extent of apoptosis upon *MYC* inactivation in tumors from WT hosts (Figure 2B, WT *MYC* On versus Off, p = 0.05). Moreover, the apoptosis in regressing tumors from WT hosts was not significantly different from that of regressing tumors in either $RAG2^{-/-}$ or $CD4^{-/-}$ hosts (Figure 2B, WT versus $RAG2^{-/-}$, $CD4^{-/-}$ *MYC* Off, p = 0.3 and 0.3, respectively). Finally there was a small but statistically insignificant increase in the levels of apoptosis upon *MYC* inactivation in $RAG2^{-/-}$ or $CD4^{-/-}$ hosts (Figure 2B, $RAG2^{-/-}$, $CD4^{-/-}$ *MYC* On versus Off, p = 0.07 and 0.09, respectively). Hence, the absence of the immune system may slightly impede apoptosis of tumor cells upon *MYC* inactivation.

Next, changes in cellular proliferation upon *MYC* inactivation were measured by Ki67 staining. *MYC* inactivation in tumors from WT and immunodeficient hosts resulted in a significant reduction in Ki67 staining (Figures 2A and 2B, WT, $RAG2^{-/-}$, $CD4^{-/-}$ *MYC* On *versus* *MYC* Off, p < 0.01). Interestingly, in comparison to WT hosts, $RAG2^{-/-}$ but not $CD4^{-/-}$ hosts, underwent a statistically significant further decrease in Ki67 staining upon *MYC* inactivation (WT versus $RAG2^{-/-}$ or $CD4^{-/-}$ *MYC* Off, p = 0.02 or p < 0.05, respectively). Thus, the absence of the host immune system either has no effect or modestly enhances the effect of *MYC* inactivation in inducing proliferative arrest.

Immune System Is Required to Induce Cellular Senescence and the Shutdown of Angiogenesis

We have reported that upon *MYC* inactivation tumor cells undergo cellular senescence (Wu et al., 2007) and the shutdown of angiogenesis (Giuriato et al., 2006). We examined the role of both processes. Tumors from WT hosts expressed a 20-fold increase in senescence-associated acidic β-gal (SA-β-Gal) activity upon *MYC* inactivation and demonstrated a 26- and 6-fold increase in senescence-associated markers, p16INK4a and p21, respectively, upon *MYC* inactivation (Figures 3A and 3B). In contrast, *MYC* inactivation in tumors in $RAG2^{-/-}$ and $CD4^{-/-}$ mice did not result in increased SA-β-Gal or the induction of p16INK4a or p21 (Figures 3A and 3B, WT versus $RAG2^{-/-}$ *MYC* Off SA-β-Gal, p = 0.01, p16 staining p = 0.002, p21 staining p = 0.01; WT versus $CD4^{-/-}$, *MYC* Off SA- β-Gal, p = 0.009, p16 staining, p = 0.0005, p21 staining, p = 0.004).

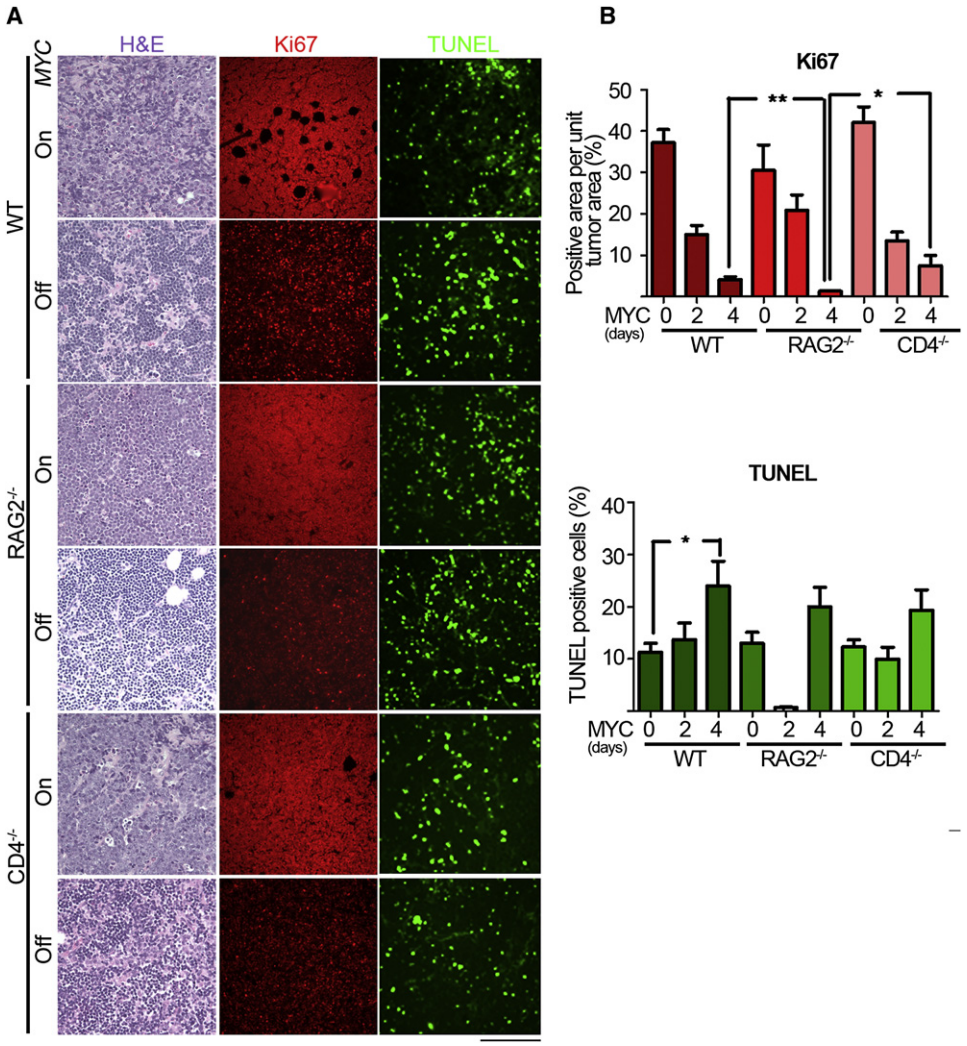

Figure 2. The Immune System Does Not Influence Apoptosis or Proliferative Arrest upon *MYC* Inactivation

(A) Micrographs of hematoxylin and eosin staining (left panel), TUNEL (middle panel), and Ki67 (right panel) immunostaining of tumors derived from untreated (*MYC* On) and 4 day dox-treated mice (*MYC* Off) from WT (top panel), RAG2$^{-/-}$ (middle panel), and CD4$^{-/-}$ (bottom panel) hosts. Scale bar = 100 μm.

(B) Quantitative representation of Ki67 (top panel) and TUNEL (bottom panel) immunostaining shown in (A) for 0, 2, and 4 days after *MYC* inactivation. Quantification of TUNEL and Ki67 immunostaining is presented as the average percentage of TUNEL-positive cells and area of Ki67-positive regions, respectively, within the tumors. At least five different fields from three different tumors injected with at least two different tumor cell lines for each different condition. Statistical significance (p value evaluated by unpaired Student's t test) is shown. *$p < 0.01$, **$p < 0.001$, ***$p < 0.0001$. Error bars are represented as ± SEM.

Thus, in immune deficient mice, *MYC* inactivation is impeded from inducing cellular senescence in tumor cells. Notably, CD4$^+$ T cells specifically appeared to be required.

We determined if an intact immune system was required for *MYC* inactivation to induce the shutdown of angiogenesis associated with the secretion of TSP-1, a potent antiangiogenic protein (Giuriato et al., 2006; Kazerounian et al., 2008; Lawler, 2000). Upon *MYC* inactivation there was a 3.5-fold induction of TSP-1 in tumors from WT hosts but not in RAG2$^{-/-}$ or CD4$^{-/-}$ hosts (Figure 4A, WT versus RAG2$^{-/-}$, CD4$^{-/-}$ *MYC* Off, $p = 0.001$). Furthermore, while tumors in WT mice demonstrated very little change in mean vascular density (MVD) as measured by CD31 staining upon *MYC* inactivation (Figure 4B), RAG2$^{-/-}$ and CD4$^{-/-}$ mice exhibited a 5- and 12-fold, respectively, increase in tumor MVD upon *MYC* inactivation (Figures 4A and 4B, RAG2$^{-/-}$ *MYC* On versus Off, $p < 0.0001$; CD4$^{-/-}$ *MYC* On versus Off, $p = 0.07$). Thus, the absence of CD4$^+$ T cells impairs the ability of *MYC* inactivation to induce cellular senescence as well as shutdown angiogenesis.

Finally, TSP-1 expression requires host immune cells and specifically CD4$^+$ T cells. Indeed, we found that TSP-1 protein expression is markedly decreased in spleens of immune compromised versus wild-type hosts (Figure S2A). Further, we show that activated CD4$^+$ T cells express TSP-1 (Figure S2B).

CD4$^+$ T Cells Home to the Tumor and Are Sufficient to Restore Sustained Tumor Regression

We examined if CD4$^+$ T cells were homing to the tumor site upon oncogene inactivation. Upon adoptive transfer into RAG2$^{-/-}$ hosts, luciferase$^+$ CD4$^+$ T cells rapidly localized to the tumor

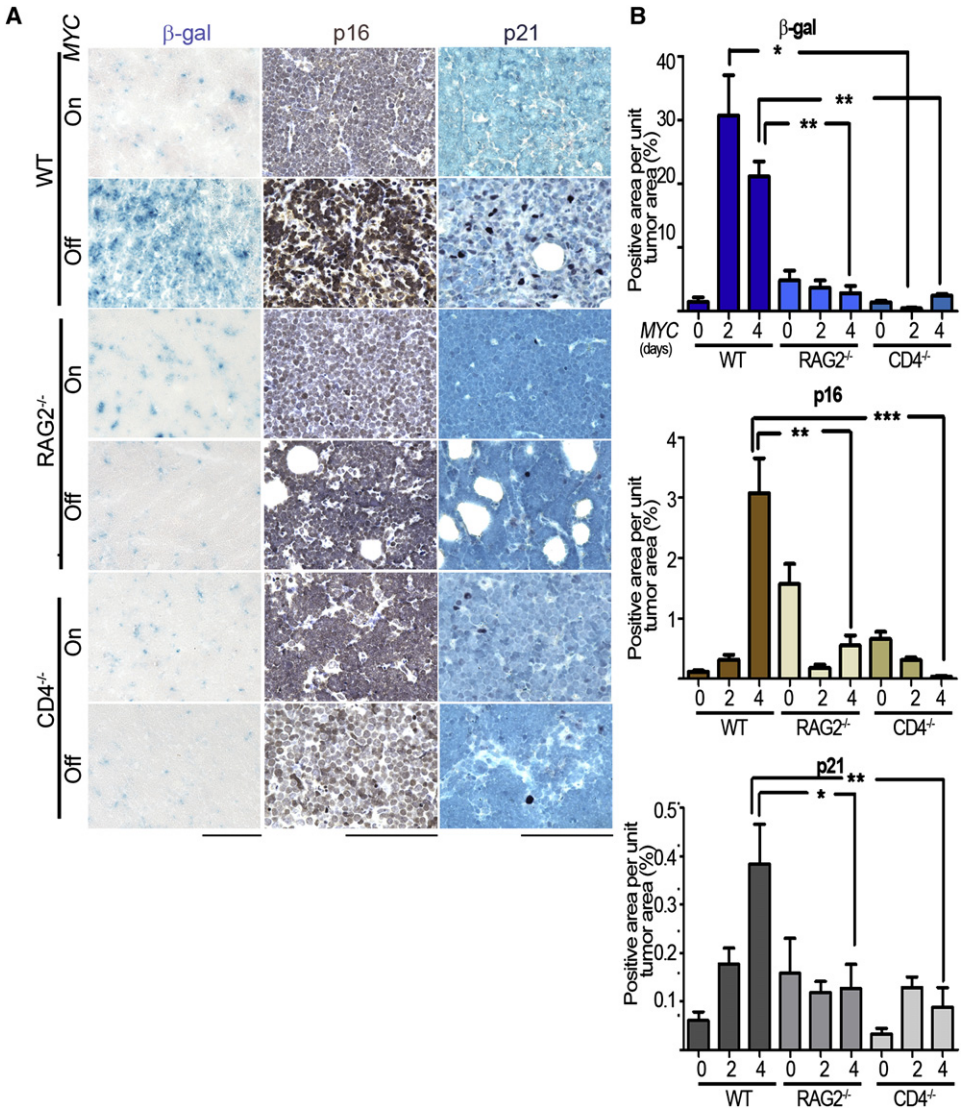

Figure 3. An Intact Immune System Is Required for the Induction of Cellular Senescence upon *MYC* Inactivation

(A) Micrographs of senescence associated β-galactosidease (SA β-gal, left panel), p16 (middle panel), and p21 (right panel) immunostaining of tumors derived from untreated (*MYC* On) and 4 day dox-treated (*MYC* Off) mice of the indicated genotypes. Scale bar = 100 μm.

(B) Quantification of SA-β-gal (top panel), p16 (middle panel), and p21 (bottom panel) staining shown in (A) for 0, 2, and 4 days after *MYC* inactivation. Quantification is presented as the average percentage of positively stained regions within the tumors. At least five different fields from three different tumors injected with at least two different tumor cell lines were analyzed for each different condition. Statistical significance (p value evaluated by unpaired Student's t test) is shown. *p < 0.01, **p < 0.001, ***p < 0.0001. Error bars are ± SEM.

site upon *MYC* inactivation as seen by bioluminescence imaging of these tumors before and after *MYC* inactivation (Figure 5A). Inactivating this oncogene causes $CD4^+$ T cells to localize at the tumor site as early as 4 days after oncogene inactivation, peak at day 12 and persist up to 3 weeks after *MYC* inactivation. Thus, *MYC* inactivation is associated with trafficking of $CD4^+$ T cells to sites of tumor involvement. Notably, $CD4^+$ T cell-depleted luciferase$^+$ splenocytes also localized to the site of the tumor upon *MYC* inactivation, suggesting the recruitment of additional host immune effector populations (Figure S3A).

Next, we evaluated if we could restore the ability of *MYC* inactivation to induce sustained tumor regression in immune compromised hosts by adoptively transferring specific lymphocyte populations into $RAG2^{-/-}$ mice. By FACS analysis, we confirmed reconstitution of effector cells (Figure S3B). As expected, $RAG2^{-/-}$ mice adoptively transferred with splenic lymphocytes exhibited sustained regression (Figure 6B). $RAG2^{-/-}$ hosts demonstrated a significant amount of MRD after *MYC* inactivation compared with WT hosts (Figures 5B and 5C, $RAG2^{-/-}$ versus WT, p = 0.007). Reconstitution of immunodeficient hosts with naive $CD8^+$ T cells continued to have a significant burden of MRD (Figure 5C, $RAG2^{-/-}CD8^+$ versus WT, p = 0.03), whereas reconstitution of $RAG2^{-/-}$ hosts with naive $CD4^+$ T cells completely eliminated MRD, similar to WT hosts upon *MYC* inactivation (Figure 5C, $RAG2^{-/-}CD4^+$ versus WT, p = 0.09). Moreover, $RAG2^{-/-}$ hosts adoptively transferred with $CD4^+$ T cells

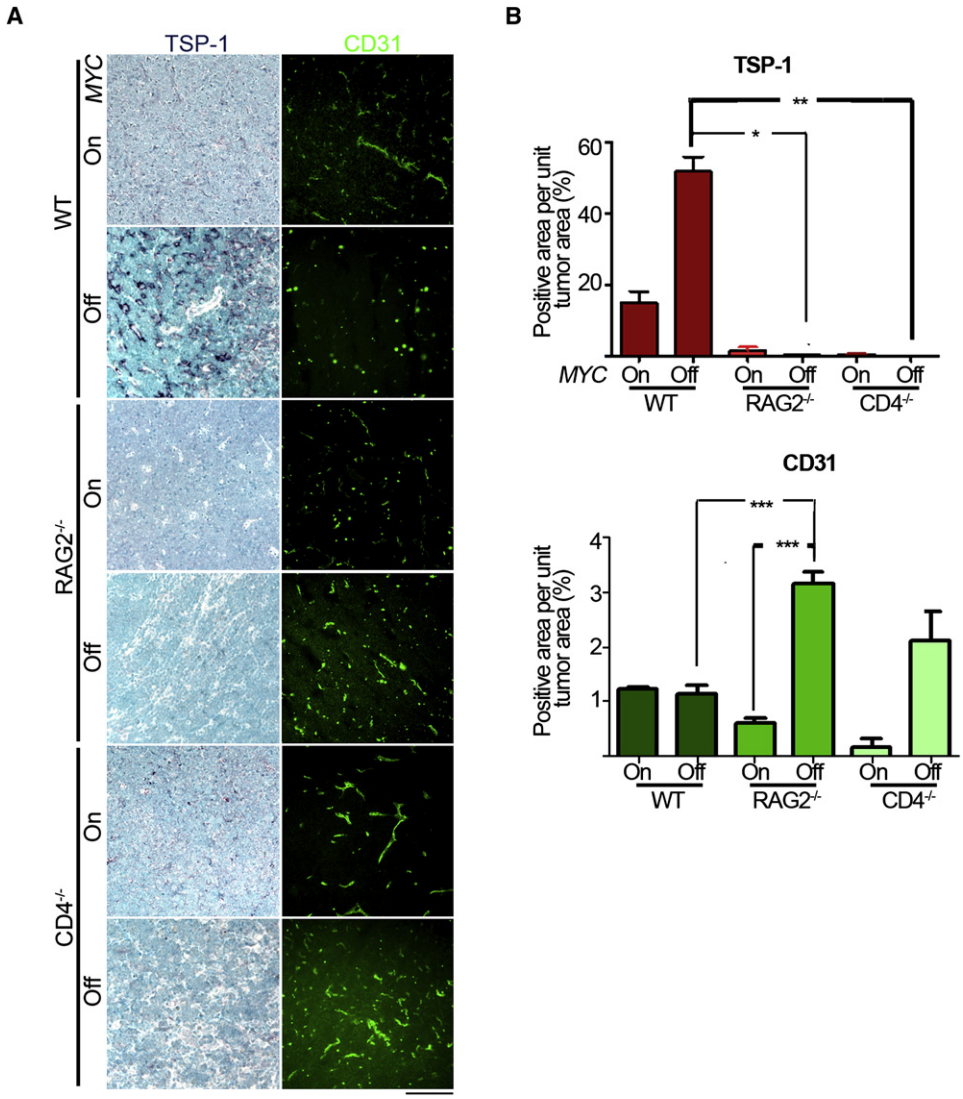

Figure 4. An Intact Immune System Is Required for the Inhibition of Angiogenesis upon *MYC* Inactivation

(A) Micrographs of TSP-1 (left panel) and CD31 (right panel) immunohistochemical and immunofluorescence staining of tumors derived from untreated (*MYC* On) and 4 day dox-treated (*MYC* Off) mice of the indicated genotypes. Scale bar = 100 μm.

(B) Quantification of TSP-1 (top panel) and CD31 (bottom panel) staining shown in (A). Quantification is presented as the average percentage of positively stained regions within the tumors. At least five different fields from two different tumors were analyzed for each different condition. Statistical significance (p value evaluated by unpaired Student's t test) is shown. *$p < 0.01$, **$p < 0.001$, ***$p < 0.0001$. Error bars are ± SEM.

See also Figure S2.

exhibited statistically significant prolonged tumor-free survival compared with RAG2$^{-/-}$ or RAG2$^{-/-}$ hosts reconstituted with CD8^{+} T cells (Figures 5B and 5D, RAG2$^{-/-}$ versus RAG2$^{-/-}$ CD4^{+}, p = 0.007, RAG2$^{-/-}$CD4^{+} versus RAG2$^{-/-}$CD8^{+}, p = 0.03). Hence, restoration of CD4^{+} T cells alone was sufficient for the ability of *MYC* inactivation to eliminate MRD and induce sustained tumor regression.

Host Immune System Is Required to Elicit Changes in Chemokine Expression

We measured relative fold changes in cytokine production in tumors growing in WT or RAG2$^{-/-}$ hosts after *MYC* inactivation (Figure 6A). *MYC* inactivation in tumors from WT compared with RAG2$^{-/-}$ hosts revealed an upregulation of antiproliferative and antiangiogenic ("antitumor") cytokines that suggest potential involvement by other immune effectors. Eotaxin-1 and IL-5 (Figure 6A, WT versus RAG2$^{-/-}$ fold change upon *MYC* inactivation p = 0.02 and p = 0.003, respectively) are potent T_H2 cytokines that have been implicated in the recruitment of an eosinophil-mediated antitumor inflammatory response (Simson et al., 2007). IFN-γ was observed to increase over 4-fold upon *MYC* inactivation in the WT hosts with virtually no change in the absence of the host immune system (WT versus RAG2$^{-/-}$ fold change upon *MYC* inactivation p = 0.03) while TNF-α was significantly downregulated in RAG2$^{-/-}$ hosts (RAG2$^{-/-}$ *MYC* On versus Off, p = 0.02); its upregulation was close to statistical

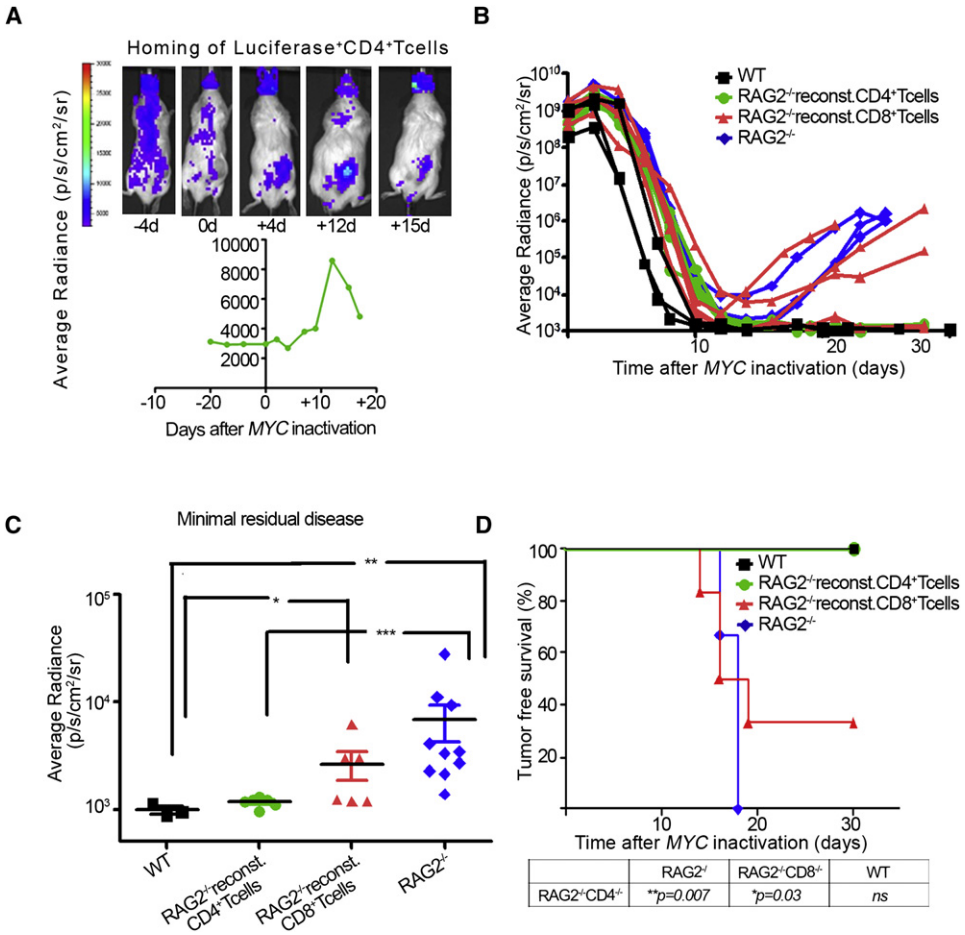

Figure 5. CD4⁺ T Cells Home to the Tumor and Are Sufficient to Induce Sustained Tumor Regression upon *MYC* Inactivation

(A) Bioluminescence signal of luciferase⁺CD4⁺ T cells that home to the tumor microenvironment. RAG2$^{-/-}$ mice were reconstituted with luciferase⁺ CD4⁺ T cells and unlabeled tumor cell lines were injected s.c. 8 days post reconstitution. *MYC* was inactivated when tumors grew to a size of 1000 mm^3. Data are represented as bioluminescence signal (average radiance) plotted against time after *MYC* inactivation (n = 3).

(B) Tumor regression and relapse kinetics measured by bioluminescence imaging. RAG2$^{-/-}$ mice were reconstituted with CD4⁺ (RAG2$^{-/-}$reconst.CD4⁺T cells, n = 5) or CD8⁺ (RAG2$^{-/-}$reconst. CD8⁺T cells, n = 6) T cells from WT mice. Eight days after reconstitution, luciferase⁺ tumor cell lines were injected s.c. *MYC* was inactivated when tumors in all hosts reached a comparable bioluminescence signal. Data are presented as bioluminescence signal (average radiance) plotted against time after *MYC* inactivation. WT (n = 3) and RAG2$^{-/-}$ (n = 3) mice were used as positive and negative controls.

(C) Quantification of minimum residual disease. Bioluminescence signals of tumors at their maximally regressed state are plotted against genotype. Statistical significance (p value evaluated by unpaired Student's t test) is shown. *p < 0.01, **p < 0.001, ***p < 0.0001. Error bars are ± SEM.

(D) Kaplan Meier curves of tumor-free survival in the reconstituted RAG2$^{-/-}$, RAG2$^{-/-}$, and WT mice. Log-rank test was used compare the survival curves. Data are representative of three experiments. Statistics were performed including all data: n = 14, RAG reconstituted with CD8⁺ T cells: n = 12. reconst. = reconstituted with.

See also Figure S3.

significance in the WT hosts (WT *MYC* On versus Off, p = 0.07). Both cytokines have been shown by many to be critical mediators of potent CD4⁺ antitumor activity (Qin and Blankenstein, 2000; Thomas and Hersey, 1998). Interestingly, MCP-1, a potent chemoattractant of inflammatory tumor-associated macrophages (TAMs), specifically, tumor-promoting M2 macrophages (Allavena et al., 2008; Hu et al., 2009), was significantly downregulated in the tumors from immunodeficient hosts compared with WT (WT versus RAG2$^{-/-}$ fold change upon *MYC* inactivation p = 0.008).

Also, the downregulation of "protumor" cytokines was measured in tumors from WT and RAG2$^{-/-}$ hosts. Vascular endothelial growth factor (VEGF) was downregulated almost 4-fold in WT hosts (WT *MYC* On versus Off, p = 0.01), whereas no change in its expression could be detected in tumors from immunodeficient hosts. IL-β decreased significantly close to 2-fold (WT versus RAG2$^{-/-}$ fold change upon *MYC* inactivation, p = 0.02); downregulation of these two cytokines suggests enhanced suppression of angiogenesis in the presence of an intact host immune system upon *MYC* inactivation (Kowanetz and Ferrara, 2006; Shchors et al., 2006).

Finally, RAG2$^{-/-}$ hosts that had been reconstituted with CD4⁺ T cells exhibited similar changes in chemokine expression to WT hosts upon *MYC* inactivation (Figure S4B). The antitumor

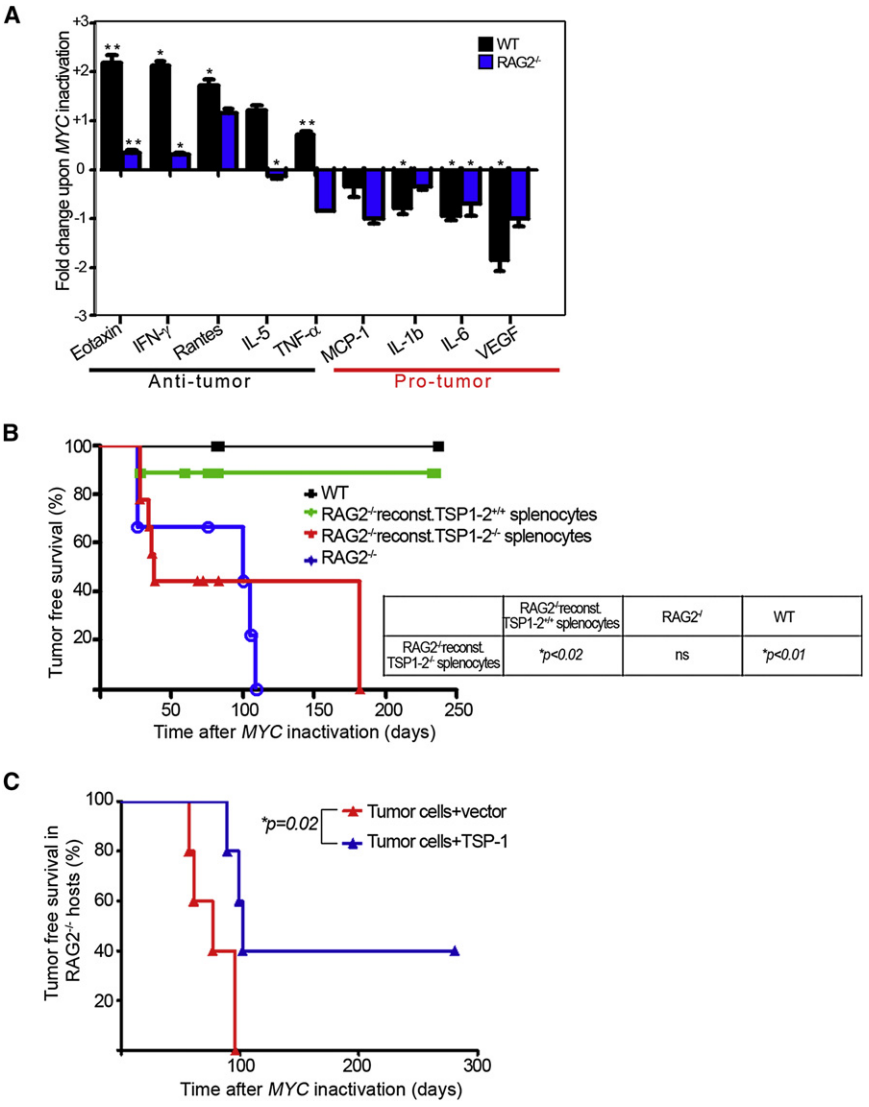

Figure 6. Cytokines Produced by the Immune System Contribute to Sustained Tumor Regression upon *MYC* Inactivation

(A) Graphical representation of fold change of indicated cytokines upon *MYC* inactivation in tumors from WT and RAG2$^{-/-}$ hosts. Tumors from WT and RAG2$^{-/-}$ mice were harvested at tumor onset and 4 days after *MYC* inactivation and run on a luminex platform to check for protein expression of 21 different cytokines. The significant fold changes in the various cytokines upon *MYC* inactivation were $\log_2$ transformed and plotted for various pro- and antitumor cytokines. *p < 0.01, **p < 0.001. Asterisks above the bars represent significance in cytokine expression upon *MYC* inactivation in the indicated host. Error bars are ± SEM.

(B) Kaplan-Meier curves of tumor-free survival of reconstituted RAG2$^{-/-}$, RAG2$^{-/-}$, and WT mice. RAG2$^{-/-}$ mice were reconstituted with splenocytes from WT (n = 18) or TSP-1,2$^{-/-}$ (n = 16) mice i.v. Eight days post reconstitution, mice were transplanted with lymphoma cells s.c. *MYC* was inactivated when tumors were 1000 mm^3. WT (n = 8) and RAG2$^{-/-}$ (n = 11). Log-rank test was used to analyze survival of indicated genotypes. Data are representative three experiments.

(C) Kaplan-Meier curves of tumor-free survival of RAG2$^{-/-}$ mice injected with TSP-1 transfected tumor cell lines (n = 5) or vector transfected control tumor cell lines (n = 5). A p53$^{-/-}$ conditional *MYC* lymphoma cell line was used.

See also Figure S4.

cytokines (eotaxin, IFN-γ and RANTES) increased, while the protumor cytokine, VEGF decreased in protein expression (Figure S4B). Thus, the host immune status is responsible for the regulation of changes in cytokine expression.

TSP Expression Is Required for Sustained Tumor Regression upon *MYC* Inactivation

Our results suggested to us the possibility that specific cytokines may be critical to the remodeling of the tumor and the tumor microenvironment upon *MYC* inactivation. We used two approaches to investigate the role of TSP-1. First, we reconstituted RAG2$^{-/-}$ mice with splenocytes from either TSP-1,2$^{+/+}$ (WT) or TSP-1,2$^{-/-}$ mice. Both TSP-1 and 2 have been implicated in the inhibition of angiogenesis and have similar structural domains (Kazerounian et al., 2008; Lawler, 2000). By FACS analysis, we verified equivalent immune reconstitution (Figure S4A). Indeed, RAG2$^{-/-}$ mice reconstituted with TSP-1,2$^{-/-}$ splenocytes completely failed to protect from sustained tumor regression upon *MYC* inactivation compared to RAG2$^{-/-}$ mice reconstituted with WT splenocytes (Figure 6B, relapse rate WT versus TSP-1,2$^{-/-}$, 10% versus 100%, p = 0.02). We conclude that TSP expression in immune effectors is important for sustained tumor regression upon *MYC* inactivation.

Next, we addressed whether we could bypass the requirement for TSP-1 expression from host immune cells by artificially introducing TSP-1 into tumor cells. We compared tumor recurrence upon *MYC* inactivation in RAG2$^{-/-}$ hosts of tumors infected with a vector control versus tumors infected with a TSP-1 expression vector. TSP-1 overexpressing tumors exhibited a delay in the kinetics (mean latency 80 versus 102 days) and a decreased frequency of tumor recurrence (40% versus 100%) resulting in a statistically significant survival advantage (Figure 6C, RAG2$^{-/-}$ TSP-1^{+} versus RAG2$^{-/-}$, p = 0.02). Thus, TSP-1 overexpression of tumor cells is sufficient to increase the duration and frequency of sustained tumor regression upon *MYC* inactivation in immune compromised hosts.

Cyclosporine A Treatment of Primary Tumors Impedes Senescence and Shutdown of Angiogenesis

To examine if similar results would be observed in primary transgenic tumors, we determined the influence of the pharmacological suppression of the host immune system with cyclosporine A (Shevach, 1985) on the consequences of *MYC* inactivation.

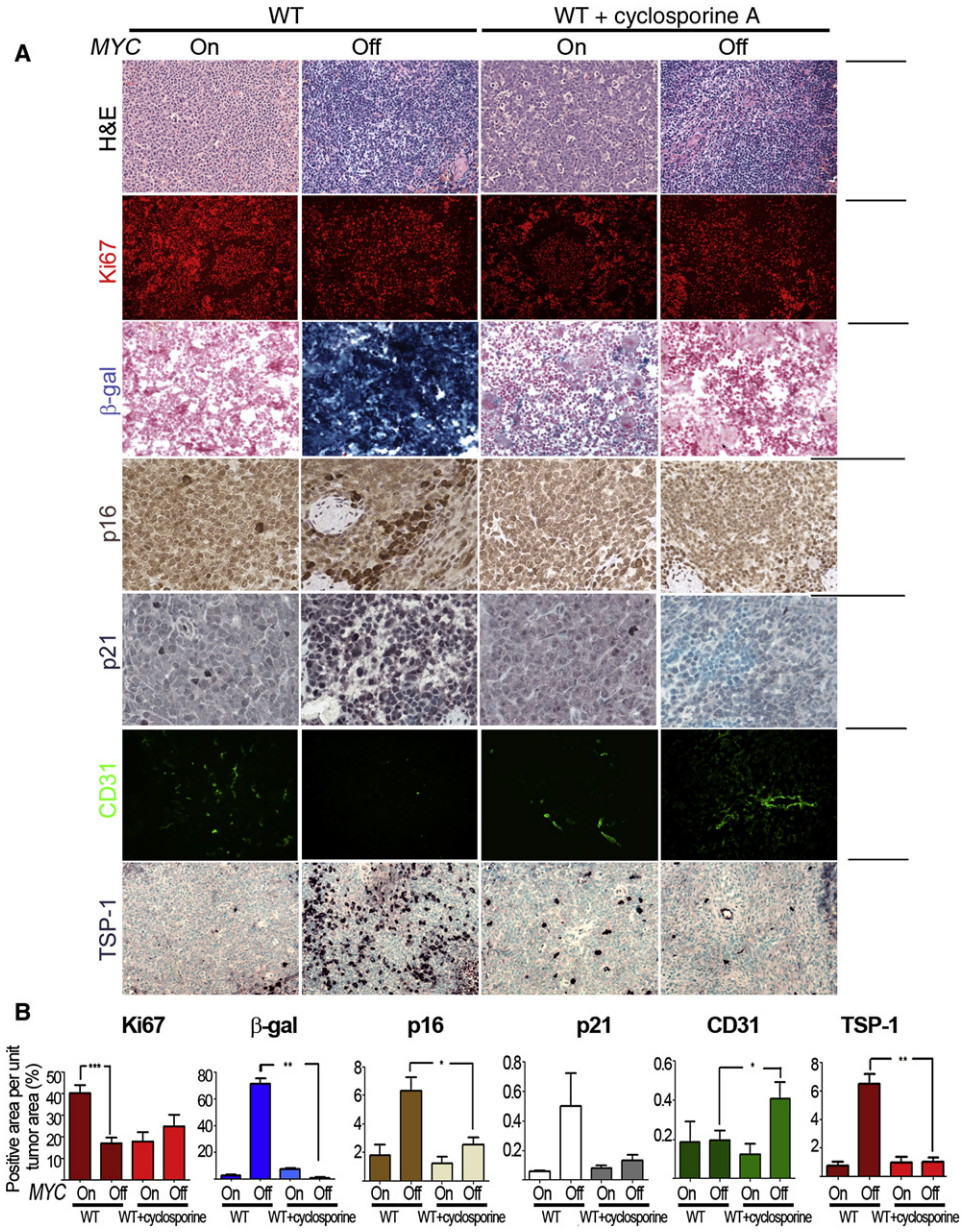

Figure 7. Cyclosporine A Treatment Inhibits Induction of Senescence and Inhibition of Angiogenesis in Tumors from Primary *MYC*-Induced T-ALL

(A) Micrographs of hematoxylin and eosin, Ki67, SA-β-gal, p16, p21, CD31, and TSP-1 immunostaining (ordered from top to bottom) of tumors derived from untreated and cyclosporine A-treated primary tumor bearing mice (*MYC* On and 4 day dox-treated *MYC* Off). Scale bar = 100 μm.

(B) Quantification of immunostaining shown in (A). Ordered from left to right, the graphs represent quantification of Ki67, SA-β-gal, p16, p21, CD31, and TSP-1 expression. Quantification is the average percentage of positively stained regions within the tumors. At least five different fields from two different tumors were analyzed. Statistical significance (p value evaluated by unpaired Student's t test) is shown. *$p < 0.01$, **$p < 0.001$, ***$p < 0.0001$. Error bars are ± SEM.

See also Figure S5.

Cyclosporine A did not have any direct effects on the proliferation of tumor cells in vitro (Figure S5). Cyclosporine A treated primary transgenic mice illustrated a marked inhibition on the ability of *MYC* inactivation to induce both cellular senescence as measured by staining for SA β-galactosidase (70% versus 1%; $p < 0.01$), p16 (6% versus 2%; $p < 0.05$), and p21 (0.5% versus 0.1%, $p < 0.01$) as well as the suppression of angiogenesis as measured by decrease in staining for CD31 (0.2% versus 0.4%, $p = 0.05$) and the induction of TSP-1 (6% versus 1%, $p = 0.0006$) (Figures 7A and 7B). Thus, cyclosporine A blocked the ability of *MYC* inactivation to induce senescence and shut down angiogenesis. We observed no effects on apoptosis as measured by TUNEL staining (data not shown). However, cyclosporine A treatment may suppress the ability of *MYC* inactivation

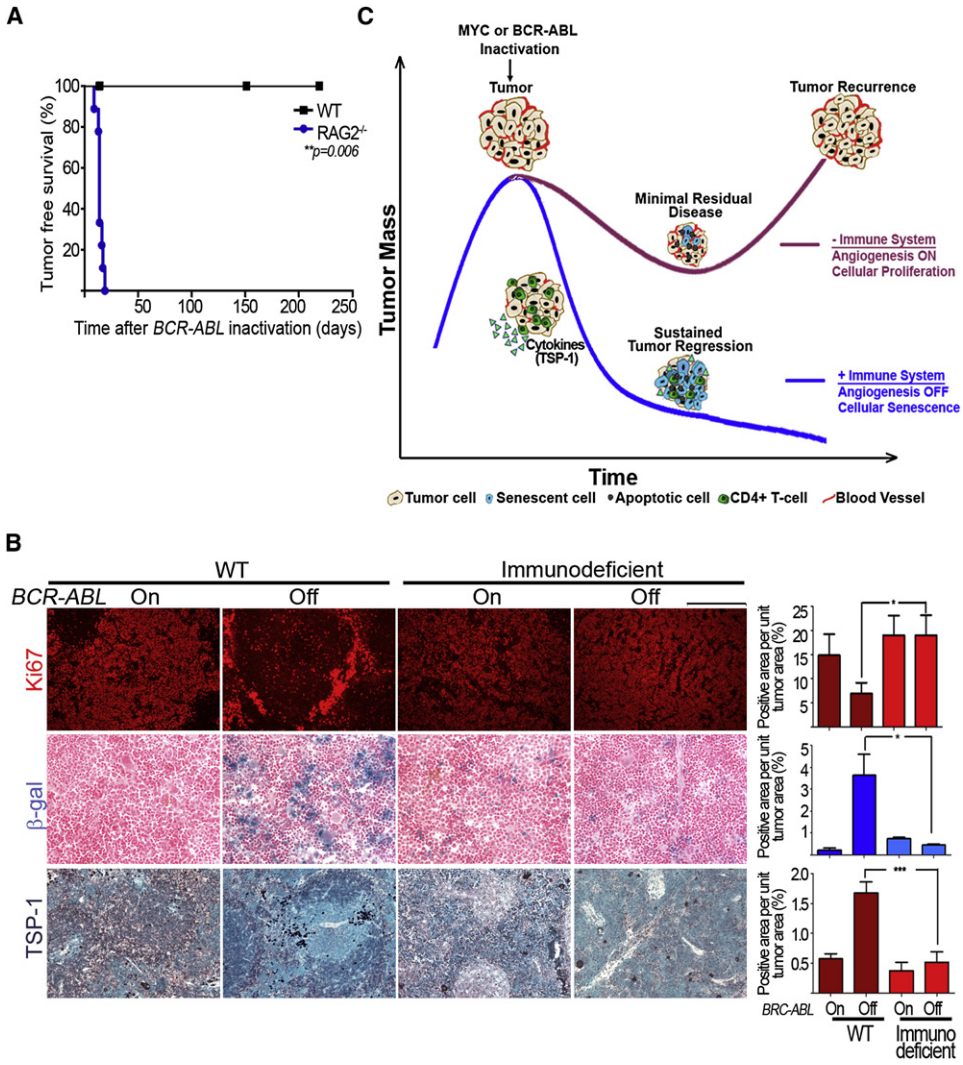

Figure 8. An Intact Immune System Is Required for Sustained Regression of Tumors in a Conditional Mouse Model of *BCR-ABL*-Induced B-ALL

(A) Kaplan-Meier curves of tumor-free survival of RAG2$^{-/-}$ (n = 9) and WT (n = 4) mice transplanted with unlabelled leukemia cells i.p. When mice were moribund with tumor, *BCR-ABL* was inactivated, and mice were scored for relapse.

(B) Micrographs and quantification of Ki67, SA-β-gal, and TSP-1 immunostaining (ordered from top to bottom) of tumors derived from untreated (*BCR-ABL* On) and doxycycline-treated (*BCR-ABL* Off) wild-type and immunodeficient tumor-bearing mice. Scale bar = 100 μm. Quantification is average percentage of positively stained regions. At least five different fields from two different tumors were analyzed for each different condition. Statistical significance (p value evaluated by unpaired Student's t test) is shown. *p < 0.01, **p < 0.001, ***p < 0.0001.

(C) Model for role of immune system in eliciting oncogene addiction.

See also Figure S6.

to induce proliferative arrest. Interestingly, cyclosporine A seemed to inhibit proliferation during tumor progression when *MYC* was still activated. This suggests, that when *MYC* is on, T cells might promote tumor formation indicating the dual nature of the immune response in cancer (de Visser et al., 2006).

Immune System Is Required for Sustained Regression of *BCR-ABL*-Induced B Cell Acute Lymphocytic Leukemia (B-ALL)

To determine if our results would generalize to another model of hematopoietic tumorigenesis, we used a conditional transgenic model of *BCR-ABL*-induced pro-B cell lymphocytic leukemia (B-ALL) (Huettner et al., 2000). First, we determined if host immune status influenced the ability of *BCR-ABL* inactivation to induce sustained tumor regression. Similar to *MYC* inactivation, tumors upon *BCR-ABL* inactivation underwent sustained tumor regression in wild-type hosts while 100% of the immunodeficient hosts relapsed within 14 days of *BCR-ABL* inactivation (Figure 8A, WT versus RAG2$^{-/-}$, p = 0.006). Hence, *BCR-ABL* inactivation also induces sustained tumor regression only in immune intact hosts.

Upon *BCR-ABL* inactivation, Ki67 expression showed a non-significant decrease in tumors transplanted into wild-type hosts but no change in tumors transplanted into immunodeficient

hosts. Ki67 expression was higher in tumors transplanted into immunodeficient hosts compared with those transplanted into immune intact hosts (Figure 8B, WT *BCR-ABL* off versus immunodeficient *BCR-ABL* off $p = 0.03$). Cellular senescence increased upon *BCR-ABL* inactivation in tumors from wild-type hosts versus immunodeficient hosts as measured by increased SA-β-gal staining (4% versus 0.4%, $p = 0.05$). Finally, there was a 3-fold increase in TSP-1 upon *BCR-ABL* inactivation in tumors from immunocompetent hosts while TSP-1 expression did not change upon *BCR-ABL* inactivation in immunodeficient hosts (Figure 8B, TSP-1 panel, WT *BCR-ABL* on *versus BCR-ABL* off, $p < 0.0001$; WT *BCR-ABL* Off versus immunodeficient *BCR-ABL* Off, $p = 0.0001$). We were unable to measure any significant CD31 expression in any of the tumors. Hence, *BCR-ABL* inactivation also induces sustained tumor regression only in immune intact hosts.

DISCUSSION

Oncogene addiction has been presumed to be a cell autonomous process. Here, we have shown that interactions between the tumor microenvironment and the immune system are essential for sustained tumor regression upon oncogene inactivation. In the absence of an intact immune system, we see a 10- to 1000-fold reduction in the rate, extent, and duration of tumor regression upon *MYC* inactivation. The absence of $CD4^+$ T cells alone was sufficient to markedly impede sustained tumor regression. Thus, oncogene addiction is not necessarily cell autonomous. $CD4^+$ T cells may play a critical role in enabling *MYC* inactivation to elicit changes in the microenvironment and in cytokine expression that appear to be required for cellular senescence and the shutdown of angiogenesis. TSP-1 must be expressed by immune effectors to cooperate with *MYC* inactivation to induce tumor regression. Our results generalized to primary tumors from *MYC*-induced T-ALL bearing hosts that had been treated with the immunosuppressive agent cyclosporine A and a conditional transgenic model of *BCR-ABL*-induced B-ALL. Oncogene inactivation generally may induce tumor regression through immune cell-dependent mechanisms.

Our observations are consistent with a multitude of reports that document the role of the immune system in neoplasia (de Visser et al., 2005, 2006; Dunn et al., 2002; Soucek et al., 2007). Tumors coevolve in the context of an intact immune system through the process of immune editing, resulting in tumor elimination, dormancy, or evolving to escape the immune system and progress to full malignancy (Dunn et al., 2002; Guerra et al., 2008; Teng et al., 2008). Upon *MYC* inactivation, a massive recruitment of $CD4^+$ T cells occurs that is associated with marked changes in cytokine production in the tumor microenvironment leading to cellular senescence and the shutdown of angiogenesis. TSP-1 is one of the critical chemokines. Interestingly, immune effector recruitment and associated changes in chemokines occur upon restoration of the tumor suppressor p53 in both liver cancer (Xue et al., 2007) and upon *MYC* inactivation in lymphoma (Giuriato et al., 2006).

Provocatively, $CD4^+$ T cells emerged as the critical host effector population for sustained tumor regression upon *MYC* inactivation. Notably, hosts deficient in $CD4^+$ T cells exhibited impaired kinetics, degree and durability of tumor regression as well as reduced senescence and suppression of angiogenesis upon *MYC* inactivation. The reconstitution of $CD4^+$ T cells into $RAG2^{-/-}$ hosts alone was capable of restoring the ability of *MYC* inactivation to induce sustained tumor regression. The reconstitution of $CD4^+$ T cells into $RAG2^{-/-}$ hosts had more potent effects on tumor regression compared with the depletion of these cells, perhaps reflecting that in hosts that are congenitally defective for a specific immune compartment there may be compensation from other immune effectors (Xing et al., 1998).

$CD4^+$ T cells have been previously implicated in the restraint of tumor growth through regulation of antigen dependent mechanisms involving either macrophages or cytotoxic T cells (Corthay et al., 2005; Dranoff et al., 1993; Qin and Blankenstein, 2000). Intriguingly, host $CD4^+$ T cells sculpted the tumor's response to *MYC* inactivation, likely not by their modest influence upon apoptosis or proliferation, but by dramatically inducing cellular senescence and the shutdown of angiogenesis, processes previously suggested by us to be integral to the ability of *MYC* inactivation to effect sustained tumor regression. Two of the hallmarks of oncogene addiction, both the induction of cellular senescence and the suppression of angiogenesis, have been linked to the expression of cytokines known to be expressed by $CD4^+$ T cells (Acosta et al., 2008; Beatty and Paterson, 2001; Kuilman et al., 2008; Muller-Hermelink et al., 2008).

Thus, $CD4^+$ T cells are one important component of the mechanism of tumor regression upon oncogene inactivation. Other host immune effectors are likely to contribute, and we recognize that other innate and adaptive immune compartments are also likely to be involved including macrophages, NK cells, mast cells, and B cells. Recent work suggests that mast cells and macrophages both may be critical (Soucek et al., 2007; Xue et al., 2007). Indeed, it is possible that $CD4^+$ T cells are mediating part of the effects we have observed by recruiting these effector populations.

TSP-1 is critical for the mechanism by which host immune effectors mediate tumor regression upon *MYC* inactivation. TSP-1 is a potent cytokine that has been implicated in the regulation of many cellular processes including the regulation of angiogenesis (Jimenez et al., 2000; Kazerounian et al., 2008; Lawler, 2000; Short et al., 2005; Zaslavsky et al., 2010). Furthermore, TSP-1 also has been suggested to regulate lymphocyte homing and function (Li et al., 2006) and appears to be required for the ability of $CD4^+$ T cells to contribute to sustained regression upon oncogene inactivation.

Additionally, other cytokines including eotaxin-1, IL-5, IFN-γ and TNF-α are possible candidates for mediating the changes in cellular senescence and angiogenesis upon *MYC* inactivation, consistent with reports that these chemokines may be involved in these processes (Beatty and Paterson, 2001; Beyne-Rauzy et al., 2004). The downregulation of other cytokines such as VEGF, IL-1β, and MCP-1 could also contribute (Kowanetz and Ferrara, 2006; Shchors et al., 2006; Su et al., 2010). IFN-γ and TNF-α have been previously implicated in the regulation of cellular quiescence and angiogenesis (Beatty and Paterson, 2001; Beyne-Rauzy et al., 2004; Kuilman et al., 2008; Muller-Hermelink et al., 2008), and eotaxin-1 and IL-5 have demonstrated potent antitumor activity in numerous mouse models of cancer

(Simson et al., 2007). Notably, tumor regression induced by the restoration of p53 expression was also associated with marked changes in chemokine expression (Xue et al., 2007).

In primary transgenic tumor hosts, an immune compromised state induced via treatment with cyclosporine A greatly impeded the consequences of oncogene inactivation. Therefore, our results generalize in the case when endogenous tumor-host interactions evolved throughout tumorigenesis. Cyclosporine A treatment is well known to increase the frequency of hematological malignancies in patients (Cockburn and Krupp, 1989; Opelz and Dohler, 2004). Hence, this agent may impede sensitivity to oncogene-directed therapies.

An immune intact host was also found to be required for *BCR-ABL* inactivation to induce sustained tumor regression in B-ALL. Similar to *MYC* inactivation, inactivation of the *BCR-ABL* oncogene resulted in the induction of cellular senescence, the shutdown of tumor angiogenesis, and ultimately sustained tumor regression only in the presence of the host immune system. However, different from *MYC* inactivation, *BCR-ABL* inactivation appeared to be less capable of suppressing cellular proliferation. Hence, the host immune system appears to be generally important in mediating the consequences of oncogene inactivation.

Thus, oncogene addiction is a consequence of both cell autonomous processes such as proliferative arrest and apoptosis as well as host-immune-dependent mechanisms such as cellular senescence and angiogenesis (Figure 8C). Upon oncogene inactivation, tumor cells are eliminated primarily in a cell autonomous manner. However, the kinetics of tumor cell elimination and the extent of tumor elimination, or minimal residual disease, as well as the durability of sustained tumor regression are all dictated by the presence of an immune system and appear to be strongly associated with its ability to elicit cellular senescence and shut down angiogenesis. These processes may contribute to the constraint of minimal residual disease (Aguirre-Ghiso, 2007). $CD4^+$ T cells are a critical component to this phenomenon and TSP-1 emerges as a possible cytokine regulating these processes. Other immune effectors and chemokines/cytokines (including IFN-γ, eotaxin-1, IL-5, TNF-α, and MCP-1) are likely to be involved. Immune cells and inflammation can be important to the pathogenesis of cancer through many effects on the tumor microenvironment (Coussens and Werb, 2002; Greten and Karin, 2004; Xue et al., 2007).

In general, the deficiency in $CD4^+$ T cells may render the treatment of tumors in patients less efficacious and impede the complete elimination of tumor cells. Indeed, AIDS patients exhibit not only a more than 100-fold increased frequency of lymphomas often associated with *MYC* overexpression but are much less responsive to therapy (Boshoff and Weiss, 2002; Carbone, 2003). Hence, $CD4^+$ T cells may contribute to the efficacy of therapeutic agents.

Our results suggest that screening methods used to identify therapies that rely on the in vitro study of cell lines or in vivo analysis of xenograft models in immune compromised hosts may underestimate the efficacy of a therapy by failing to faithfully recapitulate tumor-host interactions (Ronnov-Jessen and Bissell, 2009; Weigelt and Bissell, 2008). Moreover, the active modulation of $CD4^+$ T cell function may enhance the efficacy of therapeutics for cancer (Gattinoni et al., 2006; Lake and Robinson, 2005). Thus, a combination of targeted oncogene inactivation with immunotherapy may be a particularly efficacious anticancer therapy.

EXPERIMENTAL PROCEDURES

Transgenic Mice

The generation and characterization of Tet system transgenic lines for conditional expression of MYC, have been described (Felsher and Bishop, 1999). $CD4^{-/-}$, $CD8^{-/-}$, $CD4^{-/-}CD8^{-/-}$, and $RAG2^{-/-}$ mice were generously provided in the FVB/N background by Lisa Coussens (University of California, San Francisco). TSP-$1,2^{-/-}$ mice were generously provided by Ben Barres (Stanford University). $Luciferase^+$L2G85 mice were generously provided by Robert Negrin (Stanford University). Tet-o-BCR-ABL mice were generously provided by Daniel Tenen (Harvard University). Genotyping was performed by PCR on genomic DNA from tails. All animal experiments were approved by Stanford's Administrative Panel on Laboratory Animal Care (APLAC) and in accordance with institutional and national guidelines.

Tumor Surveillance and Tumorigenicity Assays

Mice that were moribund with tumor were either humanely euthanized or treated with doxycycline in their drinking water (100 μg/ml) to follow tumor regression and relapse. Statistical comparison of Kaplan-Meier curves is based on the log-rank test. Further details can be found in Supplementary Experiemental Procedures.

Reconstitution of $RAG2^{-/-}$ mice

$RAG2^{-/-}$ mice were injected intravenously (i.v.) with either (1) 20×10^6 splenocytes from WT or TSP-$1,2^{-/-}$ mice or (2) $4X10^6$ $CD4^+$ or $CD8^+$ T cells isolated from spleens and lymph nodes of WT mice using magnetically activated cell sorting (MACS). Eight days post reconstitution, mice were bled from the tail vein and $CD4^+$ and $CD8^+$ T cell reconstitution was verified using FACS.

In Vivo Bioluminescence Imaging

Mice with tumors were anesthetized with a combination of inhaled isoflorane/oxygen delivered by the Xenogen XGI-8 5-port Gas Anaesthesia System. The substrate **d**-luciferin (150 mg/kg) was injected into the animal's peritoneal cavity 10 min before imaging. Animals were then placed into a light-tight chamber and imaged with an IVIS-200 cooled CCD camera (Xenogen, Alameda, CA) (Contag et al., 1997). Living Image was used to collect, archive, and analyze photon fluxes and transform them into pseudocolor images by using Living Image software (Xenogen). At least five mice per group were injected with tumors expressing luciferase.

Luminex Cytokine Assay

The concentration of 21 cytokines was measured from tumor tissue lysates from WT and $RAG2^{-/-}$ mice at tumor onset and 4 days after *MYC* inactivation. Concentrations were measured using Luminex xMAP technology. Data were obtained as mean fluorescence intensity based on a standard curve generated for each cytokine. Further details can be found in Supplementary Experiemental Procedures.

SUPPLEMENTAL INFORMATION

Supplemental Information includes Supplemental Experimental Procedures and six figures and can be found online at doi:10.1016/j.ccr.2010.10.002.

ACKNOWLEDGMENTS

This manuscript is dedicated to the memory of Julie Do. We thank Ron Levy, Mina Bissell, Kwan Hyuck, Lisa Coussens, Peter Choi, and other members of the Felsher laboratory for their helpful suggestions; Robert Negrin, Lisa Coussens, and Ben Barres for providing transgenic mice; Pauline Chu for generating histology samples; Anet James for assistance with microscopy; Yael Resenberg-Hasson for assistance with the luminex cytokine assay. This work was funded by the Burroughs Welcome Fund Career Award, the Damon Runyon Foundation Lilly Clinical Investigator Award, NIH RO1 grant number CA 089305, 105102, National Cancer Institute's In-vivo Cellular and Molecular

Imaging Center grant number CA 114747, Integrative Cancer Biology Program grant number CA 112973, NIH/NCI PO1 grant number CA034233, the Leukaemia and Lymphoma Society Translational Research grant number R6223-07 (D.W.F.), NIH R01 grant number CA 118374 (S.R.), Stanford Graduate Fellowship (K.R.) Lymphoma Research Foundation and the Leukemia and Lymphoma Society (A.C.F.). Additionally, P.B. and A.K. were funded by a Howard Hughes Medical Institute Research Training Fellowship for Medical Students and a Stanford Medical Scholars Research Fellowship.

Received: April 6, 2010
Revised: August 25, 2010
Accepted: October 1, 2010
Published: November 15, 2010

REFERENCES

Acosta, J.C., O'Loghlen, A., Banito, A., Guijarro, M.V., Augert, A., Raguz, S., Fumagalli, M., Da Costa, M., Brown, C., Popov, N., et al. (2008). Chemokine signaling via the CXCR2 receptor reinforces senescence. Cell *133*, 1006–1018.

Aguirre-Ghiso, J.A. (2007). Models, mechanisms and clinical evidence for cancer dormancy. Nat. Rev. Cancer *7*, 834–846.

Allavena, P., Sica, A., Solinas, G., Porta, C., and Mantovani, A. (2008). The inflammatory micro-environment in tumor progression: the role of tumor-associated macrophages. Crit. Rev. Oncol. Hematol. *66*, 1–9.

Andreu, P., Johansson, M., Affara, N.I., Pucci, F., Tan, T., Junankar, S., Korets, L., Lam, J., Tawfik, D., DeNardo, D.G., et al. (2010). FcRgamma activation regulates inflammation-associated squamous carcinogenesis. Cancer Cell *17*, 121–134.

Beatty, G., and Paterson, Y. (2001). IFN-gamma-dependent inhibition of tumor angiogenesis by tumor-infiltrating CD4+ T cells requires tumor responsiveness to IFN-gamma. J. Immunol. *166*, 2276–2282.

Beyne-Rauzy, O., Recher, C., Dastugue, N., Demur, C., Pottier, G., Laurent, G., Sabatier, L., and Mansat-De Mas, V. (2004). Tumor necrosis factor alpha induces senescence and chromosomal instability in human leukemic cells. Oncogene *23*, 7507–7516.

Birkeland, S.A., Storm, H.H., Lamm, L.U., Barlow, L., Blohme, I., Forsberg, B., Eklund, B., Fjeldborg, O., Friedberg, M., Frodin, L., et al. (1995). Cancer risk after renal transplantation in the Nordic countries, 1964-1986. Int. J. Cancer *60*, 183–189.

Boshoff, C., and Weiss, R. (2002). AIDS-related malignancies. Nat. Rev. Cancer *2*, 373–382.

Boxer, L.M., and Dang, C.V. (2001). Translocations involving c-myc and c-myc function. Oncogene *20*, 5595–5610.

Bui, J.D., Uppaluri, R., Hsieh, C.S., and Schreiber, R.D. (2006). Comparative analysis of regulatory and effector T cells in progressively growing versus rejecting tumors of similar origins. Cancer Res. *66*, 7301–7309.

Carbone, A. (2003). Emerging pathways in the development of AIDS-related lymphomas. Lancet Oncol. *4*, 22–29.

Cockburn, I.T., and Krupp, P. (1989). The risk of neoplasms in patients treated with cyclosporine A. J. Autoimmun. *2*, 723–731.

Contag, C.H., Spilman, S.D., Contag, P.R., Oshiro, M., Eames, B., Dennery, P., Stevenson, D.K., and Benaron, D.A. (1997). Visualizing gene expression in living mammals using a bioluminescent reporter. Photochem. Photobiol. *66*, 523–531.

Corthay, A., Skovseth, D.K., Lundin, K.U., Rosjo, E., Omholt, H., Hofgaard, P.O., Haraldsen, G., and Bogen, B. (2005). Primary antitumor immune response mediated by CD4+ T cells. Immunity *22*, 371–383.

Coussens, L.M., and Werb, Z. (2002). Inflammation and cancer. Nature *420*, 860–867.

Crowe, N.Y., Smyth, M.J., and Godfrey, D.I. (2002). A critical role for natural killer T cells in immunosurveillance of methylcholanthrene-induced sarcomas. J. Exp. Med. *196*, 119–127.

Dave, S.S., Wright, G., Tan, B., Rosenwald, A., Gascoyne, R.D., Chan, W.C., Fisher, R.I., Braziel, R.M., Rimsza, L.M., Grogan, T.M., et al. (2004). Prediction of survival in follicular lymphoma based on molecular features of tumor-infiltrating immune cells. N. Engl. J. Med. *351*, 2159–2169.

de Visser, K.E., Korets, L.V., and Coussens, L.M. (2005). De novo carcinogenesis promoted by chronic inflammation is B lymphocyte dependent. Cancer Cell *7*, 411–423.

de Visser, K.E., Eichten, A., and Coussens, L.M. (2006). Paradoxical roles of the immune system during cancer development. Nat. Rev. Cancer *6*, 24–37.

Dougan, M., and Dranoff, G. (2009). Unit 20.11 The immune response to tumors. Curr. Protoc. Immunol. Published online April 1, 2009. 10.1002/0471142735.im2011s85.

Dranoff, G., Jaffee, E., Lazenby, A., Golumbek, P., Levitsky, H., Brose, K., Jackson, V., Hamada, H., Pardoll, D., and Mulligan, R.C. (1993). Vaccination with irradiated tumor cells engineered to secrete murine granulocyte-macrophage colony-stimulating factor stimulates potent, specific, and long-lasting anti-tumor immunity. Proc. Natl. Acad. Sci. USA *90*, 3539–3543.

Dunn, G.P., Bruce, A.T., Ikeda, H., Old, L.J., and Schreiber, R.D. (2002). Cancer immunoediting: from immunosurveillance to tumor escape. Nat. Immunol. *3*, 991–998.

Dunn, G.P., Koebel, C.M., and Schreiber, R.D. (2006). Interferons, immunity and cancer immunoediting. Nat. Rev. Immunol. *6*, 836–848.

Felsher, D.W. (2003). Cancer revoked: oncogenes as therapeutic targets. Nat. Rev. Cancer *3*, 375–380.

Felsher, D.W. (2008). Oncogene addiction versus oncogene amnesia: perhaps more than just a bad habit? Cancer Res. *68*, 3081–3086, discussion, 3086.

Felsher, D.W., and Bishop, J.M. (1999). Reversible tumorigenesis by MYC in hematopoietic lineages. Mol. Cell *4*, 199–207.

Galon, J., Costes, A., Sanchez-Cabo, F., Kirilovsky, A., Mlecnik, B., Lagorce-Pages, C., Tosolini, M., Camus, M., Berger, A., Wind, P., et al. (2006). Type, density, and location of immune cells within human colorectal tumors predict clinical outcome. Science *313*, 1960–1964.

Gatti, R.A., and Good, R.A. (1971). Occurrence of malignancy in immunodeficiency diseases. A literature review. Cancer *28*, 89–98.

Gattinoni, L., Powell, D.J., Jr., Rosenberg, S.A., and Restifo, N.P. (2006). Adoptive immunotherapy for cancer: building on success. Nat. Rev. Immunol. *6*, 383–393.

Giuriato, S., Ryeom, S., Fan, A.C., Bachireddy, P., Lynch, R.C., Rioth, M.J., van Riggelen, J., Kopelman, A.M., Passegue, E., Tang, F., et al. (2006). Sustained regression of tumors upon MYC inactivation requires p53 or thrombospondin-1 to reverse the angiogenic switch. Proc. Natl. Acad. Sci. USA *103*, 16266–16271.

Greten, F.R., and Karin, M. (2004). The IKK/NF-kappaB activation pathway-a target for prevention and treatment of cancer. Cancer Lett. *206*, 193–199.

Guerra, N., Tan, Y.X., Joncker, N.T., Choy, A., Gallardo, F., Xiong, N., Knoblaugh, S., Cado, D., Greenberg, N.M., and Raulet, D.H. (2008). NKG2D-deficient mice are defective in tumor surveillance in models of spontaneous malignancy. Immunity *28*, 571–580.

Hu, H., Sun, L., Guo, C., Liu, Q., Zhou, Z., Peng, L., Pan, J., Yu, L., Lou, J., Yang, Z., et al. (2009). Tumor cell-microenvironment interaction models coupled with clinical validation reveal CCL2 and SNCG as two predictors of colorectal cancer hepatic metastasis. Clin. Cancer Res. *15*, 5485–5493.

Huettner, C.S., Zhang, P., Van Etten, R.A., and Tenen, D.G. (2000). Reversibility of acute B-cell leukaemia induced by BCR-ABL1. Nat. Genet. *24*, 57–60.

Jain, M., Arvanitis, C., Chu, K., Dewey, W., Leonhardt, E., Trinh, M., Sundberg, C.D., Bishop, J.M., and Felsher, D.W. (2002). Sustained loss of a neoplastic phenotype by brief inactivation of MYC. Science *297*, 102–104.

Jimenez, B., Volpert, O.V., Crawford, S.E., Febbraio, M., Silverstein, R.L., and Bouck, N. (2000). Signals leading to apoptosis-dependent inhibition of neovascularization by thrombospondin-1. Nat. Med. *6*, 41–48.

Kazerounian, S., Yee, K.O., and Lawler, J. (2008). Thrombospondins in cancer. Cell. Mol. Life Sci. *65*, 700–712.

Kohrt, H.E., Nouri, N., Nowels, K., Johnson, D., Holmes, S., and Lee, P.P. (2005). Profile of immune cells in axillary lymph nodes predicts disease-free survival in breast cancer. PLoS Med. *2*, e284. 10.1371/journal.pmed.0020284.

Kowanetz, M., and Ferrara, N. (2006). Vascular endothelial growth factor signaling pathways: therapeutic perspective. Clin. Cancer Res. *12*, 5018–5022.

Kuilman, T., Michaloglou, C., Vredeveld, L.C., Douma, S., van Doorn, R., Desmet, C.J., Aarden, L.A., Mooi, W.J., and Peeper, D.S. (2008). Oncogene-induced senescence relayed by an interleukin-dependent inflammatory network. Cell *133*, 1019–1031.

Lake, R.A., and Robinson, B.W. (2005). Immunotherapy and chemotherapy–a practical partnership. Nat. Rev. Cancer *5*, 397–405.

Lawler, J. (2000). The functions of thrombospondin-1 and-2. Curr. Opin. Cell Biol. *12*, 634–640.

Li, S.S., Liu, Z., Uzunel, M., and Sundqvist, K.G. (2006). Endogenous thrombospondin-1 is a cell-surface ligand for regulation of integrin-dependent T-lymphocyte adhesion. Blood *108*, 3112–3120.

Meyer, N., and Penn, L.Z. (2008). Reflecting on 25 years with MYC. Nat. Rev. Cancer *8*, 976–990.

Muller-Hermelink, N., Braumuller, H., Pichler, B., Wieder, T., Mailhammer, R., Schaak, K., Ghoreschi, K., Yazdi, A., Haubner, R., Sander, C.A., et al. (2008). TNFR1 signaling and IFN-gamma signaling determine whether T cells induce tumor dormancy or promote multistage carcinogenesis. Cancer Cell *13*, 507–518.

Opelz, G., and Dohler, B. (2004). Lymphomas after solid organ transplantation: a collaborative transplant study report. Am. J. Transplant. *4*, 222–230.

Pelengaris, S., Khan, M., and Evan, G. (2002). c-MYC: more than just a matter of life and death. Nat. Rev. Cancer *2*, 764–776.

Pham, S.M., Kormos, R.L., Landreneau, R.J., Kawai, A., Gonzalez-Cancel, I., Hardesty, R.L., Hattler, B.G., and Griffith, B.P. (1995). Solid tumors after heart transplantation: lethality of lung cancer. Ann. Thorac. Surg. *60*, 1623–1626.

Qin, Z., and Blankenstein, T. (2000). CD4+ T cell–mediated tumor rejection involves inhibition of angiogenesis that is dependent on IFN gamma receptor expression by nonhematopoietic cells. Immunity *12*, 677–686.

Reiman, J.M., Kmieciak, M., Manjili, M.H., and Knutson, K.L. (2007). Tumor immunoediting and immunosculpting pathways to cancer progression. Semin. Cancer Biol. *17*, 275–287.

Ronnov-Jessen, L., and Bissell, M.J. (2009). Breast cancer by proxy: can the microenvironment be both the cause and consequence? Trends Mol. Med. *15*, 5–13.

Rossi, D., and Zlotnik, A. (2000). The biology of chemokines and their receptors. Annu. Rev. Immunol. *18*, 217–242.

Shachaf, C.M., Kopelman, A.M., Arvanitis, C., Karlsson, A., Beer, S., Mandl, S., Bachmann, M.H., Borowsky, A.D., Ruebner, B., Cardiff, R.D., et al. (2004). MYC inactivation uncovers pluripotent differentiation and tumour dormancy in hepatocellular cancer. Nature *431*, 1112–1117.

Shankaran, V., Ikeda, H., Bruce, A.T., White, J.M., Swanson, P.E., Old, L.J., and Schreiber, R.D. (2001). IFNgamma and lymphocytes prevent primary tumour development and shape tumour immunogenicity. Nature *410*, 1107–1111.

Shanker, A., Verdeil, G., Buferne, M., Inderberg-Suso, E.M., Puthier, D., Joly, F., Nguyen, C., Leserman, L., Auphan-Anezin, N., and Schmitt-Verhulst, A.M. (2007). CD8 T cell help for innate antitumor immunity. J. Immunol. *179*, 6651–6662.

Sharma, S.V., and Settleman, J. (2007). Oncogene addiction: setting the stage for molecularly targeted cancer therapy. Genes Dev. *21*, 3214–3231.

Shchors, K., Shchors, E., Rostker, F., Lawlor, E.R., Brown-Swigart, L., and Evan, G.I. (2006). The Myc-dependent angiogenic switch in tumors is mediated by interleukin 1beta. Genes Dev. *20*, 2527–2538.

Shevach, E.M. (1985). The effects of cyclosporin A on the immune system. Annu. Rev. Immunol. *3*, 397–423.

Short, S.M., Derrien, A., Narsimhan, R.P., Lawler, J., Ingber, D.E., and Zetter, B.R. (2005). Inhibition of endothelial cell migration by thrombospondin-1 type-1 repeats is mediated by beta1 integrins. J. Cell Biol. *168*, 643–653.

Simson, L., Ellyard, J.I., Dent, L.A., Matthaei, K.I., Rothenberg, M.E., Foster, P.S., Smyth, M.J., and Parish, C.R. (2007). Regulation of carcinogenesis by IL-5 and CCL11: a potential role for eosinophils in tumor immune surveillance. J. Immunol. *178*, 4222–4229.

Smyth, M.J., Cretney, E., Kershaw, M.H., and Hayakawa, Y. (2004). Cytokines in cancer immunity and immunotherapy. Immunol. Rev. *202*, 275–293.

Soucek, L., Lawlor, E.R., Soto, D., Shchors, K., Swigart, L.B., and Evan, G.I. (2007). Mast cells are required for angiogenesis and macroscopic expansion of Myc-induced pancreatic islet tumors. Nat. Med. *13*, 1211–1218.

Su, X., Ye, J., Hsueh, E.C., Zhang, Y., Hoft, D.F., and Peng, G. (2010). Tumor microenvironments direct the recruitment and expansion of human Th17 cells. J. Immunol. *184*, 1630–1641.

Swann, J.B., Vesely, M.D., Silva, A., Sharkey, J., Akira, S., Schreiber, R.D., and Smyth, M.J. (2008). Demonstration of inflammation-induced cancer and cancer immunoediting during primary tumorigenesis. Proc. Natl. Acad. Sci. USA *105*, 652–656.

Teng, M.W., Swann, J.B., Koebel, C.M., Schreiber, R.D., and Smyth, M.J. (2008). Immune-mediated dormancy: an equilibrium with cancer. J. Leukoc. Biol. *84*, 988–993.

Thomas, W.D., and Hersey, P. (1998). TNF-related apoptosis-inducing ligand (TRAIL) induces apoptosis in Fas ligand-resistant melanoma cells and mediates CD4 T cell killing of target cells. J. Immunol. *161*, 2195–2200.

van der Bruggen, P., Traversari, C., Chomez, P., Lurquin, C., De Plaen, E., Van den Eynde, B., Knuth, A., and Boon, T. (1991). A gene encoding an antigen recognized by cytolytic T lymphocytes on a human melanoma. Science *254*, 1643–1647.

Weigelt, B., and Bissell, M.J. (2008). Unraveling the microenvironmental influences on the normal mammary gland and breast cancer. Semin. Cancer Biol. *18*, 311–321.

Weinstein, I.B., and Joe, A. (2008). Oncogene addiction. Cancer Res. *68*, 3077–3080; discussion, 3080.

Weinstein, I.B., and Joe, A.K. (2006). Mechanisms of disease: oncogene addiction–a rationale for molecular targeting in cancer therapy. Nat. Clin. Pract. Oncol. *3*, 448–457.

Willimsky, G., and Blankenstein, T. (2005). Sporadic immunogenic tumours avoid destruction by inducing T-cell tolerance. Nature *437*, 141–146.

Wu, C.H., van Riggelen, J., Yetil, A., Fan, A.C., Bachireddy, P., and Felsher, D.W. (2007). Cellular senescence is an important mechanism of tumor regression upon c-Myc inactivation. Proc. Natl. Acad. Sci. USA *104*, 13028–13033.

Xing, Z., Wang, J., Croitoru, K., and Wakeham, J. (1998). Protection by CD4 or CD8 T cells against pulmonary Mycobacterium bovis bacillus Calmette-Guerin infection. Infect. Immun. *66*, 5537–5542.

Xue, W., Zender, L., Miething, C., Dickins, R.A., Hernando, E., Krizhanovsky, V., Cordon-Cardo, C., and Lowe, S.W. (2007). Senescence and tumour clearance is triggered by p53 restoration in murine liver carcinomas. Nature *445*, 656–660.

Zaslavsky, A., Baek, K.H., Lynch, R.C., Short, S., Grillo, J., Folkman, J., Italiano, J.E., Jr., and Ryeom, S. (2010). Platelet-derived thrombospondin-1 (TSP-1) is a critical negative regulator and potential biomarker of angiogenesis. Blood *115*, 4605–4613.

Zitvogel, L., Apetoh, L., Ghiringhelli, F., Andre, F., Tesniere, A., and Kroemer, G. (2008). The anticancer immune response: indispensable for therapeutic success? J. Clin. Invest. *118*, 1991–2001.

Leukemia Research 36 (2012) 98–103

Contents lists available at SciVerse ScienceDirect

Leukemia Research

journal homepage: www.elsevier.com/locate/leukres

Treatment of higher risk myelodysplastic syndrome patients unresponsive to hypomethylating agents with ON 01910.Na☆

Mahesh Seetharam[a], Alice C. Fan[b], Mai Tran[a], Liwen Xu[b], John P. Renschler[b], Dean W. Felsher[b], Kunju Sridhar[a], Francois Wilhelm[c], Peter L. Greenberg[a,*]

[a] Department of Medicine (Hematology), Stanford University Cancer Center, Stanford, CA, USA
[b] Department of Medicine (Oncology), Stanford University Cancer Center, Stanford, CA, USA
[c] Onconova Therapeutics Inc., Newtown, PA, USA

ARTICLE INFO

Article history:
Received 17 June 2011
Received in revised form 13 August 2011
Accepted 23 August 2011
Available online 14 September 2011

Keywords:
MDS
Treatment
ON 01910.Na
Rigosertib
Nanoimmunoassay
AKT signaling pathway

ABSTRACT

In a Phase I/II clinical trial, 13 higher risk red blood cell-dependent myelodysplastic syndrome (MDS) patients unresponsive to hypomethylating therapy were treated with the multikinase inhibitor ON 01910.Na. Responses occurred in all morphologic, prognostic risk and cytogenetic subgroups, including four patients with marrow complete responses among eight with stable disease, associated with good drug tolerance. In a subset of patients, a novel nanoscale immunoassay showed substantially decreased AKT2 phosphorylation in CD34+ marrow cells from patients responding to therapy but not those who progressed on therapy. These data demonstrate encouraging efficacy and drug tolerance with ON 01910.Na treatment of higher risk MDS patients.

1. Introduction

The myelodysplastic syndromes (MDS) are a heterogenous spectrum of diseases with disparate clinical manifestations and outcomes. Based on the International Prognostic Scoring System (IPSS) risk categorization, patients are stratified into risk disease regarding their potential for survival or progression to acute myeloid leukemia (AML) with IPSS Intermediate-2 and High risk patients being at higher risk for poor clinical outcomes [1].

Upon patients' progression to higher risk disease, therapies aimed at altering disease natural history have been used [2–4]. For patients eligible for high intensity therapy, allogeneic hematopoietic stem cell transplantation (HSCT) is considered. However, for the majority of patients lacking a suitable donor or ineligible for high intensity therapy, lower intensity treatments with hypomethylating therapy using the DNA methyltransferase inhibitors (DNMTIs) 5-azacitidine or decitabine have been used for treatment [3,4]. Although these lower intensity therapies have been beneficial for a portion of these MDS patients, patients may lack responsiveness or relapse after initial response.

For patients who have not responded to or have progressed after an initial response to DNMTIs and are not HSCT candidates, therapeutic options are generally limited to investigational therapies, in addition to supportive care. These patients have relatively short survival (4.3–5.6-month medians) and a high risk of leukemic transformation [5,6]. These patients, in general, are also poor candidates for other therapies due to advanced age or significant co-morbidities.

A number of compounds have been investigated in an attempt to improve treatment options for this subset of patients who have failed or are resistant to hypomethylating agent treatment. One such strategy is to therapeutically target cell cycle regulators, as altered cell cycle is a central feature of human malignancy and dysfunctional signaling in tumors ultimately affects cell cycle progression. Cell cycle progression is coordinated by cyclin/cyclin-dependent kinase (CDK) complexes and CDK inhibitors. Kinase activation generates phosphorylation cascades and mitotic spindle formation.

ON 01910.Na is a styryl sulfone mitotic and multikinase inhibitor which inhibits Polo-1 kinase (Plk1), phosphatidyl inositol-3 (PI3) kinase, AKT and mitogen activated kinase (MAPK) pathways [7–9]. The drug inhibits cell cycle progression, as well as

☆ Presented in part at the American Society of Hematology meeting, Orlando, December 2010, Abstract #4010.

* Corresponding author at: Hematology Division, Stanford University Cancer Center, 875 Blake Wilbur Drive, Stanford, CA 94305, USA. Tel.: +1 650 725 8355; fax: +1 650 723 1269.
E-mail address: peterg@stanford.edu (P.L. Greenberg).

0145-2126/$ – see front matter © 2011 Elsevier Ltd. All rights reserved.
doi:10.1016/j.leukres.2011.08.022

synergizing with cytotoxic drugs, selectively inducing mitotic arrest and apoptosis of cancer cells (including human lymphoma cells), while being relatively non-toxic for normal cells, mediated via the PI3, mammalian target of rapamycin (mTOR) and AKT pathways [7–9]. These effects lead to tumor regression in in vivo animal models [10]. In addition, Plk1 is a critical cell cycle kinase which affects mitotic progression, spindle assembly and centrosome maturation [11]. Its inhibition leads to mitotic arrest and apoptosis [12]. Conversely, its ectopic over-expression leads to neoplastic progression [13]. Increased expression of Plk1 is noted in many human tumors, including leukemia [14].

In Phase I/II studies ON 01910.Na has shown promising therapeutic results and drug tolerance in patients with advanced solid tumors [15,16], as well as in pilot in vitro and in vivo studies of MDS pts, including those with trisomy 8 [17–19]. Correlative investigations have demonstrated that ON 01910.Na inhibited cyclin D1 accumulation and was selectively toxic to trisomy 8 cells while promoting maturation of diploid cells in CD34+ cells of trisomy 8 MDS patients treated with this drug [17–19].

With this background we designed a Phase I/II trial to evaluate the safety and potential efficacy of ON 01910.Na in higher risk MDS patients whose disease had not responded to hypomethylating agents. As ON 01910.Na is a kinase inhibitor, we measured the changes in intracellular AKT signaling as an exploratory biologic correlative adjunct for our study. The PI3K/AKT signaling pathway is essential for different physiological processes of cell growth, survival and suppression of apoptosis, and its constitutive activation has been implicated in the pathogenesis as well as the progression of a wide variety of neoplasias, including AML and MDS [20–22]. A novel and highly sensitive nano-fluidic proteomic immunoassay method (NIA) has recently been developed to quantify changes in phosphorylated protein isoforms in MDS and other tumor specimens [23,24]. We utilized this detection method to investigate oncoprotein expression and phosphorylation in our patients' marrow samples, assessing CD34+ marrow intracellular AKT2 phosphorylation, a biomarker of apoptotic and cell cycle signaling [25], pre- and post-treatment.

2. Patients and methods

The objectives of this Phase I/II study were to evaluate the efficacy and safety of ON 01910.Na treatment in achieving marrow responses or hematological improvement (HI) in patients with trisomy 8 cytogenetics or those classified as IPSS Intermediate-1, Intermediate-2 or High risk whose disease had failed to respond to at least 4 cycles of hypomethylating agents or were intolerant of these drugs. All patients had been unresponsive to a median of six cycles (range 4–13) of hypomethylating agent therapy (6 post-azacytidine, 6 post-decitabine, and 1 patient treated with both agents). In addition, at baseline, all patients were red blood cell (RBC) transfusion-dependent. All patients had reviewed and signed informed consent forms according to the guidelines of the Stanford Investigational Review Board prior to their entry into the trial.

The patients (9 males, 4 females) had IPSS Intermediate-1 ($n = 4$), Intermediate-2 ($n = 2$) and High ($n = 7$) risk MDS subtypes and the cohort was comprised of patients with RAEB-1 (5 patients), RAEB-2 (4 patients) and RAEB-T (4 patients), with a median age of 75 years (range 65–86) and 1.5-year median (range 0.5–4.6) prior duration of MDS. Their cytogenetic profile included 6 patients with normal cytogenetics and 7 with abnormal cytogenetics (5 with trisomy 8 and 1 complex). This was a higher risk patient cohort, with nine of the 13 patients being IPSS Intermediate-2 or High at study entry. As the four Intermediate-1 patients were RBC transfusion dependent and had failed to respond to hypomethylating agents (after prior first line therapy), they were thus in a higher risk status than Intermediate-1 patients who would have been seen at their time of diagnosis.

Patients were required to have at least one clinically significant cytopenia and to have a baseline serum creatinine of <2 mg/dL and AST/ALT less than twice the upper limit of normal. They could not have received treatment with standard MDS therapies or investigational therapy within 4 weeks of starting ON 01910.Na.

The planned total study duration was 33 weeks, which included a 2-week screening phase, a 27-week dosing phase, and a 4-week follow-up phase that began after the last dose of ON 01910.Na. Beginning at week 4, patients were assessed for response. Marrow exams were performed at baseline, and after the first, third, fifth and seventh cycles, and at other times as clinically indicated.

Prior dosing regimens for the drug in MDS have ranged from 800 to 1500 mg/m^2/day for 2 days weekly for 3 out of 4 weeks or from 650 to 1700 mg/m^2/day for 3–6 days every 2 weeks as an continuous intravenous infusion (CIVI) [19,26]. The initial two patients received ON 01910.Na at a dose of 800 mg/m^2/day CIVI × 2 days/week × 3 weeks/month cycle. However, subsequent clinical data (Onconova Investigator's Brochure, January 25, 2010) led to recommendations to alter the treatment regimen, wherein the remaining 11 patients received the drug at a dose of 1800 mg/day CIVI × 3 days every 2 weeks/month cycle for the first 2 months, then monthly. These treatments were given in monthly cycles for a planned seven-month course of treatment.

ON 01910.Na (rigosertib) was supplied by Onconova Therapeutics Inc., Newtown, PA, as a sterile, concentrated solution in labeled, sealed glass vials stored at 2–8 °C. Just prior to dosing, the ON 01910.Na concentrate was diluted with aqueous infusion solution. Reconstituted ON 01910.Na was kept at room temperature and drug administration was started within 2 h of reconstitution via an infusion set with an in-line 1.2 μm filter. Infusion bags were changed every 24 h and a new infusion bag was administered for each of the following 24 h until completion of the total infusion time. The therapy was provided to patients as outpatients with drug placed in a portable infusion set, with their daily return to the nursing unit for changing the infusion bags and stopping the infusion at the end of the 3-day treatment.

2.1. Statistical methods

The response rates and the bone marrow blast and hematopoietic response (hematologic improvement, HI-E, HI, N, HI-P) rates were determined according to International Working Group (IWG) 2006 criteria [27]. Overall survival was estimated using the Kaplan–Meier method. Analysis of the primary efficacy endpoints and safety and toxicity features were performed on all enrolled patients who received at least one dose of ON 01910.Na.

2.2. Biologic correlative studies

2.2.1. Cell separation

For biologic correlative studies, aliquots of marrow samples obtained from patients pre- and post-treatment were enriched for CD34+ cells, as previously described [28]. The CD34+ marrow cell suspensions were stored frozen in heat-inactivated fetal bovine serum plus 10% dimethylsulfoxide in liquid nitrogen, were thawed at 37 °C into pre-warmed phosphate buffered saline (PBS) and washed once in PBS immediately before NIA analysis.

2.2.2. Nano-fluidic proteomic immunoassay (NIA)

The NIA experiments were performed using a Nanopro1000 instrument (Cell Biosciences, Santa Clara, CA) [29] as previously described [23]. Total AKT2 protein expression and its various phosphorylated isoforms were detected using a rabbit polyclonal antibody that recognizes mouse and human AKT2 (Cell Signaling Technology Inc., Boston, MA, #3063). NIA is able to quantify phosphorylated and unphosphorylated isoforms of signaling proteins in a sample, using a single antibody that recognizes all isoforms of the protein. Therefore, changes in relative phosphorylation of a protein can be measured. Quantitation of AKT2 phosphorylated and unphosphorylated protein peaks was performed using Compass (version 1.8.0) analysis software, using Gaussian peaks with variable widths, as previously described [23].

3. Results

3.1. Clinical responses

Thirteen patients were entered into the study and all were evaluable for efficacy and toxicity (Table 1). Patients received a median of six cycles (range 2–7) of treatment, with five patients completing the planned 7 cycles. Responses according to IWG 2006 criteria were: Partial response (1), stable disease (SD) 8, including 2 with transient (2 months) hematologic improvement (HI) (2; 1 HI-E, N, 1 HI-P, N) (#111, 112), and 4 with marrow complete responses (CRs) (Tables 1 and 2). The patients with marrow CRs had survivals of 5–17+ months. Five patients had progressive disease (PD), including 4 who transformed to AML while on trial. Overall survival from time of study entry was 10 months median (range 3–17) (Fig. 1); three patients remain alive, with a median time of 14 months (Table 2). Responses occurred in all FAB, IPSS and cytogenetic subgroups. Of the five patients with trisomy 8, two with stable disease (#101, 104) demonstrated a decrease in proportion

Table 1
Clinical status, treatment and responses of individual MDS patients to ON 01910.Na.

Patient	Age/gender	Modified FAB	IPSS category	Treatment cycles, number	Marrow response	Developed AML	Survival (months)
101	80M	RAEB-T	High[h]	7	SD		17
102	74M	RAEB-2	Int-2	3[a]	SD		11
103	73M	RAEB-1	Int-1	7	SD		10
104	77M	RAEB-1	Int-2[h]	7	SD (mCR)		8
105	66M	RAEB-1	Int-1	1[b]	SD (mCR)		13+
106	78M	RAEB-2	High	1[c]	PD	Yes	4
108	65F	RAEB-1	Int-1	7	SD (mCR)		17+
110	76M	RAEB-T	High	7	SD (PR)		8
111	86M	RAEB-T	High	5[a]	SD[f] → PD		12
112	81F	RAEB-2	High[h]	5[d]	SD[g] → PD		14+
117	75F	RAEB-2	High[h]	3[c,e]	PD skin (mCR)	Yes	5
121	80M	RAEB-T	High[h]	1[c]	PD	Yes	3
122	76F	RAEB-1	Int-1	5[c]	SD → PD	Yes	8

Modified FAB includes RAEB-1, RAEB-2 as defined by the WHO classification. RAEB, refractory anemia with excess blasts, RAEB-T, refractory anemia with excess blasts in transformation; Int, intermediate; SD, stable disease; PD, progressive disease; mCR, marrow complete response; PR, partial response.
Survival measured from time of study entry.
[a] Discontinued treatment due to infection related to refractory neutropenia.
[b] Discontinued treatment due to severe dysuria.
[c] Discontinued treatment due to PD (AML).
[d] Discontinued treatment due to PD (RAEBT).
[e] Discontinued treatment due to leukemia cutis despite marrow CR; overt AML 1 month later
Hematologic responses:
[f] Transient hematologic improvement-erythroid, neutrophils (HI-E,N).
[g] Transient hematologic improvement-neutrophils, platelets (HI-N,P).
[h] Trisomy 8 cytogenetics.

Table 2
Responses to therapy with ON 01910.Na related to baseline clinical features.

	Patients	Stable disease	Marrow complete response	Progressive disease	Survival (months)
Modified FAB morphologic subgroup					
RAEB-1	5	4	3	1	10 [8, 8, 10, 13+, 17+]
RAEB-2	4	2	1	2	8 [4, 5, 11, 14+]
RAEB-T	4	2 (1PR)	0	2	10 [3, 8, 12, 17]
IPSS category					
Intermediate-1	4	3	2	1	11.5 [8, 10, 13+, 17+]
Intermediate-2	2	1	1	1	9.5 [8, 11]
High	7	4 (1PR)	1	3	8 [3, 4, 5, 8, 12, 14+, 17]
All patients	13	8	4	5	10 [3–17]

Modified FAB includes RAEB-1, RAEB-2 as defined by the WHO classification. PR, partial response.

of trisomy 8 marrow cells from 65% to 15% and 80% to 13% after treatment, whereas the three remaining patients with PD had no such decrements. No other cytogenetic responses were noted in the two other pts with abnormal cytogenetics.

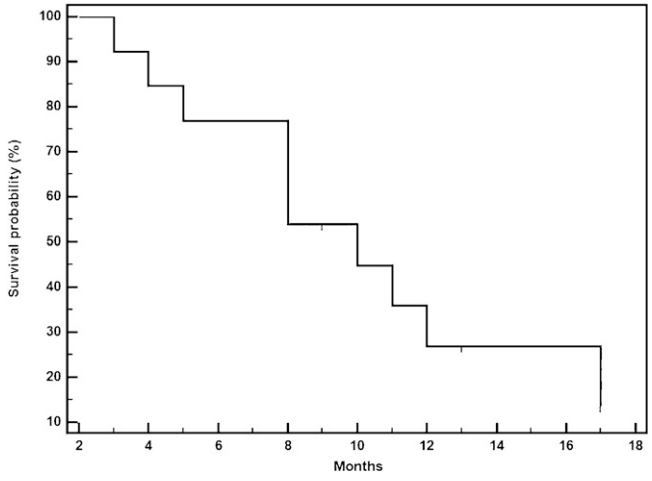

Fig. 1. Overall survival of patients treated with ON 01910.Na from the onset of start of study drug therapy (Kaplan–Meier curve).

3.2. Side effects

Grade 3/4 non-hematologic drug-related or possibly related toxicities occurred in 4 patients: 1 diarrhea, 1 dysuria, 1 fatigue, 1 epistaxis; two patients had pulmonary infections unrelated to study drug. Five patients were able to complete all 7 cycles of treatment. Per protocol guidelines, 5 patients discontinued treatment due to disease progression (4 to AML, 1 to RAEBT) (Table 1). One patient stopped therapy due to drug toxicity (severe dysuria) and two patients had treatment stopped due to infection related to their underlying neutropenias.

3.3. Biologic analyses

Using NIA, we analyzed intracellular phosphorylation of AKT2 and its isoforms in CD34+ marrow cells from five patients. The assays were performed to compare signaling at baseline and after initiating ON 01910.Na treatment (Table 3). In three responders, AKT2 phosphorylation substantially decreased by 12–19% following cycle 1. In contrast, in two patients who progressed on treatment, AKT 2 phosphorylation decreased by only 2% or increased by 19% post therapy. NIA is able to measure changes in different phosphorylated states of AKT2 (22,23,29); thus, we were able to further resolve changes in AKT2 phosphorylation into distinct phosphorylated states (Fig. 2). Interestingly, the decrease in overall phosphorylation was predominantly due to a decrease in

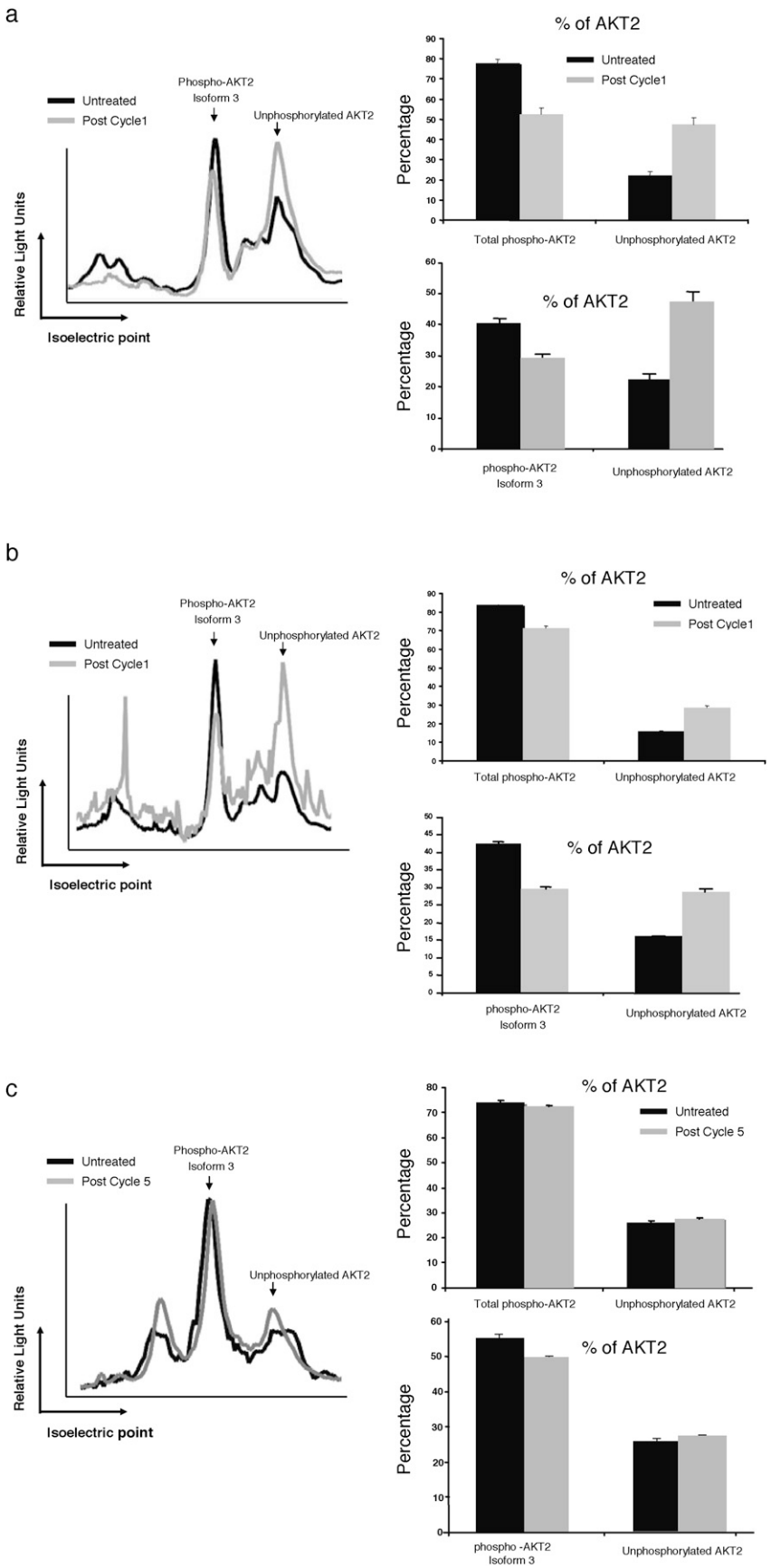

Fig. 2. Treatment effects of ON 01910.Na on AKT2 phosphorylation using nanoimmunoassay (NIA) analysis: decreased phosphorylation in CD34+ marrow cells in (a) a responding MDS patient (#101) with stable disease, (b) in a responding patient (#104) with marrow complete response, and (c) in a nonresponder (#111) whose disease progressed on treatment.

Table 3
Nanoimmunoassay (NIA) quantification of AKT2 isoforms in CD34+ bone marrow cells from MDS patients treated with ON 01910.Na.

Patients	Clinical response	% change in phospho-AKT2 levels[a]	% change in phospho-AKT2 isoform 3 levels[a]
101	Stable disease	19% decrease	22% decrease
104	Marrow CR	15% decrease	36% decrease
105	Marrow CR	12% decrease	25% decrease
111	Progressive disease	2% decrease	10% decrease
121	Progressive disease	18% increase	22% increase

[a] Percentage (%) change following cycle 1 compared to pretreatment, except for patient 111, who was evaluated post cycle 5 at time of disease progression.

phosphorylated AKT2 isoform 3, by 22–36% in each of the three responders, whereas it either decreased only 10% or increased 22% in two non-responders whose disease progressed (Table 3). In these patients, assays performed at sequential time points up to seven cycles of treatment showed similar changes as those found following cycle 1.

4. Discussion

Based on our study, ON 01910.Na appears to be active in patients with higher risk MDS who have failed to respond to hypomethylating agent therapy. A high degree of stable disease was achieved in the patients during their treatment period. Transient marrow CRs occurred in four patients. The drug was tolerated relatively well with few adverse effects. As hematologic toxicity was uncommon in these previously heavily treated patients despite decreasing marrow blastic proliferation, this suggests that the drug had limited negative effects on the patients' residual hematopoietic reserve. Although responsiveness was noted frequently in either the stabilization or improvement of marrow blasts, there was little improvement in hematologic parameters. Responses occurred in all FAB, IPSS and cytogenetic subgroups. The median 10-month survival from time of study entry compares favorably with the 4.3–5.6-month medians previously reported in higher risk MDS patients whose disease failed to respond to hypomethylating agents [5,6]. Effective clinical responses have been seen with this drug in other advanced human neoplasms [16,17].

Most current methods of protein detection are insensitive to detecting subtle changes in oncoprotein activation that underlie critical hematopoietic signaling processes. The requirement for large numbers of cells precludes serial cell sampling for assessing a response to therapeutics. Thus, in order to accurately measure oncoprotein expression and activation in our marrow specimens, we utilized the nano-fluidic proteomic immunoassay detection method (NIA) [23]. This method separates proteins by isoelectric focusing, followed by antibody detection of specific epitopes with chemiluminescence and quantifies total and low abundance protein isoforms. It has also previously been shown to measure changes in the expression and activation of a variety of other onco/signaling proteins with high accuracy and sensitivity in preclinical and clinical specimens of hematopoietic malignancies, before and during treatment [23,29,30].

The serine/threonine kinase AKT functions as a critical mediator of signaling downstream of PI3 kinase and is essential for different physiological processes. Its constitutive activation has been implicated in the pathogenesis and the progression of a wide variety of neoplasias, including MDS and AML [20–22]. Protein and mRNA levels of the Akt2 isoform increase with the pathological grade of malignant gliomas and its down-regulation induced apoptosis in a variety of tumor cells [31]. Our NIA analysis of bone marrow cells sampled before and after ON 01910.Na treatment demonstrated substantially decreased AKT2 phosphorylation of marrow CD34+ cells in the three MDS patients assayed who responded to treatment, whereas in two patients who did not respond and whose disease progressed, there was no decrease (or Ševen an increase). Notably, NIA resolved different phosphorylated isoforms of AKT2, and uncovered a decrease in responders in phosphorylation predominantly occurring in isoform 3. These findings are of interest as AKT signaling, including that for AKT2, is a critical pathway for metabolic signaling, protection against tumor cell apoptosis, cancer cell invasion and chemoresistance in AML [25,31–33]. Altered levels of AKT2 phosphorylation, particularly for isoform 3, may correlate with response to ON 01910.Na. Extension of these preliminary studies are needed to determine whether the changes in AKT2 isoform 3 may be useful to provide a potential surrogate biologic marker for responsiveness to ON 01910.Na therapy.

In summary, the responsiveness, median survival and drug tolerance of these higher risk MDS patients to ON 01910.Na are encouraging. However, a randomized Phase III clinical trial is required to clarify the potential survival advantage and for decreasing AML progression of this therapy in such patients, particularly those whose disease failed to respond to hypomethylating agents. Such a Phase III trial is now underway, based in part on results of this study. Use of surrogate biomarker correlates such as NIA of intracellular phosphorylation of relevant signaling proteins should prove useful for determining drug mechanism of action and for patient evaluation and selection on therapeutic trials with this and other kinase inhibitors.

Funding

This study was supported in part by the Clinical and Translational Science Award 1UL1 RR025744 for the Stanford Center for Clinical and Translational Education and Research (Spectrum) from the National Center for Research Resources, National Institutes of Health, Onconova Therapeutics Inc., the Leukemia & Lymphoma Society (SCOR grant), Veterans Administration Palo Alto Health Care System (resources and use of facilities) [PLG]; NIH/NCI (K23 [ACF]); and NIH/NCI (P-01 ICMIC, P-01 LPPG [DWF, LX]).

Conflict of interest statement

Peter Greenberg received research funding for this study from Onconova Therapeutics Inc. Francois Wilhelm is Chief Medical Officer and Senior Vice President at Onconova Therapeutics Inc. Dean Felsher is on the Scientific Advisory Board for Cell Biosciences. The other co-authors declare no competing financial interests.

Acknowledgements

Contributions. The study was designed by P.L.G., M.S. and A.C.F. The manuscript was written by P.L.G. and A.C.F. Clinical coordination and management and data collection was performed by M.T., M.S., and P.L.G. CD34+ cell enrichment was performed by K.S. Data analysis and interpretation was performed by P.L.G. and A.C.F. The nanoimmunoassay studies were performed by A.C.F., L.X., J.P.R. and D.W.F. The study was monitored by Onconova Therapeutics Inc. in accordance with good clinical practice requirements and all data were entered into a validated clinical trial database. Final data and the manuscript were reviewed by all investigators.

References

[1] Greenberg P, Cox C, LeBeau MM, et al. International scoring system for evaluating prognosis in myelodysplastic syndromes. Blood 1997;89:2079–88.
[2] Greenberg PL, Attar E, Bennett JM, et al. NCCN practice guidelines for myelodysplastic syndromes, version 2.2011. J Natl Compr Cancer Netw 2011;9:30–56.

[3] Fenaux P, Mufti GJ, Hellstrom-Lindberg E, et al. Efficacy of azacitidine compared with that of conventional care regimens in the treatment of higher-risk myelodysplastic syndromes: a randomised, open-label, phase III study. Lancet Oncol 2009;10:223–32.
[4] Kantarjian HM, O'Brien S, Shan J, et al. Update of the decitabine experience in higher risk myelodysplastic syndrome and analysis of prognostic factors associated with outcome. Cancer 2007;109:265–73.
[5] Jabbour E, Garcia-Manero G, Batty N, et al. Outcome of patients with myelodysplastic syndrome after failure of decitabine therapy. Cancer 2010;116: 3830–4.
[6] Prébet T, Gore SD, Esterni B, et al. Outcome of high-risk myelodysplastic syndrome after azacitidine treatment failure. J Clin Oncol 2011;29:3322–7.
[7] Gumireddy K, Reddy MV, Cosenza SC, et al. ON 01910, a non-ATP-competitive small molecule inhibitor of Plk1, is a potent anticancer agent. Cancer Cell 2005;7:275–86.
[8] Chun AW, Cosenza SC, Taft DR, et al. Preclinical pharmacokinetics and in vitro activity of ON 01910.Na, a novel anti-cancer agent. Cancer Chemother Pharmacol 2009;65:177–86.
[9] Prasad A, Park IW, Allen H, et al. Styryl sulfonyl compounds inhibit translation of cyclin D1 in mantle cell lymphoma cells. Oncogene 2009;28:1518–28.
[10] Smits VA, Klompmaker R, Arnaud L, et al. Polo-like kinase-1 is a target of the DNA damage checkpoint. Nat Cell Biol 2000;2:672–6.
[11] Liu X, Erikson RL. Polo-like kinase (Plk)1 depletion induces apoptosis in cancer cells. Proc Natl Acad Sci U S A 2003;100:5789–94.
[12] Eckerdt F, Yuan J, Strebhardt K. Polo-like kinases and oncogenesis. Oncogene 2005;24:267–76.
[13] Renner AG, Dos Santos C, Recher C, et al. Polo-like kinase 1 is overexpressed in acute myeloid leukemia and its inhibition preferentially targets the proliferation of leukemic cells. Blood 2009;114:659–62.
[14] Schöffski P. Polo-like kinase (PLK) inhibitors in preclinical and early clinical development in oncology. Oncologist 2009;14:559–70.
[15] Jimeno A, Li J, Messersmith WA, Laheru D, et al. Phase I study of ON 01910.Na, a novel modulator of the Polo-like kinase 1 pathway, in adult patients with solid tumors. J Clin Oncol 2008;26:5504–10.
[16] Jimeno A, Chan A, Cusatis G, et al. Evaluation of the novel mitotic modulator ON 01910.Na in pancreatic cancer and preclinical development of an ex vivo predictive assay. Oncogene 2009;28:610–8.
[17] Sloand EM, Pfannes L, Chen G, et al. CD34 cells from patients with trisomy 8 myelodysplastic syndrome (MDS) express early apoptotic markers but avoid programmed cell death by up-regulation of antiapoptotic proteins. Blood 2007;109:2399–405.
[18] Sloand EM, Pfannes L, Reddy R, et al. Suppression of cyclin D1 by ON 01910.Na is associated with decreased survival of trisomy 8 myelodyplastic bone marrow progenitors: a potential targeted therapy. Blood (ASH Annual Meeting Abstracts) 2007;110 [Abstract 822].
[19] Shenoy A, Pfannes L, Wilhelm F, et al. Suppression of cyclin D 1 (CD1) by on ON 01910.Na is associated with decreased survival or trisomy 8 myelodysplastic bone marrow: a potential targeted therapy for trisomy 8 MDS. Blood (ASH Annual Meeting Abstracts) 2008;112 [Abstract 1651].
[20] Park S, Chapuis N, Tamburini J, et al. Role of the PI3K/AKT and mTOR signaling pathways in acute myeloid leukemia. Haematologica 2010;95:819–28.
[21] Kawauchi K, Ogasawara T, Yasuyama M, et al. The PI3K/Akt pathway as a target in the treatment of hematologic malignancies. Anticancer Agents Med Chem 2009;9:550–9.
[22] Follo MY, Mongiorgi S, Bosi C, et al. The Akt/mammalian target of rapamycin signal transduction pathway is activated in high-risk myelodysplastic syndromes and influences cell survival and proliferation. Cancer Res 2007;67:4287–94.
[23] Fan AC, Deb-Basu D, Orban M, et al. Nano-fluidic proteomic assay for serial quantitative analysis of oncoprotein expression and phosphorylation in clinical specimens. Nat Med 2009;15:566–71.
[24] Fan AC, Dermody JL, Kong C, et al. Nanoscale quantification of phosphorylated and unphosphorylated ERK and MEK isoforms differentiates tumor and nontumor clinical specimens. Mol Cancer Ther 2009;8(Dec (Suppl.)):B178.
[25] Perego P, Cossa G, Zuco V, et al. Modulation of cell sensitivity to antitumor agents by targeting survival pathways. Biochem Pharmacol 2010;80:1459–65.
[26] Seetharam M, Tran M, Fan AC, et al. Treatment of higher risk myelodysplastic syndrome patients unresponsive to hypomethylating agents with ON 01910.Na. Blood (ASH Annual Meeting Abstracts) 2010;116 [Abstract 4010].
[27] Cheson BD, Greenberg PL, Bennett JM, et al. Clinical application and proposal for modification of the international working group (IWG) response criteria in myelodysplasia. Blood 2006;108:419–25.
[28] Sridhar K, Ross D, Tibshirani R, et al. Relationship of differential gene expression profiles in CD34+ myelodysplastic syndrome marrow cells to disease subtype and progression. Blood 2009;114:4847–58.
[29] O'Neill RA, Bhamidipati A, Bi X, et al. Isoelectric focusing technology quantifies protein signaling in 25 cells. Proc Natl Acad Sci U S A 2006;31(103):16153–8.
[30] Fan AC, Dermody JL, Kong C, et al. Nanoscale approaches to define biologic signatures and measure proteomic response to targeted therapies in hematologic and solid tumors. In: Proc 4th AACR international conference on molecular diagnostics in cancer therapeutic development. 2010 [Abstract #84317_1 (PR6)].
[31] Mure H, Matsuzaki K, Kitazato KT, et al. Akt2 and Akt3 play a pivotal role in malignant gliomas. Neuro Oncol 2010;12:221–32.
[32] Grandage VL, Gale RE, Linch DC, et al. PI3-kinase/Akt is constitutively active in primary acute myeloid leukaemia cells and regulates survival and chemoresistance via NF-kappaB, mapkinase and p53 pathways. Leukemia 2005;19:586–94.
[33] Martelli AM, Nyåkern M, Tabellini G, et al. Phosphoinositide 3-kinase/Akt signaling pathway and its therapeutical implications for human acute myeloid leukemia. Leukemia 2006;20:911–2.

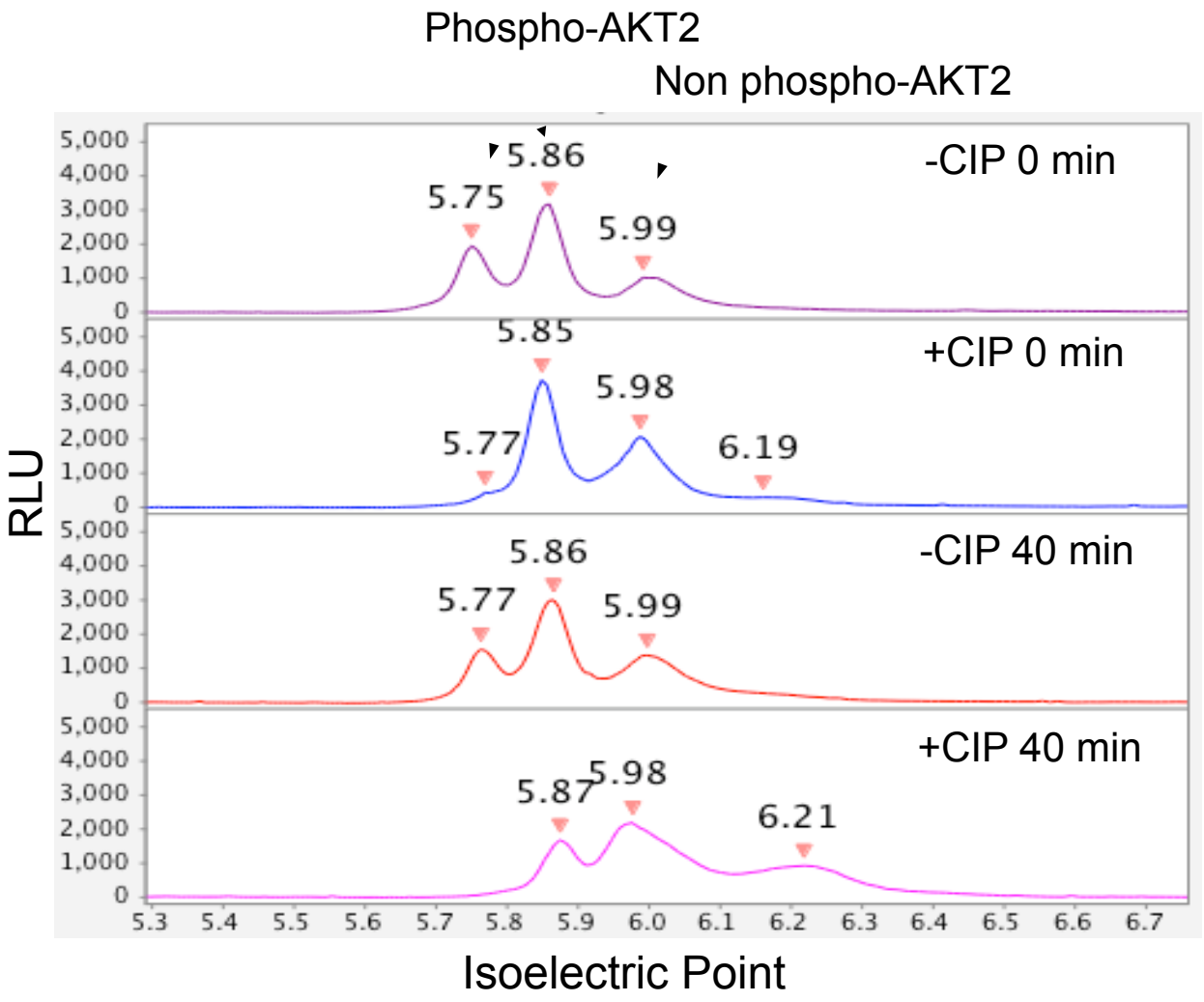

Figure 1: Identification of AKT2 Phospho-isoforms in TF1 Cells (Phosphatase Treatment). The TF1 cells were pelleted and snap frozen in liquid N_2 and kept in -80°C until use. The cell pellet was lysed with MPER buffer containing protease inhibitors. The protein amount was measured with BCA kit. The same amount of protein from each cell lysate was incubated with CIP at 37°C for certain time. subjected for NIA analyses.

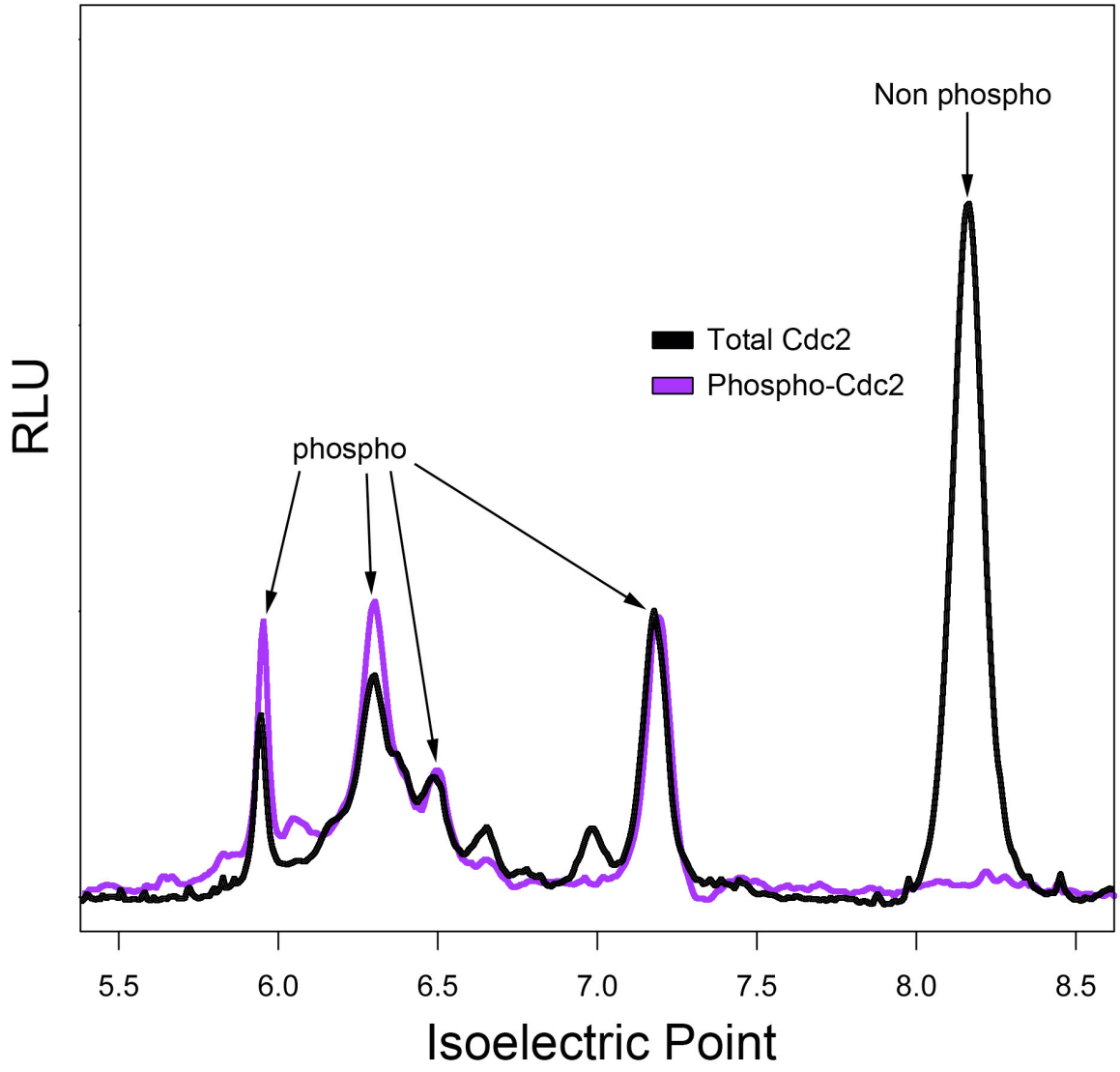

Figure 2: Identification of CDC2 Phospho-isoforms in TF1 Cells (Profile Alignment between pCDC2 Antibody and CDC2 Antibody). The TF1 cells were pelleted and snap frozen in liquid N_2 and kept in -80°C until use. The cell pellet was lysed with MPER buffer containing phosphatase and protease inhibitors. The protein amount was measured with BCA kit. The same amount of protein from each cell lysate was subjected for NIA analyses.

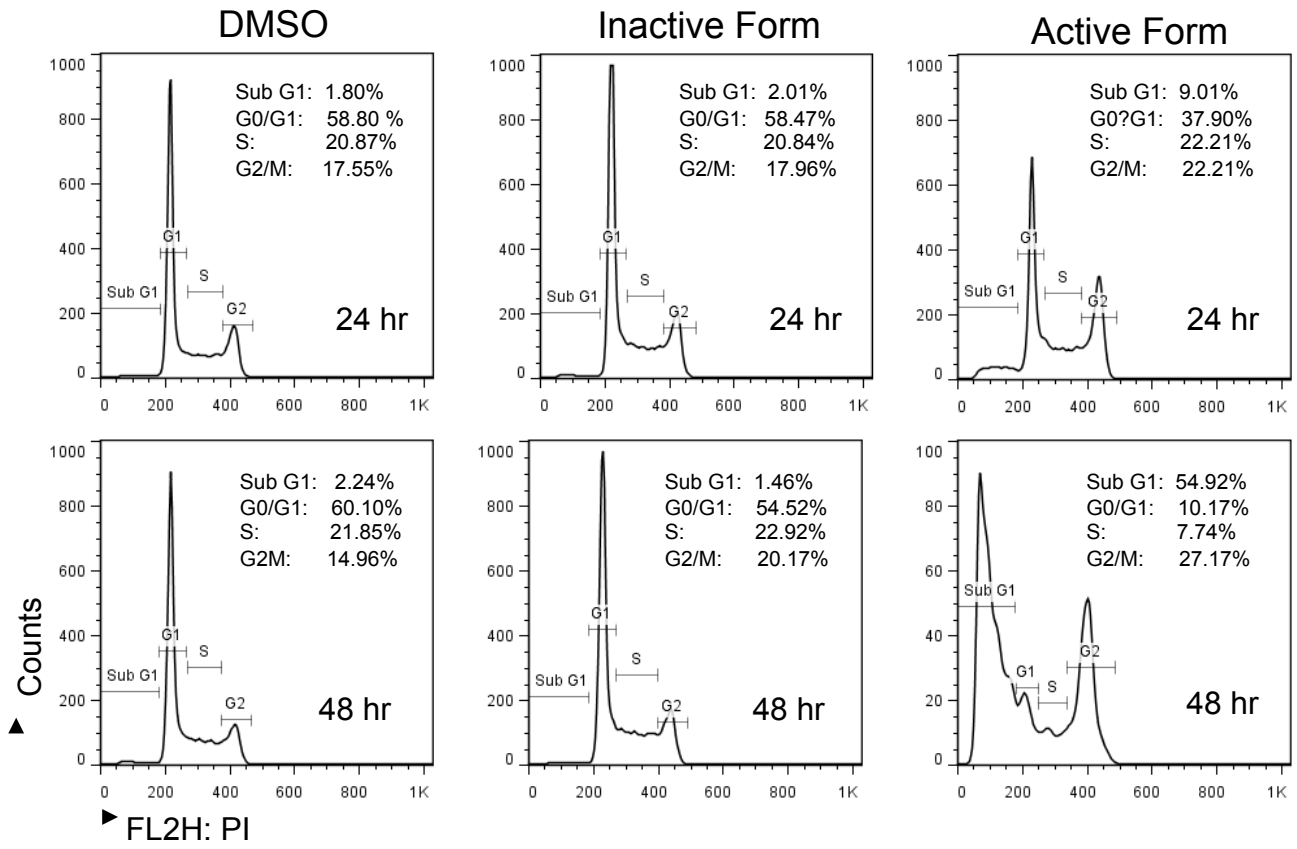

Figure 3: 24 Hour Treatment of ON01910.Na (0.3μM) Starts Cell Cycling Arrest and Apoptosis in TF1 Cells (PI Staining). TF1 cells were grown in RPMI medium containing 10% fetal bovine serum and GM-CSF. Cells were treated with 0.3 μM ON01910.Na (active form), ON019911.Na (inactive form), or DMSO. Cells were collected and fixed for promidium iodide (PI) staining at various time points of the treatments. One million fixed cells were used for PI staining FACS analysis.

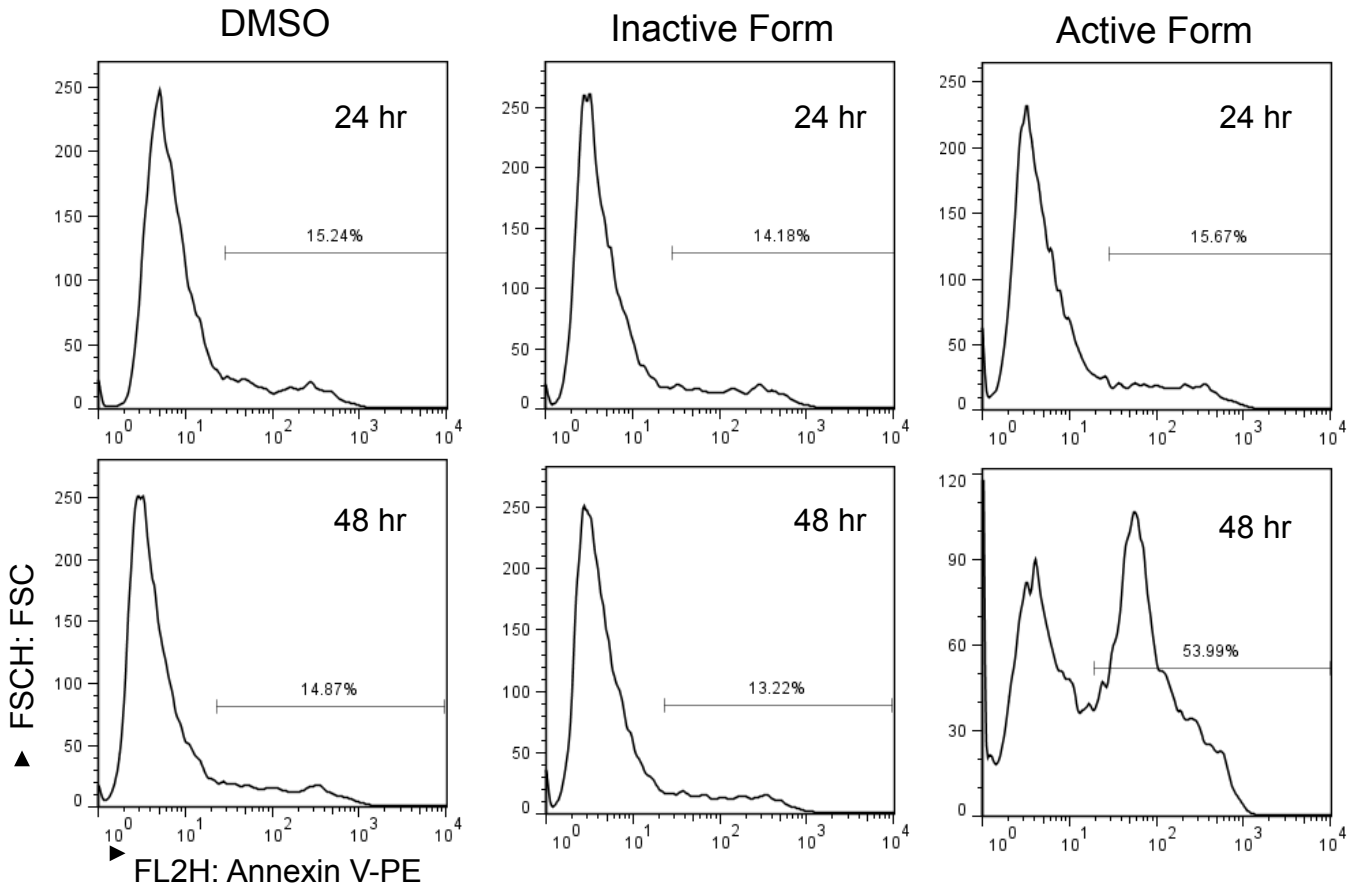

Figure 4: 24 Hour Treatment of ON01910.Na (0.3μM) Starts Cell Cycling Apoptosis in TF1 Cells (Annex V Staining). TF1 cells were grown in RPMI medium containing 10% fetal bovine serum and GM-CSF. Cells were treated with 0.3 μM ON01910.Na (active form), ON019911.Na (inactive form), or DMSO. Cells were collected and fixed for Annex V staining at various time points of the treatments. One million fixed cells were used for Annexin V staining FACS analysis.

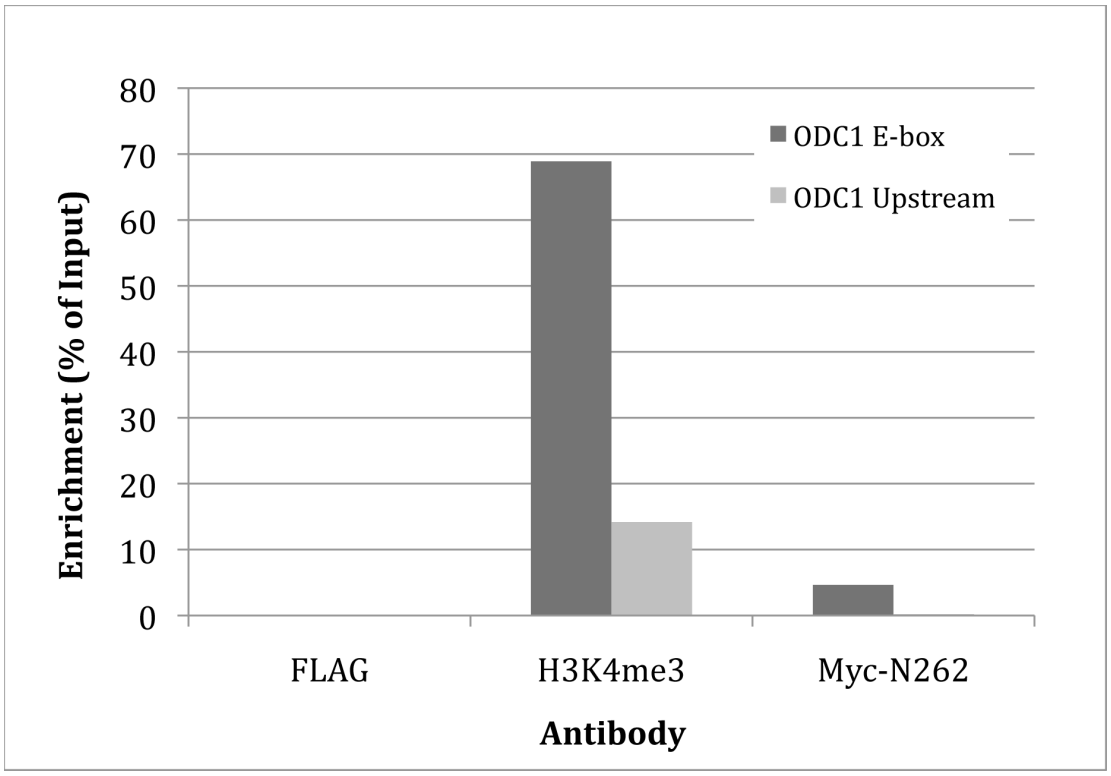

Figure 5: Bar Graph Shows qPCR Validation of AutoChIP Enrichment. Enrichment for H3K4me3 is quite high, with Odc1 e-box signal being ~5-6 times that of the upstream control region. Enrichment for Myc is relative lower, but still enriched considering that the background noise from both the Odc1 upstream control and the FLAG control are low.

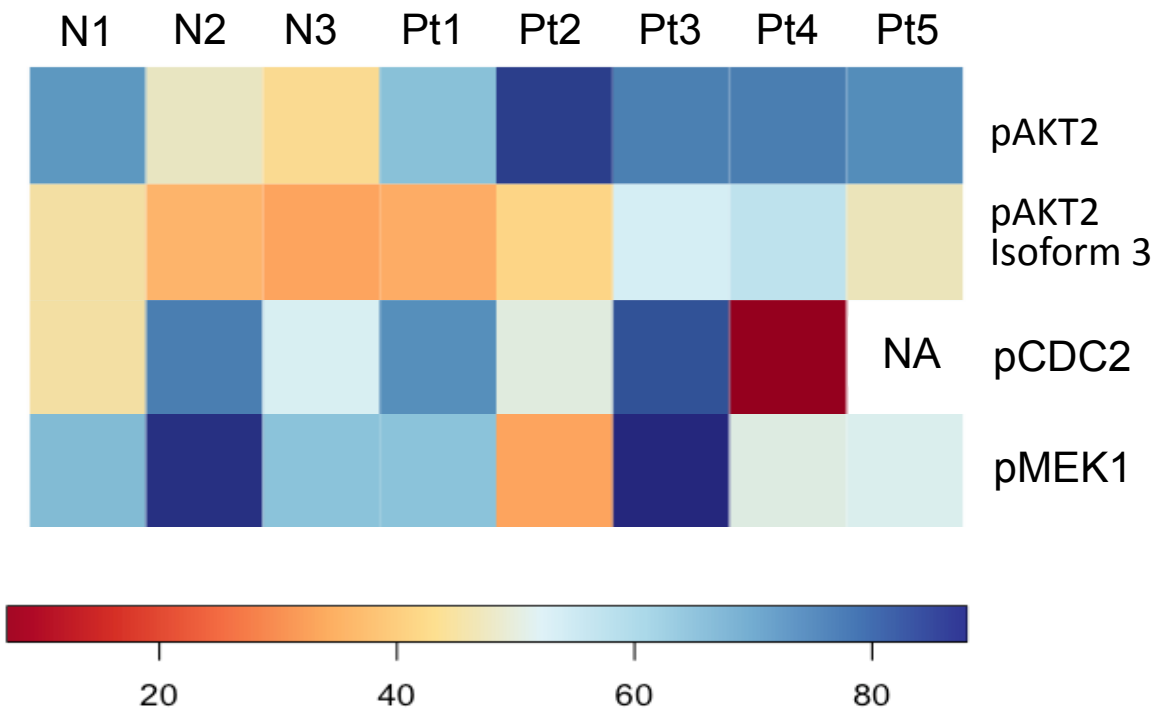

Figure 6: There Are No Specific Distribution Patterns for Basal Levels of pAKT2, AKT2 Isoform 3, pCDC2, and pMEK1 in CD34+ Bone Marrow Cells between MDS Patients and Normal Bone Marrow Donors. Heat map was generated from NIA data with R64 program.

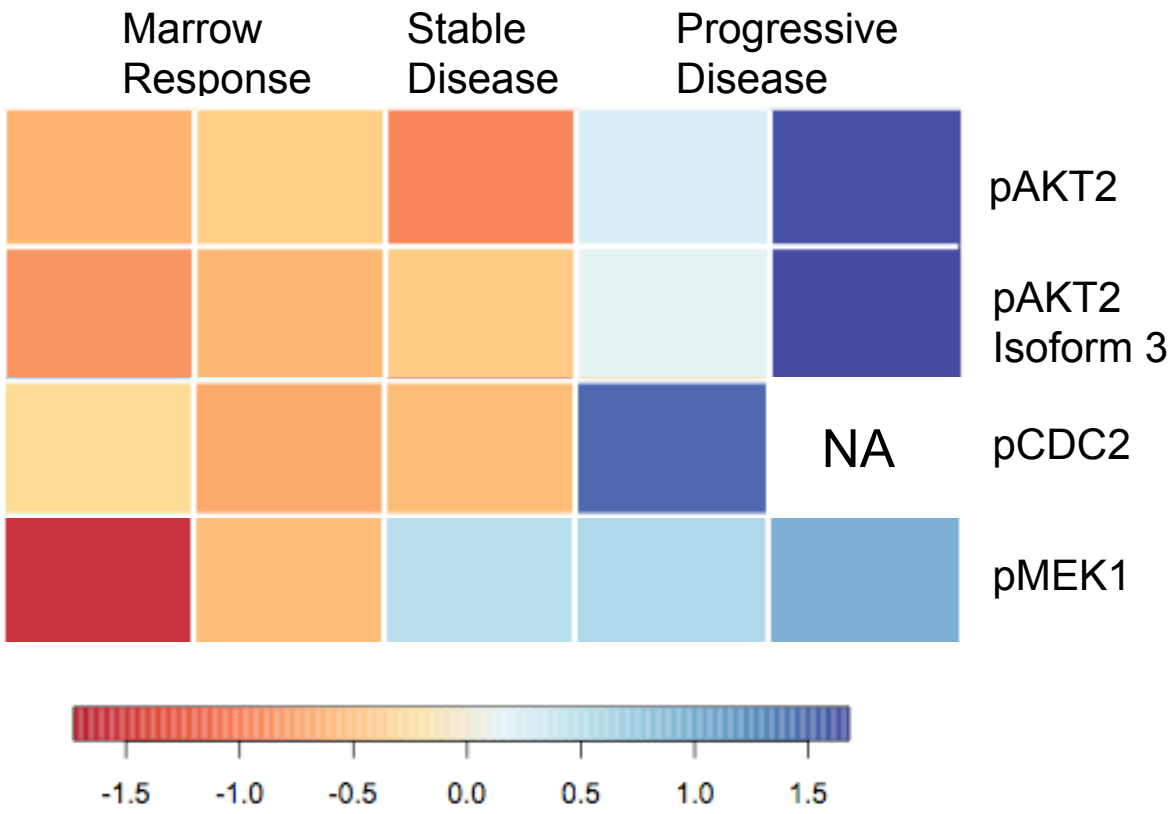

Figure 7: Heat Map Reveals A Correlation between Changes of pAKT2, pAKT2-isoform 3, pCDC2, and pMEK1 of Five Patients and Their Clinical Responses. Heat map was generated from NIA data with R64 program. Fold changes of peak area%. Scaled by column: mean=0, STD=1.

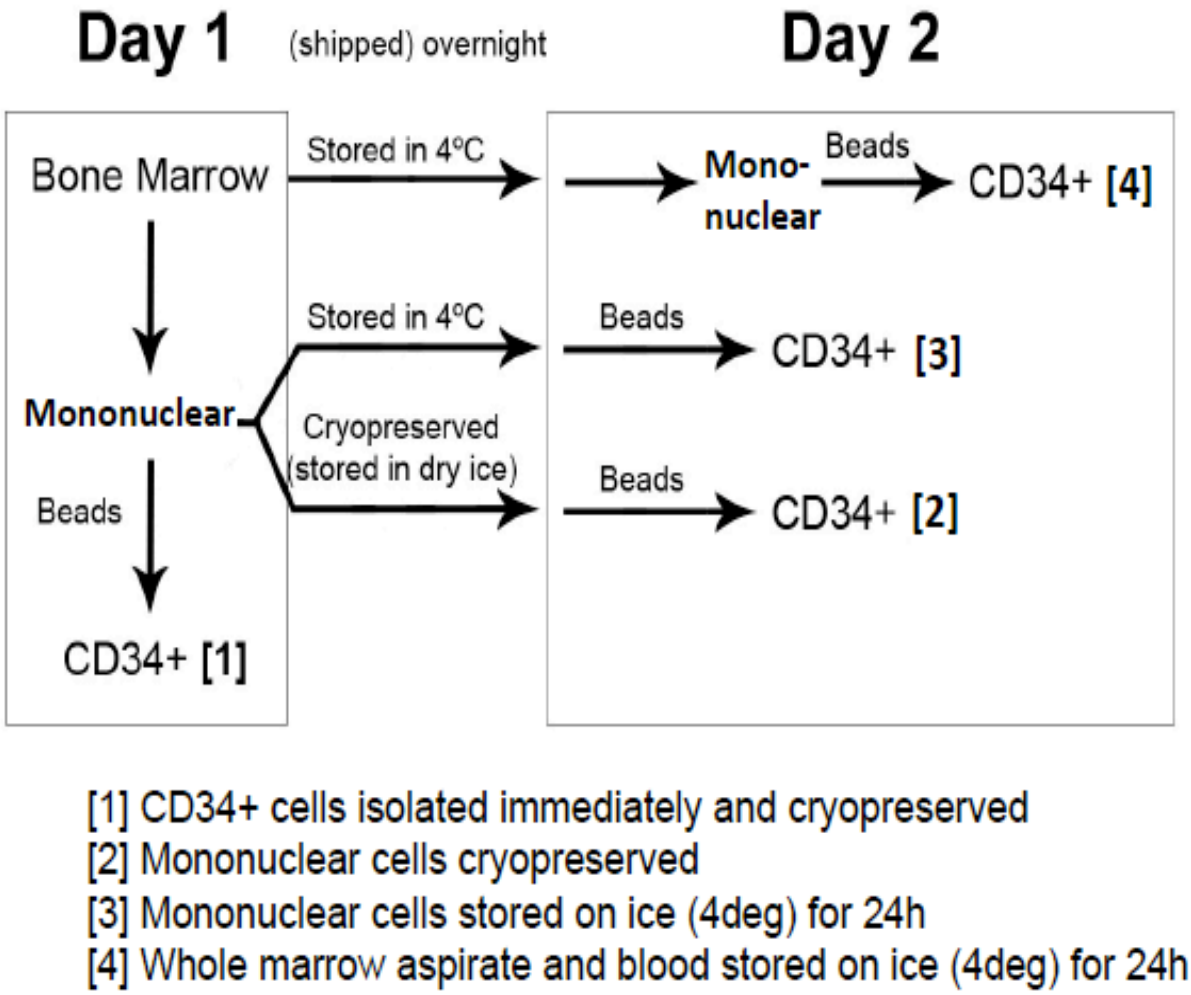

[1] CD34+ cells isolated immediately and cryopreserved
[2] Mononuclear cells cryopreserved
[3] Mononuclear cells stored on ice (4deg) for 24h
[4] Whole marrow aspirate and blood stored on ice (4deg) for 24h

Figure 8: Bone Marrow Specimen Processing Conditions. This scheme shows different processing and storage conditions to purify CD34+ cells from patient bone marrow samples.

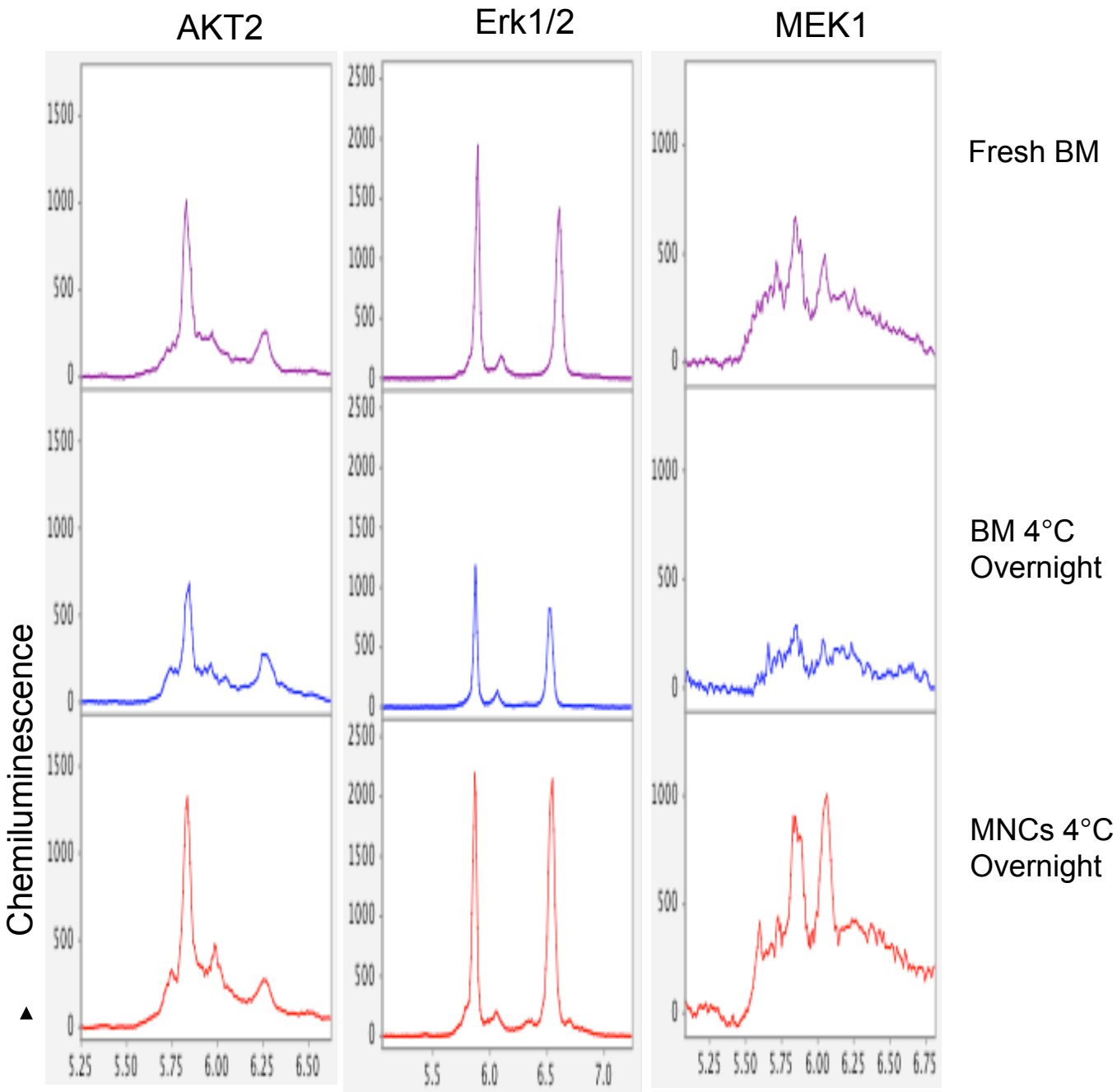

Figure 9: Bone Marrow Can Be Stored Overnight at 4°C Prior to CD34+ Cell Isolation for NIA Analysis. Mononuclear cells [MNC] are isolated from whole bone marrow (BM) with a ficoll gradient, then CD34+ cells are isolated using magnetic beads. (a) All steps occurred immediately after collection, (b) BM was stored overnight at 4o C, then the next day, MNCs were isolated, followed by CD34+ cell isolation, or (c) MNC were isolated immediately, then stored overnight at 4o C, then CD34+ cells were isolated the next day.

Table 1. List of MYC target genes identified from H3K4me3 AutoChIP-seq.

Gene Name	Organism	Cell Type	Description	Function
ACADM	human	U-937 monocyte, P493 lymphocyte, HL60	acyl-Coenzyme A dehydrogenase, C-4 to C-12 straight chain	Metabolism, Lipid
ANXA6	rat	fibroblast	annexin A6	Vesicular trafficking
BCL2	human	U-937 monocyte, HL60, P493 lymphocyte	aspecific BCL2 ARE-binding protein 2	Apoptosis
CAPZA1	human	Burkitt's lymphoma Daudi	capping protein (actin filament) muscle Z-line, alpha 1	Cytoskeletal protein
CASP8	human	HL60, P493 lymphocyte, U-937 monocyte	caspase 8	apoptosis
CDKL3	human	Burkitt's lymphoma Daudi	cyclin-dependent kinase-like 3	protein modification, cell cycle
CFDP1	human	HL60, U-937 monocyte, Burkitt's lymphoma Daudi, P493 lymphocyte	craniofacial development protein 1; BCNT	helix-loop-helix, transcription factor
CLCN6	human	Burkitt's lymphoma Daudi	chloride channel 6	channel
CPD	rat	fibroblast	carboxypeptidase D	protein processing
EPC1	human	Burkitt's lymphoma Daudi	enhancer of polycomb homolog 1, (Drosophila)	transcription, chromatin
EPM2A	human	Burkitt's lymphoma Daudi	epilepsy, progressive myoclonus type 2, Lafora disease (laforin)	metabolism
FLOT2	human	Burkitt's lymphoma Daudi	flotillin 2	cell adhesion
HSF2BP	human	Burkitt's lymphoma Daudi	heat shock transcription factor 2 binding protein	chaperones
MCC	human	lymphocyte	mutated in colorectal cancers	growth arrest
NXN	rat	fibroblast	Nucleoredoxin 1, Red-1	transcription
PEX14	human	HL60	peroxisomal biogenesis factor 14	vesicular trafficking
PFKFB4	human	Burkitt's lymphoma Daudi	6-phosphofructo-2-kinase/fructose-2,6-biphosphatase 4	metabolism

Table 1. List of MYC target genes identified from H3K4me3 AutoChIP-seq (continued).

PLA2G6	human	Burkitt's lymphoma Daudi	phospholipase A2, group VI (cytosolic, calcium-independent)	phospholipid metabolism
POU2F1	human	Burkitt's lymphoma Daudi	POU domain, class 2, transcription factor 1	transcription
PRKDC	human	P493 lymphocyte, HL60, U-937 monocyte, Burkitt's lymphoma Daudi	DNA-dependent protein kinase, catalytic subunit	DNA repair, chromatin
RBBP8	human	Burkitt's lymphoma Daudi	retinoblastoma-binding protein 8	cell cycle
RBL1	human	Burkitt's lymphoma Daudi	retinoblastoma-like 1 (p107)	cell cycle
ROCK1	rat	kidney epithelial	Rho-associated, coiled-coil forming kinase1	signal transduction
RPS6KA5	human	Burkitt's lymphoma Daudi	ribosomal protein S6 kinase, 90kD, polypeptide 5	protein synthesis
SDF2	human	Burkitt's lymphoma Daudi	stromal cell-derived factor 2	protein modification
SLC26A4	human	Burkitt's lymphoma Daudi	solute carrier family, member 4	transport
TRAF2	human	Burkitt's lymphoma Daudi	TRAP1, TNF 1 associated protein; tumor necrosis factor receptor associated protein	apoptosis
UBE2G2	human	Burkitt's lymphoma Daudi	ubiquitin-conjugating enzyme E2G 2 (homologous to yeast UBC7)	protein degradation
ZMPSTE24	human	Burkitt's lymphoma Daudi	zinc metalloproteinase, STE24 (yeast, homolog)	membrane protein

Table 2. There are no big differences in basal levels of pAKT2, pAKT2 isoform 3, pMEK1 and pCDC2 between MDS patients and Normal Marrow donors.

Patients	Clinical status	% of pAKT2 levels	% of pAKT2 isoform 3 levels	% of pMEK1 levels	% of pCDC2 levels
AF1	**Normal**	**70.5**	**45.6**	**64.4**	**45.4**
AF2	**Normal**	**47.9**	**37.7**	**86.0**	**74.1**
AF3	**Normal**	**44.1**	**35.1**	**63.1**	**51.8**
101	MDS	63.3	36.4	63.3	71.7
104	MDS	84.0	42.6	35.2	50.2
105	MDS	73.9	52.5	87.8	80.7
111	MDS	74.0	55.7	50.1	7.4
121	MDS	71.9	47.6	51.6	NA

Table 3. Changes of pAKT2, pAKT2 isoform 3, pMEK1 and pCDC2 are correlated to clinical outcomes

Patients	Clinical response	% change in pAKT2 levels	% change in pAKT2 isoform 3 levels	% change in pMEK1 levels	% change in pCDC2 levels
101	**Stable disease**	**19% decrease**	**22% decrease**	**7% increase**	**14% increase**
104	**Marrow CR**	**15% decrease**	**36% decrease**	**47% decrease**	**133% increase**
105	**Marrow CR**	**12% decrease**	**25% decrease**	**21% decrease**	**48% decrease**
111	Progressive disease	2% decrease	10% decrease	9% increase	922% increase
121	Progressive disease	18% increase	22% increase	20% increase	NA